Viscous Stability Analysis

of

Trailing Line Vortex

Hamzeh E. Nataj

Presented in Partial Fulfillment of the Requirements

for the Degree of Master of Applied Science (Mechanical Engineering) at

Concordia University

Montréal, Québec, Canada

April 2013

Concordia University

School of Graduate Studies

This is to certify that the thesis prepared

By: HAMZEH EBRAHIM NATAJ JELODAR

Entitled: Viscous Stability Analysis of Trailing Line Vortex

and submitted in partial fulfillment of the requirements for the degree of

Master of Applied Science (Mechanical Engineering)

Complies with the regulations of the University and meets the accepted standards with respect to originality and quality.

Signed by the final examining committee:

Dr. L. KADEM	Chair
Dr. A. Dolatabadi	Examiner
Dr. S. Li, BCEE	External Examiner
Dr. G. H. Vatistas	Supervisor and Examiner
Dr. H. A. Abderrahmane	Supervisor and Examiner

Approved by MASc. Program Director, MIE Department

Dean of Faculty

Date April 8th, 2013

Abstract

This piece of work deals with the viscous stability of trailing line vortex. The perturbations are three dimensional and the viscous effects were encountered. The eigenvalue problem was solved by implementing a pseudo-spectral approach in MATLAB environment. The code was confirmed through comparing the results with those available in the literature, produced with Bachelor's vortex model as base flow.

The code was afterwards used to investigate the stability of trailing line vortex where the azimuthal component of the base flow was the one of Vatistas' vortex model. The stability of the linear modes (Kelvin's waves) was investigated for axisymmetric and asymmetric disturbances. Results for the temporal viscous unstable modes were provided. The influence of swirl parameter and Reynolds number on the growth rate, phase speed and amplitude, of the perturbations were studied.

Keywords: vortex model, Kelvin waves, stability analysis, pseudo-spectral method, trailing line vortex.

Acknowledgements

Firstly, I would like to extend my appreciation to my supervisor, Dr. George H. Vatistas for all the academic counseling and financial supports during the last year.

Indeed, the idea of developing a code for stability analysis originally came up by my co-supervisor Hamid Ait Abderrahmane. He firstly suggested building up a tool for viscous stability analysis. I wish present study would satisfactorily address the original objectives. I also appreciate all the assistance from Hossein, whenever he pointed out precious comments in developing the procedure. Also, my sincere thanks to Keoponnareay for peer review. The entire challenges in last year might have been overwhelming without her support.

I would like to acknowledge all the concerns and love I always received from my family. On the moment, I wish to visit our new family member; my nephew as well as the new house. To all of them, I dedicate this thesis, especially to my life supervisor;

‘’My BROTHER”

Table of Contents

List of Figures

Nomenclature

Latin Letters

F_i	Amplitude of travelling disturbance ($i = 1,2,3$)	
$\mathbf{i}$	Imaginary unit	$\mathbf{i}^2 = -1$
k	Axial wave number	real number
m	Azimuthal wave number	Integer
M	Number of collocation points	Pure number
p	Pressure	dimensionless
q	Vortex intensity	dimensionless
r	Radial distance	dimensionless
R	Radius of the region for truncating infinity	dimensionless
Re	Reynolds Number	
s	a- index of collocation point	
	b- displacement vector	
t	time	Sec
u	Radial component of velocity	Scalar
v	Azimuthal component of velocity	Scalar
$\boldsymbol{v}$	Velocity field	real vector
w	Axial component of velocity	Scalar

Greek Letters

Ω	Vorticity
Γ	a- Circulation
	b- Standard Chebychev basis with shifted indices

ρ	Density	Kg/m²
μ	Dynamic viscosity	Pa.sec
ν	Kinematic viscosity	m²/sec
ϕ_j	Weights of projection of F_1 on the subspace span$\{\boldsymbol{\Phi_j}\}$	Complex
$\boldsymbol{\Phi_j}$	Modified chebychev basis for radial coordinate	Functional
ψ_j	Weight of projection of F_2 on the subspace span$\{\boldsymbol{\Psi_j}\}$	Complex
$\boldsymbol{\Psi_j}$	Modified chebychev basis for azimuthal coordinate	Functional
$\boldsymbol{\omega}_\alpha$	Total growth rate, mode number α	Complex
ω_r	Growth Rate	Real
ω_i	Phase Speed	Real

Letter like symbols

$\mathbb{R}$	Real space
$\mathbb{C}$	Complex space
$\mathbb{K}$	Either Real or complex Space

Operators

$\boldsymbol{\nabla}$	gradient
$\boldsymbol{\nabla}\times$	Curl
Δ	Laplacian
∂	Partial derivative
L_{pq}	Left derivative operator in LPE $pq = 11,12,21,22$
R_{pq}	Right derivative operator in LPE $pq = 11,12,21,22$

Abbreviations

LPE	Linear Perturbation equation
TLV	Trailing Line Vortex
ODE	Ordinary Differential Equation
B.C.'s	Boundary Conditions
LHS	Left Hand Side (of equation)
RHS	Right Hand Side (of equation)

Subscripts

r, θ, z	Cylindrical coordinates
c	vortex core
M	Projection into the subspace
1	Radial coordinate
2	Azimuthal coordinate
∞	infinity

Accents

Bold	Vector
Uppercase	Base flow
lowercase	Total (Base+Disturbance)
Prime	Perturbation
Dot	Derivative respect to r
Star	Dimensional variable
Blank	Dimensionless

1. Background

1.1 Introduction

In this chapter, a brief introduction to the topic is provided beginning with inviscid vortex theory and then proceed with the initial argument published originally by Kelvin, which opened up the fascinating research area that deals with wave propagation in vortices. His approach has received enormous attention in aerodynamics and in general modern physics. Most of the fundamentals were explained in whole detail in the celebrated monograph of Saffman [1]. A Concrete illustration of this aspect can also be found in the Batchelor's classical textbook in fluid dynamics [2].

Swirling flow or so-called "Vortices" has been a dynamic field of research. Momentum is transferred from large to low scale. Vortices could also contain axial or radial flows such as bathtub vortex observed during drainage. Another important example of vortices is a paired of intense vortices that form the wake behind wingtips of airplanes. These are known to be very dangerous for smaller aircrafts flying closely thus limiting traffic in busy airports. Starting at each wingtip, this spiral flow evolves and ultimately transfers to a columnar single cell vortex. These trailing line vortices persist for long distances behind the flight path. They appear in a diverse range of incidence angle during take-off, landing or cruising at high altitudes. The drag generated by these wingtip vortices is considered to be one of the main causes of fuel inefficiency. Thus it is necessary to have a good insight of the phenomenon before venturing in understanding of vortex-dominant flows. In our opinion, rotating flow must be prioritized in numerical or experimental fluid dynamics, since it is the backbone of fluid motion as mentioned by Hermann Schlichting [3]. Furthermore, one needs a dependable insight of rotating flows in many practical cases such as retrofitting design parameters in aerospace or vortex chambers.

A concentrated vortex is an axisymmetric flow where the azimuthal component of the velocity field is much greater than the others. Jets are known to be a different type of axisymmetric flow where the axial velocity is significantly greater than other two. One can utilize asymptotical theory to draw an analogy between the stability of vortex and jets in a well-posed simulation. Taking advantage of this fact in section 3.2 where the boundary condition on the vortex centerline is assumed to be similar to what Batchelor and Gill proposed for high-speed jets [4].

A vortex is characterized by its intensity, and the core radius. We will classify vortex models in section 1.4. The core radius is the position of maximum azimuthal velocity. The vortex intensity is identified by a dimensionless variable called “q” (swirl parameter). The stability of vortex strongly depends on the swirl parameter. It was believed between researchers that a specified value should exist for swirl parameter for which the vortex is stabilized. However, the upper limit has been controversial for a while. Now it is agreed that a value of q=2.31 is the upper limit above which the inviscid Bachelor vortex becomes stable. In the case of viscous fluid this upper limit depends on the Reynolds number. The limit decreases with decreasing Reynolds number.

One is specifically interested in the stability of trailing line vortex, which appears on the wake of airplanes far from the trailing edge. The vortex developed enough and the swirling flow has a persistent columnar shape. In this case, the flow is not subjected to any external source of pressure field. Accordingly, the trailing line vortex is of unconfined columnar type. In this study, one is looking for the wave propagation inside an unconfined single cell columnar vortex. Our work parallels the approach of Khorrami [5].

The governing equations and the associated boundary conditions were discretized using the pseudo-spectral method where the Chebychev polynomials are the

basis functions [6]. The perturbation was in form of Fourier waves; as A. $e^{\mathrm{i}(kz+m\theta-\omega t)}$ and the results were evaluated for both axisymmetric and asymmetric disturbances. Axisymmetric disturbance corresponds to zero azimuthal wave number (m=0). It has been shown that this mode is not greatly influenced by viscous forces. The main instable modes are found to occur at high Reynolds swirling flow with mode (m=±1). For example, flow in a wind tunnel is the low Reynolds regime. Therefore, the major mode is expected to be of the asymmetric (m=±1) type as had been found experimentally by Maxworthy [7].

The main framework for three dimensional temporal stability was established by Duck [8] and also Lessen [9]. For the temporal stability, one look for the growth rate for a given axial and azimuthal wavenumber (k, and m). In an opposite way, spatial analysis is carried out through computing axial wave number (k) for a fixed azimuthal wavenumber and growth rate (m, and ω). In this analysis, the former case was considered.

Pedley *et al.* simulated rotating pipe flow and confirmed the main mode in results is asymmetric for m=+1 [10]. Their results were presented in terms of Rossby number, which is a common dimensionless parameter in confined vortices. Maslowe validated the results with experiments [11]. Despite the persistency of asymmetric disturbances in a rotating pipe, only the axisymmetric mode (m=0) is recognized to withstand on the trailing line vortex.

This is attributed to the small order of Reynolds number in the experimental work. However, on the wake of airplanes the flow has larger Reynolds number and therefore the viscous effects are minor. Consequently, only the axisymmetric disturbance is more likely to sustain in the well-developed section of trailing line vortex. The results

are presented in chapter 5 for two case studies of axisymmetric and asymmetric disturbances. The major difference between them was extensively discussed.

Besides the controversial issues in finding the more stable type of disturbance, it has been noted by Khorrami that the effect of viscosity must be encountered in any stability analysis of vortex flow [5]. He computed the results for axisymmetric and asymmetric disturbances, and compared his results with Lessen and Duck. He also traced the effect of Reynolds number, and concluded that viscous forces affect the asymmetric disturbances but they do not influence the axisymmetric. In this study, the effect of viscous forces on the amplification rate was also studied, however only for asymmetric disturbance. In our work the polynomial basis proposed in Mao was used [12].

The fundamentals were briefly mentioned in the first chapter. The presentation proceeds with the analytical viscous stability in chapter 2 and applied numerical method in chapter 3. They contain every aspect in the establishment of the numerical algorithm except the principals required for deriving the polynomial basis. Apparently, those could be determined through recombining standard Chebychev basis, which is completely an advanced topic in functional analysis and therefore out of our scope. The printed transcript of present procedure was also attached.

In chapter 4, the method was confirmed by comparing the results with previous studies. Ultimately, the results were presented in chapter 5 for two cases; axisymmetric and asymmetric disturbance. A qualitative assessment of the influence of swirl quantity on the wave packets was also provided. The results in chapter 5 also contain the impact of Reynolds number on the growth rate. The last results consist of topographies of instability for asymmetric disturbance.

1.2 Vorticity and Kelvin's theorem

Mathematically, the vorticity field is defined as the curl of the velocity field:

$$\boldsymbol{\Omega}^* = \boldsymbol{\nabla} \times \boldsymbol{V}^* \tag{1-1}$$

This can be expanded in cylindrical coordinates as the relation between the vorticity components (${\Omega_r}^*, {\Omega_\theta}^*, {\Omega_z}^*$) and the velocity components (U^*, V^*, W^*):

$${\Omega_r}^* = \frac{1}{r^*}\frac{\partial W^*}{\partial \bar{\theta}} - \frac{\partial V^*}{\partial z^*}, \quad {\Omega_\theta}^* = \frac{\partial U^*}{\partial z^*} - \frac{\partial W^*}{\partial r^*}, \quad {\Omega_z}^* = \frac{1}{r^*}\left(\frac{\partial (r^* V^*)}{\partial r^*} - \frac{\partial U^*}{\partial \theta^*}\right) \tag{1-2}$$

Conservation of momentum for incompressible flow in cylindrical coordinates is:

$$\rho \frac{\partial \boldsymbol{V}^*}{\partial t} + \rho \boldsymbol{V}^*.\boldsymbol{\nabla}\boldsymbol{V}^* = -\boldsymbol{\nabla}\mathrm{P}^* + \mu \Delta \boldsymbol{V}^* \tag{1-3}$$

Rate of increase of momentum at P	Net flow rate of momentum	Net pressure force	Net viscous force

The equations of motions can also be reformatted in terms of vorticity. Applying the curl operator, the momentum equation for Newtonian fluid with uniform density can be expressed by following equation, which is again is in Eulerian form:

$$\rho \frac{\partial \boldsymbol{\Omega}^*}{\partial t} + \rho \boldsymbol{V}^*.\boldsymbol{\nabla}\boldsymbol{\Omega}^* = \rho \boldsymbol{\Omega}^*.\boldsymbol{\nabla}\boldsymbol{V}^* + \mu \Delta \boldsymbol{\Omega}^* \tag{1-4}$$

Rate of increase of vorticity	Net flow rate of vorticity	Vortex stretching	Viscous diffusion

Note that $\boldsymbol{\nabla} \times \boldsymbol{\nabla} P^*$ is evidently zero for any conservative pressure field. Both velocity and vorticity are vector functions and can be localised in any point with coordinates $\boldsymbol{x} = (x, y, z)$. Equation (1-1) enables us evaluating the vorticity from velocity field. Conversely, it is also possible to compute velocity by using Biot-Savart law in $\mathbb{R}^3$:

$$\boldsymbol{V}^*(\boldsymbol{z}) = -\frac{\mathbf{1}}{\mathbf{4\pi}}\int_{\mathbb{R}^3}\frac{(\boldsymbol{x}-\tilde{\boldsymbol{x}})\times\boldsymbol{\Omega}^*(\tilde{\boldsymbol{x}})}{\|\boldsymbol{x}-\tilde{\boldsymbol{x}}\|^3}\boldsymbol{d\tilde{x}} \tag{1-5}$$

Where $\tilde{\boldsymbol{x}}$ an integration variable and the velocity field is defined in the complex space. The circulation Γ of flow is defined in a confined loop C as below:

$$\Gamma = \oint_C \mathbf{V}^*.\mathrm{d}\mathbf{s} \tag{1-6}$$

Therefore, it can be seen as the work done by velocity over a closed curve. The vortex motion was firstly formulated by Kelvin when he proposed his well-known theorem about conservation of circulation in fluid flow:

$$\frac{\mathrm{D}\Gamma}{\mathrm{D}t} = \nu\int_C (\Delta\mathbf{V}^*).\mathrm{d}\mathbf{s} \tag{1-7}$$

Where $\frac{D\Gamma}{Dt} = \frac{\partial\Gamma}{\partial t} + \boldsymbol{V}^*.\boldsymbol{\nabla}\Gamma$ and ν is kinematic viscosity. For inviscid flow, this equation could be simplified and deducted to common Helmholtz law in conservation of circulation [13].

1.3 Trailing line vortex

The mechanism of having a pair of wingtip vortex is simply caused by the difference in the pressure fields on top and bottom surfaces of wing. The high-pressure flow under the wing moves towards the top surface where the pressure is lower. This phenomenon generates a strong swirling flow at the wingtip, which is known to reduce the flight efficiency by adding the so-called induced drag. The evolution of wingtip vortex is schematically illustrated below.

These vortices obviously dissipate energy and increase total drag imposed on the aircraft. Knowing the fact that the entire aerodynamic design aims to reduce the drag as much as possible, it becomes even more important to know how they could be possibly removed. This requires proposing a reasonable condition that explicitly determines the stability or instability of the vortex. Considering a single TLV, this stability condition should be well defined in terms of fluid mechanics of a developed concentrated columnar vortex. Consequently, one should look for it as a function of major physical parameters describing the phenomenon. Regarding the vital role of swirl parameter in any q-vortex model directs us to comprehend the main idea behind the stability analysis in practice.

Broadly speaking, any stability analysis in fluid mechanics simply provides a meaningful criterion for toggling into or away from the stable flow regime which can be used in another design level. For our case, it is usually demanded to make the wingtip vortices destabilized and chaotic in order to attenuate the induced drag. As mentioned before, the criterion here is reasonably the swirl parameter. A reliable threshold for vortex stability based on “q” can contribute to address fundamental questions in aerodynamics like “how does the geometry of wingtip possibly reduce the induced drag and as a result improve the fuel efficiency?” However, it is obvious that other aspects of

this puzzle must be treated as well, for example, knowing the effect of wingtip geometry on the swirl strength of trailing vortex.

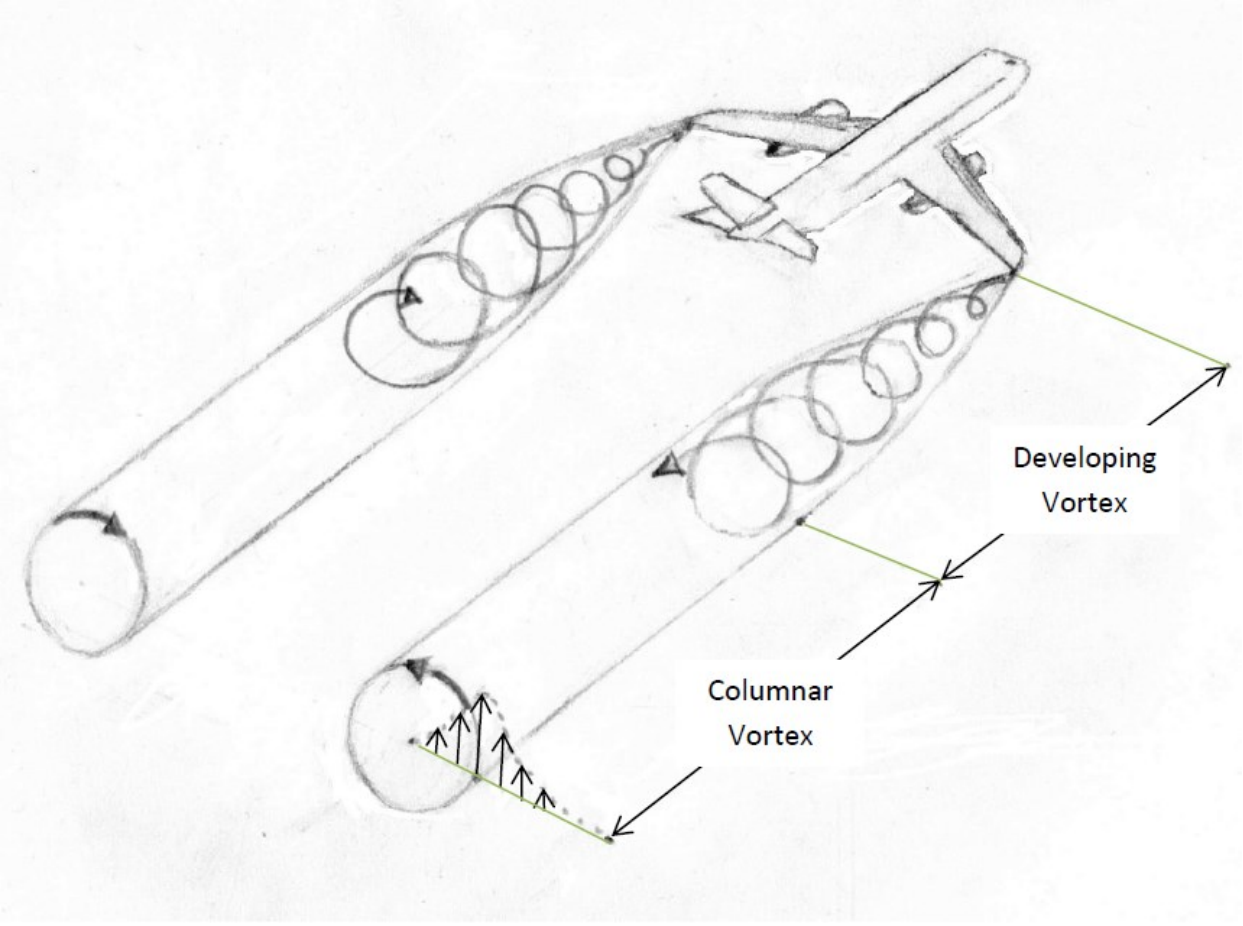

Figure 1-1 Trailing line vortex

1.4 Vortex models

In inviscid flow theory, vortex region is idealized as vortex sheets, filaments or point vortices. The simplest of all models for vortices is point-vortex model. Helmholtz established the fundamental of vortex dynamics by introducing point vortex model for inviscid incompressible swirling flow [14]. Point vortex model is applicable in ideal simulations such as in the flow of superfluid helium where a pattern of individual vortices are distinguishable and could be acceptably considered as being one dimensional. The topic of quantized vortex pattern in helium was reviewed thoroughly by Donnelly [15]. The Introductory paper by Hasimoto contains more details for the point vortex model [16].

However, such ideal models are not applicable to the current study. Stability analysis of vortices requires incorporating the base flow for columnar line vortex with axial flow, thus restricting the selection to the available vortex models.

In any incompressible vortex model, a set of dimensionless velocity components (U,V,W) in cylindrical coordinates must satisfy the axisymmetric Navier-Stokes equations for Newtonian incompressible fluid under laminar steady condition. Accordingly;

$$U\frac{\partial U}{\partial r}+W\frac{\partial U}{\partial z}-\frac{V^2}{r}=-\frac{\partial \mathrm{P}}{\partial r}+\frac{1}{\mathrm{Re}}\left(\frac{\partial^2 U}{\partial r^2}+\frac{1}{r}\frac{\partial U}{\partial r}+\frac{\partial^2 U}{\partial z^2}-\frac{U}{r^2}\right) \tag{1-8 a}$$

$$U\frac{\partial V}{\partial r}+W\frac{\partial V}{\partial z}+\frac{U.V}{r}=\frac{1}{\mathrm{Re}}\left(\frac{\partial^2 V}{\partial r^2}+\frac{1}{r}\frac{\partial V}{\partial r}+\frac{\partial^2 V}{\partial z^2}-\frac{V}{r^2}\right) \tag{1-8 b}$$

$$U\frac{\partial W}{\partial r}+W\frac{\partial W}{\partial z}=-\frac{\partial \mathrm{P}}{\partial z}+\frac{1}{\mathrm{Re}}\left(\frac{\partial^2 W}{\partial r^2}+\frac{1}{r}\frac{\partial W}{\partial r}+\frac{\partial^2 W}{\partial z^2}\right) \tag{1-8 c}$$

$$\frac{\partial U}{\partial r}+\frac{U}{r}+\frac{\partial W}{\partial z}=0 \tag{1-8 d}$$

Where all parameters became dimensionless regarding to the vortex core ($r_c{}^*$) and axial velocity at infinity ($W_\infty{}^*$) as shown below:

$$r = r^*/r_c{}^*$$

$$z = z^*/r_c{}^*$$

$$U = \frac{U^*}{W_\infty{}^*} \qquad Radial \ \ (r - direction)$$

$$V = \frac{V^*}{W_\infty{}^*} \qquad azimuthal \ \ (\theta - direction)$$

$$W = \frac{W^*}{W_\infty{}^*} \qquad axial \ \ (z - direction)$$

$$\mathrm{P} = \frac{\mathrm{P}^* - \mathrm{P}_\infty{}^*}{\rho {W_\infty{}^*}^2}$$

$$\mathrm{Re} = \frac{W_\infty{}^* . r_c{}^*}{\nu}$$

One can look at dimensionless parameters above and discover the fact that the definition of Reynolds number in equation (1-8) relies essentially on an unchangeable $r_c{}^*$. Note that the vortex core $r_c{}^*$ is the radial location of the maximum azimuthal velocity. It is indeed an indicator of the effective zone of rotating flow. Far downstream, where the trailing vortex is well developed, the core size could reasonably accepted to be constant. Consequently, the core radius is invariable for an adequately developed swirling flow regime behind the airplane and one can use it as "a priori" in the dimensionless equations. Thus, our analysis is necessarily limited to the developed region of trailing line vortex.

Azimuthal velocity is predominant in a swirling flow of this kind, and one can conclusively omit any term in the momentum equations that does not contain "V". In addition; the columnar flow assumption retrieves the independency of all variables to the axial dimension (i.e. $\frac{\partial}{\partial z} = 0$).

Therefore, equations (1-8) could then be reduced to:

$$\frac{V^2}{r} = \frac{d\mathrm{P}}{dr} \tag{1-9 a}$$

$$\frac{U}{r}\frac{d(rV)}{dr} = \frac{1}{\mathrm{Re}}\frac{d}{dr}\left(\frac{1}{r}\frac{d}{dr}(rV)\right) \tag{1-9 b}$$

$$\frac{\partial U}{\partial r} + \frac{U}{r} + \frac{\partial W}{\partial z} = 0 \tag{1-9 c}$$

Furthermore, any model should be capable of interpolating the experimental profile of the azimuthal velocity component. Fortunately, several simple (and sometimes empirical) models have been proposed to approximate well the experimental values of the velocity field and pressure distribution. The most presently popular are those of: Rankine, Scully, Sullivan, Taylor, Bachelor, Burger, Lamb-Oseen and Vatistas. The tabulated velocity components, static pressure and vorticity for some models were provided in Table 1-1 in non-dimensional form [17]:

Table 1-1

Quantity	Radial Velocity		Azimuthal Velocity	Axial Velocity	Pressure	Vorticity
Variable	$U = \frac{U^*}{{W_\infty}^*}$		$V = \frac{V^*}{{W_\infty}^*}$	$W = \frac{W^*}{{W_\infty}^*}$	$\mathrm{P} = \frac{\mathrm{P}^* - {\mathrm{P}_\infty}^*}{\rho {W_\infty}^{*2}}$	$\Omega_z = \frac{{\Omega_z}^*}{({W_\infty}^*/{r_c}^*)}$
Rankine	$0 \le r \le 1$	0	$q.r$	$-kz$	$\frac{q^2.r^2}{2}$	2q
	$1 \le r \le \infty$	$f_n(r)$	$\frac{q}{r}$	$-\frac{1}{\mathrm{Re}}\frac{z}{r}\frac{d}{dr}(rf_n(r))$	$q^2\left(1 - \frac{1}{2r^2}\right)$	0
Burgers	$-2\alpha r$		$\frac{q}{r}(1 - e^{\alpha r^2})$	$4\alpha z$	$q^2\left(1 - \frac{\beta}{\alpha ln2}\right)$	$2q.\alpha.e^{-\alpha r^2}$
Vatistas	$n = 2$	$\frac{-6r^3}{1+r^4}$	$\frac{q.r}{\sqrt{1+r^4}}$	$\frac{24z.r^2}{(1+r^4)^2}$	$\frac{2}{\pi}tan^{-1}(r^2)$	$\frac{2q}{\sqrt{(1+r^2)^3}}$

Where $\alpha = 1.256$ and $\beta = \int_r^\infty \frac{1}{r^3}\left(1 - e^{-\alpha r^2}\right)^2 dr$

In all models, the dimensionless swirl parameter is defined by

$$q = \frac{{\Gamma_\infty}^*}{2\pi . {r_c}^* . {W_\infty}^*}$$

And ${\Gamma_\infty}^*$ is the asymptotical circulation of the velocity field in $r - \theta$ plane. Regarding to its definition in (1-6), it can be evaluated either from velocity:

$${\Gamma_\infty}^* = \oint_{C_\infty} \boldsymbol{V}^* . d\boldsymbol{s} = \lim_{r^* \to +\infty} \oint_{C_\infty} V^* . r^* d\theta = 2\pi \lim_{r^* \to +\infty} (r^* . V^*)$$

This directly determines the dimensionless swirl parameter in terms of dimensionless azimuthal velocity as $q = \lim_{r \to +\infty} (rV)$. All models given in Table 1-1, share these features:

- Maximum azimuthal velocity should be located on the unit core radius (i.e. $r = 1$)
- $\lim_{r \to +\infty} (rV) = q$ Which means that all the models asymptotically act as irrotational vortex $r \to \infty; V \to \frac{q}{r}$.
- $\lim_{r \to 0} \left(\frac{V}{r}\right) = q$ or equivalently $r \to 0;\ V \to q . r$ (i.e. forced vortex).

It is crucial to know that all vortex models are solutions to the simplified Navier-Stokes equations and continuity. Since the system of equations that describes these vortices is underdetermined, their formulation starts by presuming a velocity profile and other flow parameters are obtained by the solution of the set.

The simplest and the oldest model is due to Rankine. It assumes a solid body rotation in the vortex core, and a potential flow outside the core. The maximum velocity occurs at the core radius. Burgers model is considered to match better than Rankine's to the empirical tangential velocity near the core. However, it carries additional complication in evaluating pressure drop on the vortex axis. In this study, the azimuthal component of vortex model proposed by Vatistas was used, which is known to agree well with the experimental results. Moreover, it does not have the complexities encountered

in Burger's model about computing the new parameter β. Instead, it results into an explicit formulation for pressure distribution inside the vortex core.

The radial variations of azimuthal velocity for common vortex models are presented in Figure 1-2 below [18].

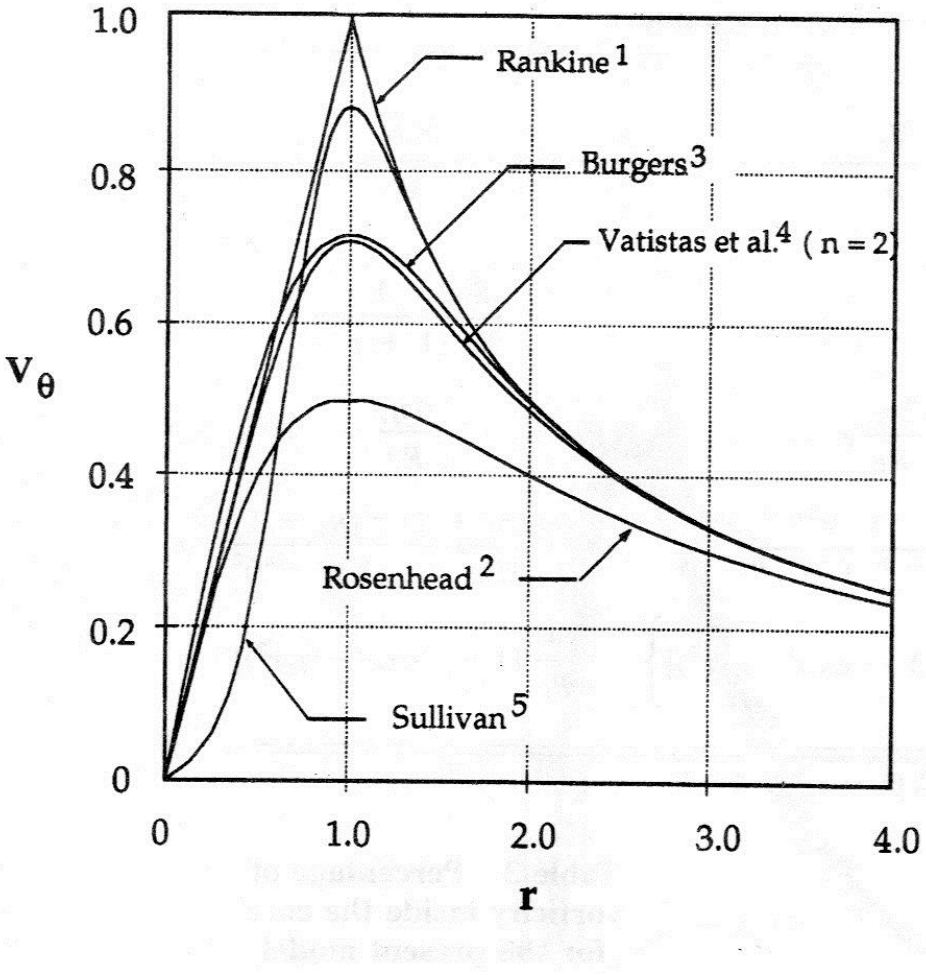

Figure 1-2 Comparison of different viscous vortex models, [18]

1.5 Waves inside vortices

Disturbances transmit throughout the flow region as travelling waves. These waves, commonly called Kelvin waves, are neutrally oscillatory and most of the time damped. Nevertheless, they are sometimes stable enough to be called solitons, which usually lead to abrupt instability and vortex breakdown as well as accompanying enlargement, stretching and dissipation [16].

These waves were discovered theoretically by Lord Kelvin during his attempt for developing the theory of vortex atoms [19]. He imposed Rankine's vortex model to three dimensional perturbation and derived the dispersion relation as below:

$$\frac{(m\Omega^2+\omega)^2}{4\Omega^2-\mathrm{g}^2}\left[\frac{\beta r_c J_{|m|}'(\beta r_c)}{J_{|m|}(\beta r_c)}+\frac{2m\Omega}{g}\right]=-|k|r_c\frac{K_{|m|}'(|k|r_c)}{K_{|m|}(|k|r_c)} \qquad (1\text{-}10)$$

With $\beta^2=\frac{k^2(4\Omega^2-g^2)}{g^2}$ and $g=m\Omega+\omega$. Where $J_{(m)}$ and $K_{(m)}$ are respectively the Bessel function and the modified Bessel function of order m [1]. Here, m=0 corresponds to axisymmetric mode and ω is the growth rate.

The presence of these waves in the vortex core was experimentally confirmed by Maxworthy [7]. Melander et al. also observed Kelvin on trailing line vortices in turbulent regimes [20].

Kelvin was apparently motivated in waves on the vortex core for developing his vortex ring model on an entirely different topic; to explain matter at the atomic level. While his approach missed the chance to receive attention in 19th century, recently his approach seems to be applicable in revealing intriguing notions in modern physics, particularly in string theory [21].

1.6 Stability analysis of vortices

The main idea of stability analysis in swirling flows is the interaction between vortices and waves. The approach is established by determining a steady state solution, which is called base flow and the stability is checked through a study of eigensolutions of the linearized perturbation equation. Indeed, stability analysis is significantly more elaborative than providing the base flow.

A body of works in recent years was restricted to Bachelor's trailing vortex. Martin Lessen firstly calculated both inviscid and viscous stability of wave modes with numerical shooting method [9]. (Duck & Pedley). On the moment, reference to the PhD thesis by K. Duraisamy for the most dependable studies in wingtip vortices [22] is made.

The most significant publication are those by Leibovich *et al.* [23] . They studied the interaction of vortex break down and unstable Kelvin waves. Moreover, they proposed a stability criteria by considering maximum strain energy and asymptotical theory [24]. Maxworthy *et al.* [7] investigated wave motions in vortex core experimentally and validated dispersion theory of solitary waves in Burger's vortex model. Lessen *et al.* implemented the first viscous stability analysis by introducing three dimensional perturbation into the base flow [9]. Extensive viscous stability analysis is available for Scully model in Khorrami [5] as well as Batchelor vortex model in Fabre and Mao [25], [12].

In the present study, the same analysis for a vortex having an azimuthal velocity from Vatistas vortex model (n=2) is applied. Selecting appropriate value for n can produce either Rankine's ($n \to \infty$) or Scully's ($n = 1$) vortices. For several practical reasons, the most widely used member of the set is the $n = 2$ (a close approximation to Oseen-Lamb and Burgers vortices), [26]. Vatistas model was found by several

researcher more suitable in describing experimental results. For instance Bagai and Leishman [27] used the *n*-family model to describe of tip-vortices at helicopter rotor wakes. The Vatistas vortex model is found to describe well the strong vortex connecting the inlet to the ground in Jet engines operating near the ground [28]. To date there are over 70 publications (in scholarly journals, monograms, reports of major scientific centers, masters and doctoral theses, and patents) that cite the original contribution, and the list grows by the day. Due to several agreeable practical and mathematical properties it is expected that this vortex model and its extensions will eventually replace the widely cited classical Rankine, Oseen-Lamb, Burgers, and Scully vortex formulations.

2. Analytical Model for Viscous Stability Analysis of Vortex

2.1 Linearization of perturbation equation

Here, the general perturbation equation is derived. The momentum and conservation equations are used in cylindrical coordinates for the velocity and pressure fields. Starting point is the full Navier-Stokes and continuity equations for an incompressible Newtonian fluid [12]:

$$\partial_t \boldsymbol{v} + (\boldsymbol{v}.\boldsymbol{\nabla})\boldsymbol{V} = -\boldsymbol{\nabla}\mathrm{p} + \mathrm{Re}^{-1}\Delta\boldsymbol{v} \qquad \text{with} \qquad \boldsymbol{\nabla}.\boldsymbol{v} = 0 \qquad (2\text{-}1)$$

In this equation $\boldsymbol{v}(r,\theta,z;t) = (u,v,w)$ and $\mathrm{p}(r,\theta,z;t)$ are respectively dimensionless velocity and pressure fields in cylindrical coordinates; in a way that:

$u \rightarrow Radial \ \ (r-direction)$

$v \rightarrow azimuthal \ \ (\theta-direction)$

$w \rightarrow axial \ \ (z-direction)$

One can expand equation (2-1) as shown below;

$$\frac{\partial u}{\partial t} + u\frac{\partial u}{\partial r} + \frac{v}{r}\frac{\partial u}{\partial \theta} + w\frac{\partial u}{\partial z} - \frac{v^2}{r} = -\frac{\partial \mathrm{p}}{\partial r} + \frac{1}{\mathrm{Re}}\left(\frac{\partial^2 u}{\partial r^2} + \frac{1}{r}\frac{\partial u}{\partial r} + \frac{1}{r^2}\frac{\partial^2 u}{\partial \theta^2} + \frac{\partial^2 u}{\partial z^2} - \frac{u}{r^2} - \frac{2}{r^2}\frac{\partial v}{\partial \theta}\right) \qquad (2\text{-}2a)$$

$$\frac{\partial v}{\partial t} + u\frac{\partial v}{\partial r} + \frac{v}{r}\frac{\partial v}{\partial \theta} + w\frac{\partial v}{\partial z} - \frac{u.v}{r} = -\frac{1}{r}\frac{\partial \mathrm{p}}{\partial \theta} + \frac{1}{\mathrm{Re}}\left(\frac{\partial^2 v}{\partial r^2} + \frac{1}{r}\frac{\partial v}{\partial r} + \frac{1}{r^2}\frac{\partial^2 v}{\partial \theta^2} + \frac{\partial^2 v}{\partial z^2} + \frac{2}{r^2}\frac{\partial u}{\partial \theta} - \frac{v}{r^2}\right) \qquad (2\text{-}2\ \mathrm{b})$$

$$\frac{\partial w}{\partial t} + u\frac{\partial w}{\partial r} + \frac{v}{r}\frac{\partial w}{\partial \theta} + w\frac{\partial w}{\partial z} = -\frac{\partial \mathrm{p}}{\partial z} + \frac{1}{\mathrm{Re}}\left(\frac{\partial^2 w}{\partial r^2} + \frac{1}{r}\frac{\partial w}{\partial r} + \frac{1}{r^2}\frac{\partial^2 w}{\partial \theta^2} + \frac{\partial^2 w}{\partial z^2}\right) \qquad (2\text{-}2\ \mathrm{c})$$

$$\frac{\partial u}{\partial r} + \frac{u}{r} + \frac{1}{r}\frac{\partial v}{\partial \theta} + \frac{\partial w}{\partial z} = 0 \qquad (2\text{-}2\ \mathrm{d})$$

All quantities were made dimensionless with the scale of free stream axial velocity $W_\infty{}^*$, and a characteristic core radius $r_c{}^*$. The dimensionless pressure equals to

$(\mathrm{p}^* - \mathrm{p}_\infty{}^*)/\rho {W_\infty}^{*2}$, and the Reynolds number is defined as $\mathrm{Re} = {W_\infty}^* {r_c}^*/\nu$ where ν is the kinematic viscosity [29].

The velocity and pressure fields are written in the form:

$$u = U + u'$$

$$v = V + v'$$

$$w = W + w'$$

$$\mathrm{p} = \mathrm{P} + \mathrm{p}'$$

Where uppercase letters denote base flow variables for single cell vortex. For brevity, the base flow field by $\boldsymbol{V}(r) = (U, V, W)$ is designated. Thereby, the following closed form can be obtained [12]:

$$\partial_t \boldsymbol{v}' + (\boldsymbol{U}.\boldsymbol{\nabla})\boldsymbol{v}' + (\boldsymbol{v}'.\boldsymbol{\nabla})\boldsymbol{V} = -\boldsymbol{\nabla}\mathrm{p}' + \mathrm{Re}^{-1}\boldsymbol{\nabla}^2\boldsymbol{v}' \qquad \text{With} \qquad \boldsymbol{\nabla}.\boldsymbol{v}' = 0 \qquad (2\text{-}3)$$

$\boldsymbol{v}'(r, \theta, z; t) = (u', v', w')$ and $\mathrm{p}'(r, \theta, z; t)$ are the introduced disturbances which are asserted in flow field and one is interested to investigate their growth rate. that the velocity $\boldsymbol{V}(r) = (U, V, W)$ is only a function of radial distance. All the terms that include derivative of the base flow respect to azimuthal and axial coordinate (e.g. $\frac{\partial U}{\partial z}$, $\frac{\partial W}{\partial \theta}$, etc.) can be eliminated. Moreover, dropping the non-linear terms in (2-3) (e.g. $\frac{u'v'}{r}, u'\frac{\partial u'}{\partial r}, \frac{v'}{r}\frac{\partial u'}{\partial \theta}$, etc.) one reaches the "Linear Perturbation Equation", given by Eqs. (2-4) [29].

It is important to point out that eliminating these terms might not be necessarily a sound assumption. Especially when the initial perturbations raise enough to the extent that the second order terms in the perturbation equation become excessively large and so are no longer negligible. Thus, neglecting non-linear terms is only admissible for elementary growth of disturbances and right after they exceed a specified value the linear

form of the perturbation equation does not describe the dispersion of instabilities accurately.

$$\frac{\partial u'}{\partial t}+U\frac{\partial u'}{\partial r}+\frac{V}{r}\frac{\partial u'}{\partial \theta}+W\frac{\partial u'}{\partial z}+u'\frac{\partial U}{\partial r}-\frac{2Vv'}{r}= \tag{2-4 a}$$

$$-\frac{\partial \mathrm{p}'}{\partial r}+\frac{1}{\mathrm{Re}}\left(\frac{\partial^2 u'}{\partial r^2}+\frac{1}{r}\frac{\partial u'}{\partial r}+\frac{1}{r^2}\frac{\partial^2 u'}{\partial \theta^2}+\frac{\partial^2 u'}{\partial z^2}-\frac{u'}{r^2}-\frac{2}{r^2}\frac{\partial v'}{\partial \theta}\right)$$

$$\frac{\partial v'}{\partial t}+U\frac{\partial v'}{\partial r}+\frac{V}{r}\frac{\partial v'}{\partial \theta}+W\frac{\partial v'}{\partial z}+u'\frac{\partial V}{\partial r}+\frac{1}{r}(Uv'+Vu')= \tag{2-4 b}$$

$$-\frac{1}{r}\frac{\partial \mathrm{p}'}{\partial \theta}+\frac{1}{\mathrm{Re}}\left(\frac{\partial^2 v'}{\partial r^2}+\frac{1}{r}\frac{\partial v'}{\partial r}+\frac{1}{r^2}\frac{\partial^2 v'}{\partial \theta^2}+\frac{\partial^2 v'}{\partial z^2}+\frac{2}{r^2}\frac{\partial u'}{\partial \theta}-\frac{v'}{r^2}\right)$$

$$\frac{\partial w'}{\partial t}+U\frac{\partial w'}{\partial r}+\frac{V}{r}\frac{\partial w'}{\partial \theta}+W\frac{\partial w'}{\partial z}+u'\frac{\partial W}{\partial r}+w'\frac{\partial W}{\partial z}= \tag{2-4 c}$$

$$-\frac{\partial \mathrm{p}'}{\partial z}+\frac{1}{\mathrm{Re}}\left(\frac{\partial^2 w'}{\partial r^2}+\frac{1}{r}\frac{\partial w'}{\partial r}+\frac{1}{r^2}\frac{\partial^2 w'}{\partial \theta^2}+\frac{\partial^2 w'}{\partial z^2}\right)$$

$$\frac{\partial u'}{\partial r}+\frac{u'}{r}+\frac{1}{r}\frac{\partial v'}{\partial \theta}+\frac{\partial w'}{\partial z}=0 \tag{2-4 d}$$

It should be emphasized that here only considered the incompressible instability was considered. The unconfined single cell vortex is our interest. Radial distance varies from singular point at origin to infinity. However, only the region (0,R) where the value of R was sufficiently chosen to be the effective zone of vortex momentum was discretized. More precisely; 0<r<R is the region where the azimuthal component V is predominant. Many researchers authenticated the fact that neglecting velocity for r>R does work satisfactorily for a numerical modal analysis. Note that components (U,V,W) and P come out of base flow field defined by chosen vortex model and fulfill the equation (1-9) as well as all the conditions proposed in section (1-4). Hence, equation (2-4), which from now on is called “LPE”, is a system of ordinary differential equation with known coefficients

(all in terms of velocity and pressure fields proposed by base flow for vortex). It must be solved to determine the evolution of the imposed disturbance (u', v', w', p')[16].

2.2 Boundary conditions for LPE

The domain of axisymmetric flow is easily recognised to be (0,∞). Accordingly, should look for a sound assumptions in two districts; first, vortex centerline (r=0), and second, free stream (r→∞). Assuming an asymptotical correlation for the compatibility condition on the vortex core;

$$\lim_{r\to 0}\frac{\partial \boldsymbol{v}'}{\partial \theta}=0 \qquad (2\text{-}5)$$

Where $\boldsymbol{v}'(r,\theta,z;t)=(u',v',w')=u'\widehat{\mathbf{e}_\mathbf{r}}+v'\widehat{\mathbf{e}_\boldsymbol{\theta}}+w'\widehat{\mathbf{e}_\mathbf{z}}$ is the total perturbation velocity field. The compatibility equation (2-5) was originally proposed by Batchelor in order to perform stability analysis of high-speed jets [4]. This assumption assures about the smoothness of solution along the centerline. Indeed, it is a deduction of the general compatibility relation for the total velocity field. Knowing that all velocity components in base flow are independent of azimuthal direction [5]. yields:

$$\frac{\partial \boldsymbol{v}'}{\partial \theta}=\frac{\partial}{\partial \theta}\left(u'\widehat{\mathbf{e}_\mathbf{r}}+v'\widehat{\mathbf{e}_\boldsymbol{\theta}}+w'\widehat{\mathbf{e}_\mathbf{z}}\right)$$

Or

$$\lim_{r\to 0}\frac{\partial \boldsymbol{v}'}{\partial \theta}=\frac{\partial u'}{\partial \theta}\widehat{\mathbf{e}_\mathbf{r}}+u'\frac{d\widehat{\mathbf{e}_\mathbf{r}}}{d\theta}+\frac{\partial v'}{\partial \theta}\widehat{\mathbf{e}_\boldsymbol{\theta}}+v'\frac{d\widehat{\mathbf{e}_\boldsymbol{\theta}}}{\partial \theta}+\frac{\partial w'}{\partial \theta}\widehat{\mathbf{e}_\mathbf{z}}+w'\frac{d\widehat{\mathbf{e}_\mathbf{z}}}{\partial \theta}$$

But

$$\frac{d\widehat{\mathbf{e}_\mathbf{r}}}{d\theta}=\widehat{\mathbf{e}_\boldsymbol{\theta}} \qquad \frac{d\widehat{\mathbf{e}_\boldsymbol{\theta}}}{d\theta}=-\widehat{\mathbf{e}_\mathbf{r}} \qquad \frac{d\widehat{\mathbf{e}_\mathbf{z}}}{d\theta}=0$$

These allows us to refine the compatibility equation as a boundary condition on r=0 as;

$$\begin{cases} \left.\dfrac{\partial u'}{\partial \theta}\right|_{r=0} = v' \\ \left.\dfrac{\partial v'}{\partial \theta}\right|_{r=0} = -u' \\ \left.\dfrac{\partial w'}{\partial \theta}\right|_{r=0} = 0 \end{cases}$$ B.C.'s for LPE on the vortex centerline (2-6 a)

In temporal stability analysis, one looks for the growth rate of transient Kelvin waves. Therefore, only the transient solutions of LPE are involved. This is arithmetically equivalent to $u' = v' = w' = 0$ at free stream; or

$$\lim_{r\to\infty} u' = \lim_{r\to\infty} v' = \lim_{r\to\infty} w' = 0$$ B.C.'s for LPE on free stream (2-6 b)

2.3 Imposing spiral disturbance on LPE

Let us now introduce asymmetric (spiral) disturbance to equation (2-4), expressed in Fourier wave form:

$$\begin{aligned} u' &= F_1(r)e^{\mathbf{i}(kz+m\theta-\boldsymbol{\omega}t)} \\ v' &= F_2(r)e^{\mathbf{i}(kz+m\theta-\boldsymbol{\omega}t)} \\ w' &= F_3(r)e^{\mathbf{i}(kz+m\theta-\boldsymbol{\omega}t)} \\ \mathrm{p}' &= F_4(r)e^{\mathbf{i}(kz+m\theta-\boldsymbol{\omega}t)} \end{aligned} \qquad (2\text{-}7)$$

Where all variables are dimensionless. Parameter k is real and represents the wavenumber on the axial coordinate. The quantity m is an integer, known as the azimuthal direction wavenumber. The growth rate is directly related to the real part of the complex variable $\boldsymbol{\omega}$.

Without loss of generality, the problem could be restricted to positive values of k and q but negative m. It is worthy to note that in order to achieve to a much cleaner LPE, many authors in inviscid analysis displace the radial disturbance by a phase angle of $\frac{\pi}{2}$ (which equals multiplication by an imaginary unit). In the present study the viscous mode analysis, whereas all the disturbances were presumed to have the same phase angle was adopted.

Note that all variables F_1, F_2, F_3 and F_4 and also their derivatives are solely in terms of radial distance of the vortex core. These perturbations are then substituted into LPE equation (2-4) and yield a linear system of ordinary differential equations as (2-8);

$$-\boldsymbol{\omega}F_1 + UF_1^{\cdot} + \dot{U}F_1 + \mathbf{i}m\frac{V}{r}F_1 - \frac{2V}{r}F_2 + \mathbf{i}kWF_1 = \\ -\dot{F_4} + \frac{1}{\mathrm{Re}}\left(\ddot{F_1} + \frac{\dot{F_1}}{r} - (m^2+1)\frac{F_1}{r^2} - \mathbf{i}\frac{2m}{r^2}F_2 - k^2F_1\right) \quad (2\text{-}8\ a)$$

$$-\boldsymbol{\omega}F_2 + UF_2^{\cdot} + \dot{V}F_1 + \mathbf{i}m\frac{V}{r}F_2 + \frac{U}{r}F_2 + \frac{V}{r}F_1 + \mathbf{i}kWF_2 = \\ -\mathbf{i}\frac{m}{r}F_4 + \frac{1}{\mathrm{Re}}\left(\ddot{F_2} + \frac{\dot{F_2}}{r} - (m^2+1)\frac{F_2}{r^2} + \mathbf{i}\frac{2m}{r^2}F_1 - k^2F_2\right) \quad (2\text{-}8\ b)$$

$$-\boldsymbol{\omega}F_3 + UF_3^{\cdot} + \dot{W}F_1 + \mathbf{i}m\frac{V}{r}F_3 + \mathbf{i}kWF_3 = \\ -\mathbf{i}kF_4 + \frac{1}{\mathrm{Re}}\left(\ddot{F_3} + \frac{\dot{F_3}}{r} - m^2\frac{F_3}{r^2} - k^2F_3\right) \quad (2\text{-}8\ c)$$

$$F_1^{\cdot} + \frac{F_1}{r} + \mathbf{i}\frac{m}{r}F_2 + \mathbf{i}kF_3 = 0 \quad (2\text{-}8\ d)$$

Where dots denote derivatives with respect to r. One can eliminate F_3 and F_4 by an elaborative algebraic manipulation and obtain a 2×2 system of ordinary differential equations in terms of variables F_1 and F_2 which are respectively correspondent to the amplitudes of the traveling disturbance wave in the radial (u') and azimuthal (v') coordinates.

One then needs to find the solution of following eigenvalue problem:

$$\boldsymbol{\omega}\begin{bmatrix} L_{11} & L_{12} \\ L_{21} & L_{22} \end{bmatrix}\begin{bmatrix} F_1 \\ F_2 \end{bmatrix} = \begin{bmatrix} R_{11} & R_{12} \\ R_{21} & R_{22} \end{bmatrix}\begin{bmatrix} F_1 \\ F_2 \end{bmatrix} \quad (2\text{-}9)$$

Linear operators L_{11}, L_{12}, L_{21}, and L_{22} are defined as below [12]:

$$L_{11} = \mathrm{Re}\left[\frac{d^2}{dr^2} + \frac{1}{r}\frac{d}{dr} - \frac{1}{r^2} - k^2\right] \tag{2-10a}$$

$$L_{12} = \mathbf{i}m\mathrm{Re}\left[\frac{1}{r}\frac{d}{dr} - \frac{1}{r^2}\right] \tag{2-10b}$$

$$L_{21} = -\frac{\mathbf{i}m}{k^2}\left[\frac{1}{r}\frac{d}{dr} + \frac{1}{r^2}\right] \tag{2-10c}$$

$$L_{22} = 1 + \frac{m^2}{k^2 r^2} \tag{2-10d}$$

Operators R_{11}, R_{12}, R_{21}, and R_{22} could be specified identically but with more terms as;

$$R_{11} = \frac{d^4}{dr^4} + \frac{2}{r}\frac{d^3}{dr^3} - \left(\frac{3}{r^2} + f + k^2\right)\frac{d^2}{dr^2} + \left(\frac{3}{r^3} - \frac{f + k^2}{r} - \frac{df}{dr} + \mathbf{i}(k\frac{dW}{dr}\mathrm{Re})\right)\frac{d}{dr} - \frac{3}{r^4} + \frac{f + k^2}{r^2} - (\frac{df}{dr})\frac{1}{r} + k^2 f + \mathbf{i}(k\frac{d^2W}{dr^2}\mathrm{Re}) \tag{2-11 a}$$

$$R_{12} = \mathbf{i}\left[\frac{m}{r}\frac{d^3}{dr^3} - \frac{2m}{r^2}\frac{d^2}{dr^2} + \left(\frac{3m}{r^3} - \frac{fm}{r}\right)\frac{d}{dr} - \frac{3m}{r^4} + \frac{fm + 2k^2 m}{r^2} - \frac{m}{r}\frac{df}{dr} + \mathbf{i}\frac{2Vk^2\mathrm{Re}}{r}\right] \tag{2-11 b}$$

$$R_{21} = -\frac{\mathbf{i}}{k^2\mathrm{Re}}\left[\frac{m}{r}\frac{d^3}{dr^3} + \frac{2m}{r^2}\frac{d^2}{dr^2} - \left(\frac{m}{r^3} + \frac{fm}{r}\right)\frac{d}{dr} + \frac{m}{r^4} - \frac{fm + 2k^2 m}{r^2} + \mathbf{i}\left(mk\frac{dW}{dr}\mathrm{Re}\right)\frac{1}{r} - \mathbf{i}(k^2 E\mathrm{Re})\right] \tag{2-11 c}$$

$$R_{22} = \frac{1}{\mathrm{Re}}\left[\left(1 + \frac{m^2}{k^2 r^2}\right)\frac{d^2}{dr^2} + \left(\frac{1}{r} - \frac{m^2}{k^2 r^3}\right)\frac{d}{dr} + \left(\frac{m^2}{k^2}\right)\frac{1}{r^4} - \left(1 + f\frac{m^2}{k^2}\right)\frac{1}{r^2} - f\right] \tag{2-11 d}$$

Where $f = k^2 + \frac{m^2}{r^2} + \mathbf{i}kWRe + \mathbf{i}\frac{mVRe}{r}$ and $E = \frac{V}{r} + \frac{dV}{dr}$ [15].

For a particular radial distance, all the expressions in (2-10) and (2-11) act as linear derivatives: $a_4D^4 + a_3D^3 + a_2D^2 + a_1D + a_0$ whereas D is $\frac{d}{dr}$ and with the coefficients a_0, a_1, ... are only functions of r. As a result, one can initially derive their linear form for r and save it for computational efficiency.

Equation (2-9) which from now its solution is our major interest, is an LPE according to introducing a 3D disturbance into an axisymmetric incompressible viscous flow. It may be regarded as an eigenvalue problem and could be solved to determine the perturbation growth rate; $\boldsymbol{\omega}$ as well as amplitudes F_1 and F_2.

The Boundary conditions of LPE were defined in section 2.2 and here they should be consistently reconstructed in terms of amplitudes F_1 and F_2. Substitution of (2-7) back into the original B.C.'s yields:

$$\begin{cases} imF_1 = F_2 \\ imF_2 = -F_1 \end{cases}$$ B.C.'s for LPE on the vortex centerline (2-12 a)

It is obvious that amplitudes F_1 and F_2 are bounded and should be asymptotically vanished far from the vortex centerline, This is equivalent to the boundary condition at $r = \infty$ as below.

$$\lim_{r\to\infty} F_1 = \lim_{r\to\infty} F_2 = 0$$ B.C.'s for LPE on free stream (2-12 b)

Consequently, the azimuthal wave number (m) requires different B.C.'s on the vortex centerline. Only m=0 and m<-1 were considered, since the boundary condition for m=-1 was obscure. The boundary conditions are listed in Table 2-1.

Table 2-1

		Radial	Azimuthal
m=0	r=0	$F_1 = \ddot{F}_1 = 0$	$F_2 = 0$
	r=∞	$F_1 = \dot{F}_1 = 0$	$F_2 = 0$
m<-1	r=0	$F_1 = \dot{F}_1 = 0$	$F_2 = \ddot{F}_2 = 0$
	r=∞	$F_1 = \dot{F}_1 = 0$	$F_2 = \ddot{F}_2 = 0$

Our main objective is investigation of the viscous stability of trailing line vortex by solving equation (2-9). Unfortunately, the perturbation equation does not have a closed form solution. Therefore, it sounds inevitable resorting to an appropriate numerical technique. The numerical method was demonstrated in the following chapter.

3. Pseudo-spectral method with Chebychev basis

3.1 Discretizing LPE in Chebychev basis

3.1.1 Compiling LPE for Chebychev collocation method

The LPE, as its compact formulation presented in equation (2-9), is a Linear ODE system and must be solved for evaluating variables $F_1(r)$ and $F_2(r)$ in semi-infinite domain $0 < r < \infty$. In such a domain, it is common to incorporate the Chebychev polynomials.

First of all, the domain should be conformed for adopting Chebychev collocation method. The original domain $(0,\infty)$ is mapped to $(-1,1)$ by introducing new variable "y" as below:

$$y = \frac{2r}{R} - 1 \qquad (3\text{-}1)$$

The scaling quantity, R, provides a way for truncating infinity. As displayed in figure 1-2, the azimuthal velocity (V) clearly falls off outside the vortex core. The azimuthal component vanishes at a sufficiently large but finite radial distance. This distance was assumed to equal to 2.5 for axisymmetric and 7.5 for asymmetric mode. In this way, the boundary condition at infinity coincides with r=R.

The vortex centerline is characterized with y=-1, and the infinity with y=1 Then equation (2-9) changes to the following form:

$$\boldsymbol{\omega}\begin{bmatrix} L_{11} & L_{12} \\ L_{21} & L_{22} \end{bmatrix}\begin{bmatrix} F_1(y) \\ F_2(y) \end{bmatrix} = \begin{bmatrix} R_{11} & R_{12} \\ R_{21} & R_{22} \end{bmatrix}\begin{bmatrix} F_1(y) \\ F_2(y) \end{bmatrix} \qquad (3\text{-}2)$$

The LPE equation (2-9) is a 2×2 ODE system in $\mathbb{K}^2$ and could be projected to a subspace that roughly has the dimension $\mathbb{K}_M \times \mathbb{K}_M{}^*$. This region is constructed by orthogonal Chebychev basis function $\{\boldsymbol{\Phi}_n\}_{n=1}^{M}$ and $\{\boldsymbol{\Psi}_n\}_{n=1}^{M}$ which satisfy B.C.'s given in Table 3-1.

Table 3-1

		Radial	Azimuthal
m=0	y=-1	$\boldsymbol{\Phi}_i = 0 \quad \frac{d^2\boldsymbol{\Phi}_i}{dy^2} = 0$	$\boldsymbol{\Psi}_i = 0$
	y=1	$\boldsymbol{\Phi}_i = 0 \quad \frac{d\boldsymbol{\Phi}_i}{dy} = 0$	$\boldsymbol{\Psi}_i = 0$
m<-1	y=-1	$\boldsymbol{\Phi}_i = 0 \quad \frac{d\boldsymbol{\Phi}_i}{dy} = 0$	$\boldsymbol{\Psi}_i = 0 \quad \frac{d^2\boldsymbol{\Psi}_i}{dy^2} = 0$
	y=1	$\boldsymbol{\Phi}_i = 0 \quad \frac{d\boldsymbol{\Phi}_i}{dy} = 0$	$\boldsymbol{\Psi}_i = 0 \quad \frac{d^2\boldsymbol{\Psi}_i}{dy^2} = 0$

The standard Chebychev basis is defined with a recurrence formulation as:

$$\Gamma_1(y) = 1 \quad \Gamma_2(y) = y \quad \Gamma_{n\,(n>2)}(y) = 2\Gamma_{n-1}(y) - \Gamma_{n-2}(y) \qquad (3\text{-}3)$$

We intentionally shifted the index of the Chebychev basis by one unit, so the corresponding functions could be fed much easier into the program. Unfortunately, the properties of standard Chebychev basis do not match with the acquired characteristics in Table 3-1. Therefore, there is a need to recombine the standard basis in a way that they fulfill all the B.C.'s at y=±1. Here the modified basis proposed by Mao [12] was incorporated.

* is either the complex space or real space.

3.1.2 Modified chebychev basis for m=0

The modified Chebychev basis for discretizing the radial disturbance (i.e. $u = U + u';\ F_1$) is:

$\boldsymbol{\Phi_1} = \Gamma_1$

$\boldsymbol{\Phi_2} = \Gamma_2$

$\boldsymbol{\Phi_3} = \Gamma_3 - \Gamma_1$

$\boldsymbol{\Phi_4} = (\Gamma_4 - \Gamma_2) - 2(\Gamma_3 - \Gamma_1)$

$\boldsymbol{\Phi_{i\ (n>4,odd)}} = \Gamma_i - \Gamma_1 - \frac{1}{4}(i-1)^2(\Gamma_3 - \Gamma_1) + \frac{1}{96}[(i-1)^4 - 4(i-1)^2](\Gamma_4 - 2\Gamma_3 - \Gamma_2 + 2\Gamma_1)$

$\boldsymbol{\Phi_{i\ (n>4,even)}} = \Gamma_i - \Gamma_2 - \frac{1}{4}(i^2 - 2i)(\Gamma_3 - \Gamma_1) + \frac{1}{96}[-(i-1)^4 - 2(i-1)^2 + 3](\Gamma_4 - 2\Gamma_3 - \Gamma_2 + 2\Gamma_1)$

Then for $i > 4$, all terms simply satisfy $\boldsymbol{\Phi_i}(y = \pm 1) = \left.\frac{d^2\boldsymbol{\Phi_i}}{dy^2}\right|_{(y=-1)} = \left.\frac{d\boldsymbol{\Phi_i}}{dy}\right|_{(y=1)} = 0$

This enables to estimate the radial amplitude of emanating disturbance, F_1 on the subspace $\mathbb{K}_{M-4} = span\{\boldsymbol{\Phi_5}, \boldsymbol{\Phi_6}, \dots, \boldsymbol{\Phi_M}\}$. Similarly, the following basis for azimuthal disturbance (i.e. $v = V + v';\ F_2$) was used;

$\boldsymbol{\Psi_1} = \Gamma_1$

$\boldsymbol{\Psi_2} = \Gamma_2$

$\boldsymbol{\Psi_{i\ (n>2,odd)}} = \Gamma_i - \Gamma_1$

$\boldsymbol{\Psi_{i\ (n>2,even)}} = \Gamma_i - \Gamma_2$

Which satisfies $\boldsymbol{\Psi_{i(i>2)}}(y = \pm 1) = 0$

$M-4$-subsequent terms from this functional vector were taken in. Then, the corresponding subspace $\mathbb{K}_{M-4} = span\{\boldsymbol{\Psi_3}, \boldsymbol{\Psi_4}, \dots, \boldsymbol{\Psi_{M-2}}\}$ has the same dimension as the radial one.

3.1.3 Modified chebychev basis for m<-1

The radial disturbance was discretized with:

$\boldsymbol{\Phi_1} = \Gamma_1$

$\boldsymbol{\Phi_2} = \Gamma_2$

$\boldsymbol{\Phi_3} = \Gamma_3 - \Gamma_1$

$\boldsymbol{\Phi_4} = \Gamma_4 - \Gamma_2$

$\boldsymbol{\Phi_{i\,(n>4,odd)}} = \Gamma_i - \Gamma_1 - \frac{1}{4}(i-1)^2(\Gamma_3 - \Gamma_1)$

$\boldsymbol{\Phi_{i\,(n>4,even)}} = \Gamma_i - \Gamma_2 - \frac{1}{8}(i^2 - 2i)(\Gamma_4 - \Gamma_2)$

That for $i > 4$, satisfy $\boldsymbol{\Phi_i}(y = \pm 1) = \left.\frac{d\boldsymbol{\Phi_i}}{dy}\right|_{(y=\pm 1)} = 0$. This provides the subspace $\mathbb{K}_{M-4} = span\{\boldsymbol{\Phi_5}, \boldsymbol{\Phi_6}, \dots, \boldsymbol{\Phi_M}\}$ which could be used for approximating F_1.

For the azimuthal disturbance, we used:

$\boldsymbol{\Psi_1} = \Gamma_1$

$\boldsymbol{\Psi_2} = \Gamma_2$

$\boldsymbol{\Psi_3} = \Gamma_3 - \Gamma_1$

$\boldsymbol{\Psi_4} = \Gamma_4 - 6\Gamma_3 - \Gamma_2 + 6\Gamma_1$

$\boldsymbol{\Psi_{i\,(n>4,odd)}} = \Gamma_i - \Gamma_1 - \frac{1}{12}[(i-1)^4 - (i-1)^2](\Gamma_3 - \Gamma_1) - \frac{1}{96}[(i-1)^4 - 4(i-1)^2](\Gamma_4 - 6\Gamma_3 - \Gamma_2 + 6\Gamma_1)$

To fulfill the B.C.'s; $\boldsymbol{\Psi_{i(i>2)}}(y = \pm 1) = \left.\frac{d^2\boldsymbol{\Psi}_{i(i>4)}}{dy^2}\right|_{(y=\pm 1)} = 0$

Then, $M - 4$-subsequent terms from this functional vector make the subspace $\mathbb{K}_{M-4} = span\{\boldsymbol{\Psi_3}, \boldsymbol{\Psi_4}, \dots, \boldsymbol{\Psi_{M-2}}\}$ which has as same dimension as of the radial disturbance.

3.1.4 Discretizing operators and approximation of LPE

We suppose M-collocation nodes by incorporating Gauss-Lobatto points:

$$y_s = -\cos\left(\frac{(s-1)\pi}{M-1}\right) \qquad for \quad s = 1,2,\dots,M \tag{3-4}$$

In pseudo-spectral collocation method, one estimates $F_1(y)$ on the basis $\{\mathbf{\Phi}_n\}_{n=5}^{M}$ and F_2 on the basis $\{\mathbf{\Psi}_n\}_{n=3}^{M-2}$.*

$$F_{1M}(y) = \sum_{n=5}^{M} \phi_n \mathbf{\Phi}_n(y) \tag{3-5a}$$

$$F_{2M}(y) = \sum_{n=3}^{M-2} \psi_n \mathbf{\Psi}_n(y) \tag{3-5b}$$

One also needs to seek for the weight coefficients $(\phi_5, \phi_6, \dots, \phi_M)$ and $(\psi_3, \psi_4, \dots, \psi_{M-2})$ by implementing simultaneous solution of the eigenvalue system in equation (3-2) for roughly M times. Now, let see what happens for the amplitudes F_{1M} and F_{2M} locally (i.e. on each collocation point). Rewriting series expansions at each collocation point; gives:

$$F_{1M}(y_s) = \sum_{n=1}^{M} \phi_n \mathbf{\Phi}_n(y_s) \tag{3-6a}$$

$$F_{2M}(y_s) = \sum_{n=1}^{M-2} \psi_n \mathbf{\Psi}_n(y_s) \tag{3-6 b}$$

Any operator in (2-10) and (2-11) either L_{11}, L_{12}, L_{21}, and L_{22}or R_{11},R_{12},R_{21}, and R_{22} depends only on the radial location which is characterized by r_s or the corresponding variable y_s defined by mapping correlation (3-1). Thus, they appear as linear derivative

*Remind that
(1) F_1 and its mutual polynomial basis correspond to radial (i.e.) direction.
(2) F_2 and its mutual polynomial basis correspond to azimuthal (i.e.) direction.
(3)M is the order of polynomials, (i.e. number of the computing terms) in the modified chebychev series

operators with constant coefficients such as $a_4 \frac{d^4}{dr^4} + a_3 \frac{d^4}{dr^4} + \ \ldots$. Thus; it would be more precise to label them locally as $L_{11}\rfloor_{@y_s}$, $L_{12}\rfloor_{@y_s}$, … and $R_{11}\rfloor_{@y_s}$, $R_{12}\rfloor_{@y_s}$, … and so on. Substituting (3-5) into (3-2) yields the local LPE on each collocation point. Therefore, each collocation point exhibits a separate eigenvalue problem as:

$$\boldsymbol{\omega} \begin{bmatrix} L_{11}\rfloor_{@y_s} & L_{12}\rfloor_{@y_s} \\ L_{21}\rfloor_{@y_s} & L_{22}\rfloor_{@y_s} \end{bmatrix} \begin{bmatrix} F_{1M}(y) \\ F_{2M}(y) \end{bmatrix} = \begin{bmatrix} R_{11}\rfloor_{@y_s} & R_{12}\rfloor_{@y_s} \\ R_{21}\rfloor_{@y_s} & R_{22}\rfloor_{@y_s} \end{bmatrix} \begin{bmatrix} F_{1M}(y) \\ F_{2M}(y) \end{bmatrix} \qquad (3\text{-}7)$$

$$\mathrm{s} = 1,2,3,4, \ldots, \ell \quad (\ell \leq M)$$

One can look back into the definition of all operators in (2-10) and (2-11) for the maximum order of derivation and verify that only for $s \geq 3$ the system of equations represented by (3-7) could result in nontrivial answer. Furthermore, it is more desirable to deal with a square matrix, taking $\ell = M - 2$ in order to generate a compact form from the discretized LPE are as shown in equation (3-8) (see appendix A);

$$
\begin{bmatrix}
\begin{bmatrix}
L_{11}\{\boldsymbol{\Phi}_5(y)\}_{@y_3} & L_{11}\{\boldsymbol{\Phi}_6(y)\}_{@y_3} & \cdots & L_{11}\{\boldsymbol{\Phi}_M(y)\}_{@y_3} \\
L_{11}\{\boldsymbol{\Phi}_5(y)\}_{@y_4} & L_{11}\{\boldsymbol{\Phi}_6(y)\}_{@y_4} & \cdots & L_{11}\{\boldsymbol{\Phi}_M(y)\}_{@y_4} \\
\vdots & \vdots & \ddots & \vdots \\
L_{11}\{\boldsymbol{\Phi}_5(y)\}_{@y_{M-2}} & L_{11}\{\boldsymbol{\Phi}_6(y)\}_{@y_{M-2}} & \cdots & L_{11}\{\boldsymbol{\Phi}_M(y)\}_{@y_{M-2}}
\end{bmatrix}
\begin{bmatrix}
L_{12}\{\boldsymbol{\Psi}_3(y)\}_{@y_3} & L_{12}\{\boldsymbol{\Psi}_4(y)\}_{@y_3} & \cdots & L_{12}\{\boldsymbol{\Psi}_{M-2}(y)\}_{@y_3} \\
L_{12}\{\boldsymbol{\Psi}_3(y)\}_{@y_4} & L_{12}\{\boldsymbol{\Psi}_4(y)\}_{@y_4} & \cdots & L_{12}\{\boldsymbol{\Psi}_{M-2}(y)\}_{@y_4} \\
\vdots & \vdots & \ddots & \vdots \\
L_{12}\{\boldsymbol{\Psi}_3(y)\}_{@y_{M-2}} & L_{12}\{\boldsymbol{\Psi}_4(y)\}_{@y_{M-2}} & \cdots & L_{12}\{\boldsymbol{\Psi}_{M-2}(y)\}_{@y_{M-2}}
\end{bmatrix}
\\
\begin{bmatrix}
L_{21}\{\boldsymbol{\Phi}_5(y)\}_{@y_3} & L_{21}\{\boldsymbol{\Phi}_6(y)\}_{@y_3} & \cdots & L_{21}\{\boldsymbol{\Phi}_M(y)\}_{@y_3} \\
L_{21}\{\boldsymbol{\Phi}_5(y)\}_{@y_4} & L_{21}\{\boldsymbol{\Phi}_6(y)\}_{@y_4} & \cdots & L_{21}\{\boldsymbol{\Phi}_M(y)\}_{@y_4} \\
\vdots & \vdots & \ddots & \vdots \\
L_{21}\{\boldsymbol{\Phi}_5(y)\}_{@y_{M-2}} & L_{21}\{\boldsymbol{\Phi}_6(y)\}_{@y_{M-2}} & \cdots & L_{21}\{\boldsymbol{\Phi}_M(y)\}_{@y_{M-2}}
\end{bmatrix}
\begin{bmatrix}
L_{22}\{\boldsymbol{\Psi}_3(y)\}_{@y_3} & L_{22}\{\boldsymbol{\Psi}_4(y)\}_{@y_3} & \cdots & L_{22}\{\boldsymbol{\Psi}_{M-2}(y)\}_{@y_3} \\
L_{22}\{\boldsymbol{\Psi}_3(y)\}_{@y_4} & L_{22}\{\boldsymbol{\Psi}_4(y)\}_{@y_4} & \cdots & L_{22}\{\boldsymbol{\Psi}_{M-2}(y)\}_{@y_4} \\
\vdots & \vdots & \ddots & \vdots \\
L_{22}\{\boldsymbol{\Psi}_3(y)\}_{@y_{M-2}} & L_{22}\{\boldsymbol{\Psi}_4(y)\}_{@y_{M-2}} & \cdots & L_{22}\{\boldsymbol{\Psi}_{M-2}(y)\}_{@y_{M-2}}
\end{bmatrix}
\end{bmatrix}
\boldsymbol{\omega}
\begin{bmatrix}
\begin{bmatrix}
R_{11}\{\boldsymbol{\Phi}_5(y)\}_{@y_3} & R_{11}\{\boldsymbol{\Phi}_6(y)\}_{@y_3} & \cdots & R_{11}\{\boldsymbol{\Phi}_M(y)\}_{@y_3} \\
R_{11}\{\boldsymbol{\Phi}_5(y)\}_{@y_4} & R_{11}\{\boldsymbol{\Phi}_6(y)\}_{@y_4} & \cdots & R_{11}\{\boldsymbol{\Phi}_M(y)\}_{@y_4} \\
\vdots & \vdots & \ddots & \vdots \\
R_{11}\{\boldsymbol{\Phi}_5(y)\}_{@y_{M-2}} & R_{11}\{\boldsymbol{\Phi}_6(y)\}_{@y_{M-2}} & \cdots & R_{11}\{\boldsymbol{\Phi}_M(y)\}_{@y_{M-2}}
\end{bmatrix}
\begin{bmatrix}
R_{21}\{\boldsymbol{\Phi}_5(y)\}_{@y_3} & R_{21}\{\boldsymbol{\Phi}_6(y)\}_{@y_3} & \cdots & R_{21}\{\boldsymbol{\Phi}_M(y)\}_{@y_3} \\
R_{21}\{\boldsymbol{\Phi}_5(y)\}_{@y_4} & R_{21}\{\boldsymbol{\Phi}_6(y)\}_{@y_4} & \cdots & R_{21}\{\boldsymbol{\Phi}_M(y)\}_{@y_4} \\
\vdots & \vdots & \ddots & \vdots \\
R_{21}\{\boldsymbol{\Phi}_5(y)\}_{@y_{M-2}} & R_{21}\{\boldsymbol{\Phi}_6(y)\}_{@y_{M-2}} & \cdots & R_{21}\{\boldsymbol{\Phi}_M(y)\}_{@y_{M-2}}
\end{bmatrix}
\end{bmatrix}
=
\begin{bmatrix}
\begin{bmatrix}
R_{12}\{\boldsymbol{\Psi}_3(y)\}_{@y_3} & R_{12}\{\boldsymbol{\Psi}_4(y)\}_{@y_3} & \cdots & R_{12}\{\boldsymbol{\Psi}_{M-2}(y)\}_{@y_3} \\
R_{12}\{\boldsymbol{\Psi}_3(y)\}_{@y_4} & R_{12}\{\boldsymbol{\Psi}_4(y)\}_{@y_4} & \cdots & R_{12}\{\boldsymbol{\Psi}_{M-2}(y)\}_{@y_4} \\
\vdots & \vdots & \ddots & \vdots \\
R_{12}\{\boldsymbol{\Psi}_3(y)\}_{@y_{M-2}} & R_{12}\{\boldsymbol{\Psi}_4(y)\}_{@y_{M-2}} & \cdots & R_{12}\{\boldsymbol{\Psi}_{M-2}(y)\}_{@y_{M-2}}
\end{bmatrix}
\begin{bmatrix}
R_{22}\{\boldsymbol{\Psi}_3(y)\}_{@y_3} & R_{22}\{\boldsymbol{\Psi}_4(y)\}_{@y_3} & \cdots & R_{22}\{\boldsymbol{\Psi}_{M-2}(y)\}_{@y_3} \\
R_{22}\{\boldsymbol{\Psi}_3(y)\}_{@y_4} & R_{22}\{\boldsymbol{\Psi}_4(y)\}_{@y_4} & \cdots & R_{22}\{\boldsymbol{\Psi}_{M-2}(y)\}_{@y_4} \\
\vdots & \vdots & \ddots & \vdots \\
R_{22}\{\boldsymbol{\Psi}_3(y)\}_{@y_{M-2}} & R_{22}\{\boldsymbol{\Psi}_4(y)\}_{@y_{M-2}} & \cdots & R_{22}\{\boldsymbol{\Psi}_{M-2}(y)\}_{@y_{M-2}}
\end{bmatrix}
\end{bmatrix}
\begin{bmatrix}
\begin{bmatrix}
\phi_5 \\ \phi_6 \\ \vdots \\ \phi_M
\end{bmatrix}
\\
\begin{bmatrix}
\psi_3 \\ \psi_4 \\ \vdots \\ \psi_{M-2}
\end{bmatrix}
\end{bmatrix}
\tag{3-8}
$$

3.1.5 Evaluating the growth rate of the travelling waves

The growth rate can be found through eigenvalue analysis of the matrix of coefficients [D] in equation (3-8). It could be shown that a set of complex answers $\boldsymbol{\omega}_1$, $\boldsymbol{\omega}_2$, $\boldsymbol{\omega}_3$, …, $\boldsymbol{\omega}_{2M-8}$ exist as:

$$\{\boldsymbol{\omega}_{\boldsymbol{\alpha}}\}_{[1:(2M-8)]} = eig\{[D]\} = eig\{[L]^{-1}.[R]\} \qquad (3\text{-}9)$$

The original definition of perturbations in equation (2-7) simply reveals the fact that it is the real part of $\boldsymbol{\omega}$ that causes perturbations u', v',w' and p′ either amplify or attenuate in time. For more illustration, let us expand one of eigenvalues:

$$\boldsymbol{\omega}_{\alpha} = \omega_r + \mathbf{i}\omega_i$$

Substituting back into (2-7), gives:

$$\begin{aligned} u' &= F_1(r)e^{\mathbf{i}(kz+m\theta-(\omega_r+\mathbf{i}\omega_i)t)} \\ &= F_1(r)e^{(\omega_i t)}e^{\mathbf{i}(kz+m\theta-\omega_r t)} \\ \Longrightarrow \qquad \|u'\| &= \|F_1\|e^{(\omega_i t)} \qquad (3\text{-}10) \\ \angle u' &= (kz + m\theta + \angle F_1) - \omega_r t \end{aligned}$$

This shows that the perturbation will be amplified when $\omega_i > 0$ and decay if $\omega_i < 0$. The neutral stability is specified by $\omega_i = 0$. The unstable region, therefore, corresponds to a positive ω_i and that is where the instabilities are intensified with a quick exponential rate. On the other hand, a negative ω_i corresponds to a flow regime, which is capable of persisting over destabilizing sources. Accordingly, zero growth rate may be seen as threshold in transition from an unstable flow to a stable one.

The eigensolutions of equation (3-9) are a spectrum of complex quantities $\boldsymbol{\omega}_{\alpha}$s that each of them accompanies with the eigenvectors $[\phi_5, \phi_6, \dots, \phi_M]'$ and $[\psi_3,$

$\psi_4, \dots, \psi_{M-2}]'$. Then, the amplitudes of traveling disturbance waves (F_1, F_2, F_3, F_4) could be deduced either universally by (3-5) or locally by (3-6).

Thereon, the most tangible parameter for investigating the growth rate of disturbance is followed through selecting the maximum real part among the eigenvalues $\boldsymbol{\omega}_1$, $\boldsymbol{\omega}_2$, $\boldsymbol{\omega}_3$, …, $\boldsymbol{\omega}_{2M-8}$:

$$\omega = \max(real(eig\{[L]^{-1}.[R]\})) \qquad (3\text{-}11)$$

Which is the growth rate of the primary mode. Matrices [L] and [R] are the matrices of coefficients on LHS and RHS of equation (3-8). Likewise, the growth rate of secondary mode is evaluated by the second largest real part. In this way, successive modes do exist depending on the number of collocation points.

3.2 Demonstrating the numerical procedure

It was been shown in previous section that the concrete criterion for stability is the growth rate from (3-11). Hence, one needs primarily to build up the matrices of coefficients $[L]_{(2M-8)\times(2M-8)}$ and $[R]_{(2M-8)\times(2M-8)}$. Now let us introduce the vector $\widehat{\boldsymbol{L_{11}}}(\boldsymbol{y})$ as below:

$$\left\{\widehat{\boldsymbol{L_{11}}}(\boldsymbol{y})\right\}_{[1:M]} = [L_{11}\{\boldsymbol{\Phi}_1(y)\} \quad L_{11}\{\boldsymbol{\Phi}_2(y)\} \quad L_{11}\{\boldsymbol{\Phi}_3(y)\} \quad L_{11}\{\boldsymbol{\Phi}_4(y)\} \quad L_{11}\{\boldsymbol{\Phi}_5(y)\} \quad L_{11}\{\boldsymbol{\Phi}_6(y)\} \quad \cdots \quad L_{11}\{\boldsymbol{\Phi}_M(y)\}]$$

The idea could be developed in designating vectors $\widehat{\boldsymbol{L_{11}}}(\boldsymbol{y})$, $\widehat{\boldsymbol{L_{21}}}(\boldsymbol{y})$, $\widehat{\boldsymbol{L_{12}}}(\boldsymbol{y})$ and $\widehat{\boldsymbol{L_{22}}}(\boldsymbol{y})$; as below

$$\left\{\widehat{\boldsymbol{L_{11}}}(\boldsymbol{y})\right\}_{[1:M]} = [L_{11}\{\boldsymbol{\Phi}_1(y)\} \quad L_{11}\{\boldsymbol{\Phi}_2(y)\} \quad L_{11}\{\boldsymbol{\Phi}_3(y)\} \quad L_{11}\{\boldsymbol{\Phi}_4(y)\} \quad L_{11}\{\boldsymbol{\Phi}_5(y)\} \quad L_{11}\{\boldsymbol{\Phi}_6(y)\} \quad \cdots \quad L_{11}\{\boldsymbol{\Phi}_M(y)\}] \tag{3-12 a}$$

$$\left\{\widehat{\boldsymbol{L_{21}}}(\boldsymbol{y})\right\}_{[1:M]} = [L_{21}\{\boldsymbol{\Phi}_1(y)\} \quad L_{21}\{\boldsymbol{\Phi}_2(y)\} \quad L_{21}\{\boldsymbol{\Phi}_3(y)\} \quad L_{21}\{\boldsymbol{\Phi}_4(y)\} \quad L_{21}\{\boldsymbol{\Phi}_5(y)\} \quad L_{21}\{\boldsymbol{\Phi}_6(y)\} \quad \cdots \quad L_{21}\{\boldsymbol{\Phi}_M(y)\}] \tag{3-12 b}$$

$$\left\{\widehat{\boldsymbol{L_{12}}}(\boldsymbol{y})\right\}_{[1:M-2]} = [L_{12}\{\boldsymbol{\Psi}_1(y)\} \quad L_{12}\{\boldsymbol{\Psi}_2(y)\} \quad L_{12}\{\boldsymbol{\Psi}_3(y)\} \quad L_{12}\{\boldsymbol{\Psi}_4(y)\} \quad \cdots \quad L_{12}\{\boldsymbol{\Psi}_{M-2}(y)\}] \tag{3-12 c}$$

$$\left\{\widehat{\boldsymbol{L_{22}}}(\boldsymbol{y})\right\}_{[1:M-2]} = [L_{22}\{\boldsymbol{\Psi}_1(y)\} \quad L_{22}\{\boldsymbol{\Psi}_2(y)\} \quad L_{22}\{\boldsymbol{\Psi}_3(y)\} \quad L_{22}\{\boldsymbol{\Psi}_4(y)\} \quad \cdots \quad L_{22}\{\boldsymbol{\Psi}_{M-2}(y)\}] \tag{3-12 d}$$

Then, the LHS of equation (3-8) could be rewritten in a more concise form as:

$$[L]_{(2M-8)\times(2M-8)} = \begin{bmatrix} \begin{bmatrix} \left\{\widehat{\boldsymbol{L_{11}}}(\boldsymbol{y_3})\right\}_{[5:M]} \\ \left\{\widehat{\boldsymbol{L_{11}}}(\boldsymbol{y_4})\right\}_{[5:M]} \\ \vdots \\ \left\{\widehat{\boldsymbol{L_{11}}}(\boldsymbol{y_{M-2}})\right\}_{[5:M]} \end{bmatrix} & \begin{bmatrix} \left\{\widehat{\boldsymbol{L_{12}}}(\boldsymbol{y_3})\right\}_{[3:M-2]} \\ \left\{\widehat{\boldsymbol{L_{12}}}(\boldsymbol{y_4})\right\}_{[3:M-2]} \\ \vdots \\ \left\{\widehat{\boldsymbol{L_{12}}}(\boldsymbol{y_{M-2}})\right\}_{[3:M-2]} \end{bmatrix} \\ \begin{bmatrix} \left\{\widehat{\boldsymbol{L_{21}}}(\boldsymbol{y_3})\right\}_{[5:M]} \\ \left\{\widehat{\boldsymbol{L_{21}}}(\boldsymbol{y_4})\right\}_{[5:M]} \\ \vdots \\ \left\{\widehat{\boldsymbol{L_{21}}}(\boldsymbol{y_{M-2}})\right\}_{[5:M]} \end{bmatrix} & \begin{bmatrix} \left\{\widehat{\boldsymbol{L_{22}}}(\boldsymbol{y_3})\right\}_{[3:M-2]} \\ \left\{\widehat{\boldsymbol{L_{22}}}(\boldsymbol{y_4})\right\}_{[3:M-2]} \\ \vdots \\ \left\{\widehat{\boldsymbol{L_{22}}}(\boldsymbol{y_{M-2}})\right\}_{[3:M-2]} \end{bmatrix} \end{bmatrix} \tag{3-13}$$

Similar notation can also be used for operators in equation (2-11); providing four vectors $\widehat{\boldsymbol{R_{11}}}(\boldsymbol{y})$, $\widehat{\boldsymbol{R_{21}}}(\boldsymbol{y})$, $\widehat{\boldsymbol{R_{12}}}(\boldsymbol{y})$and $\widehat{\boldsymbol{R_{22}}}(\boldsymbol{y})$ as:

$$\left\{\widehat{\boldsymbol{R_{11}}}(\boldsymbol{y})\right\}_{[\mathbf{1}:\boldsymbol{M}]} = [R_{11}\{\boldsymbol{\Phi}_1(y)\} \quad R_{11}\{\boldsymbol{\Phi}_2(y)\} \quad R_{11}\{\boldsymbol{\Phi}_3(y)\} \quad R_{11}\{\boldsymbol{\Phi}_4(y)\} \quad R_{11}\{\boldsymbol{\Phi}_5(y)\} \quad R_{11}\{\boldsymbol{\Phi}_6(y)\} \quad \cdots \quad R_{11}\{\boldsymbol{\Phi}_M(y)\}] \tag{3-14 a}$$

$$\left\{\widehat{\boldsymbol{R_{21}}}(\boldsymbol{y})\right\}_{[\mathbf{1}:\boldsymbol{M}]} = [R_{21}\{\boldsymbol{\Phi}_1(y)\} \quad R_{21}\{\boldsymbol{\Phi}_2(y)\} \quad R_{21}\{\boldsymbol{\Phi}_3(y)\} \quad R_{21}\{\boldsymbol{\Phi}_4(y)\} \quad R_{21}\{\boldsymbol{\Phi}_5(y)\} \quad R_{21}\{\boldsymbol{\Phi}_6(y)\} \quad \cdots \quad R_{21}\{\boldsymbol{\Phi}_M(y)\}] \tag{3-14 b}$$

$$\left\{\widehat{\boldsymbol{R_{12}}}(\boldsymbol{y})\right\}_{[\mathbf{1}:\boldsymbol{M}-\mathbf{2}]} = [R_{12}\{\boldsymbol{\Psi}_1(y)\} \quad R_{12}\{\boldsymbol{\Psi}_2(y)\} \quad R_{12}\{\boldsymbol{\Psi}_3(y)\} \quad R_{12}\{\boldsymbol{\Psi}_4(y)\} \quad \cdots \quad R_{12}\{\boldsymbol{\Psi}_{M-2}(y)\}] \tag{3-14 c}$$

$$\left\{\widehat{\boldsymbol{R_{22}}}(\boldsymbol{y})\right\}_{[\mathbf{1}:\boldsymbol{M}-\mathbf{2}]} = [R_{22}\{\boldsymbol{\Psi}_1(y)\} \quad R_{22}\{\boldsymbol{\Psi}_2(y)\} \quad R_{22}\{\boldsymbol{\Psi}_3(y)\} \quad R_{22}\{\boldsymbol{\Psi}_4(y)\} \quad \cdots \quad R_{22}\{\boldsymbol{\Psi}_{M-2}(y)\}] \tag{3-14 d}$$

Which simply let us reconfigure the RHS in equation (3-8) as below;

$$[R]_{(2M-8)\times(2M-8)} = \begin{bmatrix} \begin{bmatrix} \left\{\widehat{\boldsymbol{R_{11}}}(\boldsymbol{y_3})\right\}_{[\mathbf{5}:\boldsymbol{M}]} \\ \left\{\widehat{\boldsymbol{R_{11}}}(\boldsymbol{y_4})\right\}_{[\mathbf{5}:\boldsymbol{M}]} \\ \vdots \\ \left\{\widehat{\boldsymbol{R_{11}}}(\boldsymbol{y_{M-2}})\right\}_{[\mathbf{5}:\boldsymbol{M}]} \end{bmatrix} & \begin{bmatrix} \left\{\widehat{\boldsymbol{R_{12}}}(\boldsymbol{y_3})\right\}_{[\mathbf{3}:\boldsymbol{M}-\mathbf{2}]} \\ \left\{\widehat{\boldsymbol{R_{12}}}(\boldsymbol{y_4})\right\}_{[\mathbf{3}:\boldsymbol{M}-\mathbf{2}]} \\ \vdots \\ \left\{\widehat{\boldsymbol{R_{12}}}(\boldsymbol{y_{M-2}})\right\}_{[\mathbf{3}:\boldsymbol{M}-\mathbf{2}]} \end{bmatrix} \\ \begin{bmatrix} \left\{\widehat{\boldsymbol{R_{21}}}(\boldsymbol{y_3})\right\}_{[\mathbf{5}:\boldsymbol{M}]} \\ \left\{\widehat{\boldsymbol{R_{21}}}(\boldsymbol{y_4})\right\}_{[\mathbf{5}:\boldsymbol{M}]} \\ \vdots \\ \left\{\widehat{\boldsymbol{R_{21}}}(\boldsymbol{y_{M-2}})\right\}_{[\mathbf{5}:\boldsymbol{M}]} \end{bmatrix} & \begin{bmatrix} \left\{\widehat{\boldsymbol{R_{22}}}(\boldsymbol{y_3})\right\}_{[\mathbf{3}:\boldsymbol{M}-\mathbf{2}]} \\ \left\{\widehat{\boldsymbol{R_{22}}}(\boldsymbol{y_4})\right\}_{[\mathbf{3}:\boldsymbol{M}-\mathbf{2}]} \\ \vdots \\ \left\{\widehat{\boldsymbol{R_{22}}}(\boldsymbol{y_{M-2}})\right\}_{[\mathbf{3}:\boldsymbol{M}-\mathbf{2}]} \end{bmatrix} \end{bmatrix} \tag{3-15}$$

Ultimately, the discretized linear perturbation equation (or the approximation of LPE) receives a compact form as following:

$$\boldsymbol{\omega}[L]_{(2M-8)\times(2M-8)} \begin{bmatrix} \phi_5 \\ \phi_6 \\ \vdots \\ \phi_M \\ \psi_3 \\ \psi_4 \\ \vdots \\ \psi_{M-2} \end{bmatrix} = [R]_{(2M-8)\times(2M-8)} \begin{bmatrix} \phi_5 \\ \phi_6 \\ \vdots \\ \phi_M \\ \psi_3 \\ \psi_4 \\ \vdots \\ \psi_{M-2} \end{bmatrix} \tag{3-16}$$

The matrices of coefficients were intentionally arranged according to (3-13) and (3-15) to attain better computational performance. A subroutine that offers locally vectors $\widehat{\boldsymbol{L_{11}}}(\boldsymbol{y})$, $\widehat{\boldsymbol{L_{21}}}(\boldsymbol{y})$, ... $\widehat{\boldsymbol{L_{22}}}(\boldsymbol{y})$, and also $\widehat{\boldsymbol{R_{11}}}(\boldsymbol{y})$, $\widehat{\boldsymbol{R_{21}}}(\boldsymbol{y})$, ... $\widehat{\boldsymbol{R_{22}}}(\boldsymbol{y})$ as a function of base flow characteristics and the perturbation for a degree of precision was proposed. Such a subroutine should be considered as diagram below;

$$\begin{matrix} m \\ k \\ q \\ Re \\ M \\ y \end{matrix} \xrightarrow{f_1} \begin{matrix} \left\{\widehat{\boldsymbol{L_{11}}}(\boldsymbol{y})\right\}_{[\mathbf{1}:\boldsymbol{M}]} \\ \left\{\widehat{\boldsymbol{L_{21}}}(\boldsymbol{y})\right\}_{[\mathbf{1}:\boldsymbol{M}]} \\ \left\{\widehat{\boldsymbol{L_{12}}}(\boldsymbol{y})\right\}_{[\mathbf{1}:\boldsymbol{M}-\mathbf{2}]} \\ \left\{\widehat{\boldsymbol{L_{22}}}(\boldsymbol{y})\right\}_{[\mathbf{1}:\boldsymbol{M}-\mathbf{2}]} \end{matrix} \quad \& \quad \begin{matrix} \left\{\widehat{\boldsymbol{R_{11}}}(\boldsymbol{y})\right\}_{[\mathbf{1}:\boldsymbol{M}]} \\ \left\{\widehat{\boldsymbol{R_{21}}}(\boldsymbol{y})\right\}_{[\mathbf{1}:\boldsymbol{M}]} \\ \left\{\widehat{\boldsymbol{R_{12}}}(\boldsymbol{y})\right\}_{[\mathbf{1}:\boldsymbol{M}-\mathbf{2}]} \\ \left\{\widehat{\boldsymbol{R_{22}}}(\boldsymbol{y})\right\}_{[\mathbf{1}:\boldsymbol{M}-\mathbf{2}]} \end{matrix} \tag{3-17}$$

We shall continue now with a numerical example; by computing vector $\left\{\widehat{\boldsymbol{R_{12}}}(\boldsymbol{y_3})\right\}_{[\mathbf{1}:\mathbf{5}]}$:

$$\left\{\widehat{\boldsymbol{R_{12}}}(\boldsymbol{y})\right\}_{[\mathbf{1}:\mathbf{5}]} = [R_{12}\{\boldsymbol{\Psi}_1(y)\} \quad R_{12}\{\boldsymbol{\Psi}_2(y)\} \quad R_{12}\{\boldsymbol{\Psi}_3(y)\} \quad R_{12}\{\boldsymbol{\Psi}_4(y)\} \quad R_{12}\{\boldsymbol{\Psi}_5(y)\}]$$

The given quantities were summarized in Table 3-2

Table 3-2

$m = -2$	$k = 1.95$	$q = 0.7$	$Re = 1000$	$M = 7$	$R = 2.5$
$s = 3;\ \ y_3 = 0.5\ and\ r_3 = 1.875$					
Base Flow					
$U = 0$		$V = \frac{q}{r}\left(1 - e^{-r^2}\right)$		$W = e^{-r^2}$	
Radial (r-direction)		azimuthal (θ-direction)		axial (z-direction)	

More specifically; we are going to compute one of its arrays; $R_{12}\{\mathbf{\Psi}_4(y)\}$; at $y_3 = 0.5$ (i.e. $r_3 = 1.875$), where:

$$V = \frac{q}{r}\left(1 - e^{-r^2}\right) = 0.3622$$

$$W = e^{-r^2} = 0.0297 \tag{3-18}$$

$$\frac{dV}{dr} = \frac{-q\left(1 - e^{-r^2}\right)}{r^2} + 2qe^{-r^2} = -0.1516$$

From (2-11 b), the operator R_{12} is defined as:

$$R_{12} = \mathbf{i}\left[\frac{m}{r}\frac{d^3}{dr^3} - \frac{2m}{r^2}\frac{d^2}{dr^2} + \left(\frac{3m}{r^3} - \frac{fm}{r}\right)\frac{d}{dr} - \frac{3m}{r^4} + \frac{fm + 2k^2m}{r^2} - \frac{m}{r}\frac{df}{dr} + \mathbf{i}\frac{2Vk^2\mathrm{Re}}{r}\right] \tag{3-19}$$

Where

$$f = k^2 + \frac{m^2}{r^2} + \mathbf{i}kWRe + \mathbf{i}\frac{mVRe}{r} \tag{3-20 a}$$

$$\frac{df}{dr} = -\frac{2m^2}{r^3} + \mathbf{i}k\left(-2re^{-r^2}\right)Re + imRe\left(\frac{-2q\left(1 - e^{-r^2}\right)}{r^3} + \frac{2q}{r}e^{-r^2}\right) \tag{3-20 b}$$

Firstly, one needs to compute f and $\frac{df}{dr}$ via substituting (3-18) into (3-20):

$$f = 1.95^2 + \frac{(-2)^2}{1.875^2} + \mathbf{i}1.95 \times 0.029729 \times 1000 + \mathbf{i}\frac{(-2) \times 0.362234 \times 1000}{1.875} = 4.94 - 328.4\mathbf{i} \quad \text{(3-21 a)}$$

$$\frac{df}{dr} = -\frac{2(-2)^2}{1.875^3} + \mathbf{i} \times 1.95 \times \left(-2 \times 1.875e^{-r^2}\right)1000 + \mathbf{i}(-2)1000\left(\frac{-2 \times 0.7 \times \left(1 - e^{-1.875^2}\right)}{1.875^3} + \frac{2 \times 0.7}{1.875}e^{-1.875^2}\right) = -1.214 + 150.35\mathbf{i} \quad \text{(3-21 b)}$$

The modified Chebychev polynomial $\mathbf{\Psi}_4$ can be found for m=-2 and M=7 (see page 31);

$$\mathbf{\Psi}_4(y) = 4y^3 - 12y^2 - 4y + 12$$

that on $y_3 = 0.5$ results into

$$\mathbf{\Psi}_4(y_3) = [4y^3 - 12y^2 - 4y + 12]_{y=0.5} = 7.5 \quad \text{(3-22 a)}$$

$$\dot{\mathbf{\Psi}}_4(y_3) = [12y^2 - 24y - 4]_{y=0.5} = -13 \quad \text{(3-22 b)}$$

$$\ddot{\mathbf{\Psi}}_4(y_3) = [24y - 24]_{y=0.5} = -12 \quad \text{(3-22 c)}$$

$$\mathbf{\Psi}_4^{(3)}(y_3) = [24]_{y=0.5} = 24 \quad \text{(3-22 d)}$$

Knowing that $y = \frac{2r}{R} - 1$ gives: $\frac{d}{dr} = \frac{2}{R}\frac{d}{dy}$; $\frac{d^2}{dr^2} = \left(\frac{2}{R}\right)^2 . \frac{d^2}{dy^2}$; $\frac{d^3}{dr^3} = \left(\frac{2}{R}\right)^3 . \frac{d^3}{dy^3}$

it can then be used in equation (3-19) to obtain:

$$R_{12}\{\mathbf{\Psi}_4(y)\} = \mathbf{i}\left[\frac{m}{r}\left(\frac{2}{R}\right)^3 \frac{d^3\mathbf{\Psi}_4}{dy^3} - \frac{2m}{r^2}\left(\frac{2}{R}\right)^2 \frac{d^2\mathbf{\Psi}_4}{dy^2} + \left(\frac{3m}{r^3} - \frac{fm}{r}\right)\frac{2}{R}\frac{d\mathbf{\Psi}_4}{dy} + \left(-\frac{3m}{r^4} + \frac{fm + 2k^2m}{r^2} - \frac{m}{r}\frac{df}{dr} + \mathbf{i}\frac{2Vk^2\mathrm{Re}}{r}\right)\mathbf{\Psi}_4\right] \quad \text{(3-23)}$$

Two different approaches could be employed in evaluating above expression on the node, specified by s=3 where $y_3 = 0.5$ & $r_3 = 1.875$. We illustrate both of them on the next page.

Approach (I): One can directly substitute (3-21) and (3-22) into (3-23) and obtain:

$$R_{12}\{\boldsymbol{\Psi}_4(y)\}_{@y_3} = \mathbf{i}\left[\frac{m}{r}\left(\frac{2}{R}\right)^3 \boldsymbol{\Psi}_4{}^{(3)}(y_3) - \frac{2m}{r^2}\left(\frac{2}{R}\right)^2 \ddot{\boldsymbol{\Psi}}_4(y_3) + \left(\frac{3m}{r^3} - \frac{fm}{r}\right)\frac{2}{R}\dot{\boldsymbol{\Psi}}_4(y_3) + \left(-\frac{3m}{r^4} + \frac{fm + 2k^2m}{r^2} - \frac{m}{r}\frac{df}{dr} + \mathbf{i}\frac{2Vk^2\mathrm{Re}}{r}\right)\boldsymbol{\Psi}_4(y_3)\right]$$

$$= \mathbf{i}\left[\frac{-2}{1.875}\times\left(\frac{2}{2.5}\right)^3 \times 24 - \frac{2(-2)}{1.875^2}\times\left(\frac{2}{2.5}\right)^2 \times (-12) + \left(\frac{3(-2)}{1.875^3} - \frac{(4.94 - 328.4\mathbf{i})(-2)}{1.875}\right)\times\frac{2}{2.5}\times(-13) + \left(-\frac{3(-2)}{1.875^4} + \frac{(4.94 - 328.4\mathbf{i})(-2) + 2\times 1.95^2\times(-2)}{1.875^2} - \frac{(-2)}{1.875}(-1.214 + 150.35\mathbf{i}) + \mathbf{i}\frac{2\times 0.3622\times 1.95^2\times 1000}{1.875}\right)\times 7.5\right] = -17266.4 - 126.8\mathbf{i} \quad \text{(3-24 I)}$$

Approach (II) The operator could be expressed in polynomial form, be saved as the vector of coefficients and eventually been evaluated on the point s=3. (y=0.5):

$$R_{12}\{\boldsymbol{\Psi}_4(y)\}_{@y_3} = \mathbf{i}\left[\frac{m}{r}\left(\frac{2}{R}\right)^3 \boldsymbol{\Psi}_4{}^{(3)}(y) - \frac{2m}{r^2}\left(\frac{2}{R}\right)^2 \ddot{\boldsymbol{\Psi}}_4(y) + \left(\frac{3m}{r^3} - \frac{fm}{r}\right)\frac{2}{R}\dot{\boldsymbol{\Psi}}_4(y) + \left(-\frac{3m}{r^4} + \frac{fm + 2k^2m}{r^2} - \frac{m}{r}\frac{df}{dr} + \mathbf{i}\frac{2Vk^2\mathrm{Re}}{r}\right)\boldsymbol{\Psi}_4(y)\right]_{@y_3}$$

$$= \mathbf{i}\left[\frac{-2}{1.875}\times\left(\frac{2}{2.5}\right)^3 \times [24] - \frac{2(-2)}{1.875^2}\times\left(\frac{2}{2.5}\right)^2 \times [24y - 24] + \left(\frac{3(-2)}{1.875^3} - \frac{(4.94 - 328.41\mathbf{i})(-2)}{1.875}\right) \times\frac{2}{2.5}\times[12y^2 - 24y - 4] + \left(-\frac{3(-2)}{1.875^4} + \frac{(4.94 - 328.41\mathbf{i})(-2) + 2\times 1.95^2\times(-2)}{1.875^2} - \frac{(-2)}{1.875}(-1.214 + 150.352\mathbf{i}) + \mathbf{i}\frac{2\times 0.362234\times 1.95^2\times 1000}{1.875}\right)[4y^3 - 12y^2 - 4y + 12]\right]_{@y_3}$$

$$= [(-7265.7 - 31.8\mathbf{i})y^3 + (25160.1 + 137.2\mathbf{i})y^2 + (539.8 - 34.4\mathbf{i})y + (-22918.1 - 139.9\mathbf{i})]_{@y=0.5} = -17266.4 - 126.8\mathbf{i} \quad \text{(3-24 II)}$$

Both methods led to similar results, but approach (I) needs to have access to all values of $\boldsymbol{\Psi}_4(y_3)$,$\dot{\boldsymbol{\Psi}}_4(y_3)$,$\ddot{\boldsymbol{\Psi}}_4(y_3)$ and $\boldsymbol{\Psi}_4{}^{(3)}(y_3)$. If every arrays in the vector $\{\widehat{\boldsymbol{R_{12}}}(\boldsymbol{y_3})\}_{[1:5]}$ are considered then 5×4=20 extra variables would be required, which is equal to 20×3=60 for all the arrays $R_{12}\{\boldsymbol{\Psi}_j(y_s)\}, 3 \le j, s \le 5$. Regarding terms like $\frac{d^4}{dr^4}$ in every operator, approach (I) contains five extra matrices, that each has a dimension of

M^2, just to save all the quantities $\boldsymbol{\Psi}_j(y_s)$, $\dot{\boldsymbol{\Psi}}_j(y_s)$, $\ddot{\boldsymbol{\Psi}}_j(y_s)$, ${\boldsymbol{\Psi}_j}^{(3)}(y_s)$ and ${\boldsymbol{\Psi}_j}^{(4)}(y_s)$ $(1 \le j, s \le M)$.

In the same manner, unnecessary spaces shall be considered for all quantities $\boldsymbol{\Phi}_j(y_s)$, $\dot{\boldsymbol{\Phi}}_j(y_s)$, $\ddot{\boldsymbol{\Phi}}_j(y_s)$, ${\boldsymbol{\Phi}_j}^{(3)}(y_s)$ and ${\boldsymbol{\Phi}_j}^{(4)}(y_s)$ $(1 \le j, s \le M)$. This means that approach (I) needs 10M3 more space compared to approach (II); which in turn reveals the advantages of approach (II) in terms of computational cost.

In addition, the latter is more suitable for establishing a subroutine like (3-17). From (3-24 II):

$$R_{12}\{\boldsymbol{\Psi}_4(y)\} = (-7265.7 - 31.8\mathbf{i})y^3 + (25160.1 + 137.2\mathbf{i})y^2 + (539.8 - 34.4\mathbf{i})y + (-22918.1 - 139.9\mathbf{i})$$

$$= [0 \quad 0 \quad 0 \quad 0 \quad (-7265.7 - 31.8\mathbf{i}) \quad (25160.1 + 137.2\mathbf{i}) \quad (539.8 - 34.4\mathbf{i}) \quad (-22918.1 - 139.9\mathbf{i})] \begin{bmatrix} y^7 \\ y^6 \\ \vdots \\ y \\ 1 \end{bmatrix}$$

Similarly; $\boldsymbol{\Psi}_5(y) = 8y^4 - 8y^3 - 24y^2 + 8y + 16$ and the same approach gives:

$$R_{12}\{\boldsymbol{\Psi}_5(y)\}$$

$$= (-14531.4 - 63.6\mathbf{i})y^4 + (23499.2 + 175.2\mathbf{i})y^3 + (36868.4 + 176.9\mathbf{i})y^2 + (-27983.2 - 370.8\mathbf{i})y + (-26820.9 - 108\mathbf{i})$$

$$= [0 \quad 0 \quad 0 \quad (-14531.4 - 63.6\mathbf{i}) \quad (23499.2 + 175.2\mathbf{i}) \quad (36868.4 + 176.9\mathbf{i}) \quad (-27983.2 - 370.8\mathbf{i}) \quad (-26820.9 - 108\mathbf{i})] \begin{bmatrix} y^7 \\ y^6 \\ \vdots \\ y \\ 1 \end{bmatrix}$$

The concept can be generalized by expressing all terms $R_{12}\{\boldsymbol{\Psi}_j(y)\}, 1 \le j \le 5$ as polynomials of y and save all their coefficients in a medial matrix $\left[\mathcal{R}_{12}^{p}(j,l)\right]_{5\times 8}$. Each row in that matrix represents the coefficients of polynomials.

For example, in this case:

$[\mathcal{R}_{12}^{p}(j,l)]_{5\times 8}$ =

0	0	0	0	0	0	0	-1816.4-7.9**i**
0	0	0	0	0	0	-1816.4-7.9**i**	280.2+3.5**i**
0	0	0	0	0	-3632.9-15.9**i**	1121+13.9**i**	3632.9+18.8**i**
0	0	0	0	-7265.7-31.8**i**	25160.1+137.2**i**	539.8-34.4**i**	-22918.1-139.9**i**
0	0	0	-14531.4 - 63.6**i**	23499.2+175.2**i**	36868.4+176.9**i**	-27983.2- 370.8**i**	-26820.9-108**i**

(3-3-25)

Any row of this matrix identifies:

$$R_{12}\{\boldsymbol{\Psi}_j(y)\} = \mathcal{R}_{12}^{p}(j,1).y^7 + \mathcal{R}_{12}^{p}(j,2).y^6 + \cdots + \mathcal{R}_{12}^{p}(j,7).y + \mathcal{R}_{12}^{p}(j,8) \qquad 1 \le j \le 5$$

The vector $\{\widehat{\boldsymbol{R_{12}}(\boldsymbol{y})}\}_{[1:5]}$ is computed from:

$$\{\widehat{\boldsymbol{R_{12}}(\boldsymbol{y})}\}_{[1:5]} = [R_{12}\{\boldsymbol{\Psi}_1(y)\} \quad R_{12}\{\boldsymbol{\Psi}_2(y)\} \quad R_{12}\{\boldsymbol{\Psi}_3(y)\} \quad R_{12}\{\boldsymbol{\Psi}_4(y)\} \quad R_{12}\{\boldsymbol{\Psi}_5(y)\}]$$

$$= [y^7 \quad y^6 \quad \cdots \quad y \quad 1] \begin{bmatrix} \mathcal{R}_{12}^{p}(1,1) & \mathcal{R}_{12}^{p}(2,1) & \mathcal{R}_{12}^{p}(3,1) & \mathcal{R}_{12}^{p}(4,1) & \mathcal{R}_{12}^{p}(5,1) \\ \mathcal{R}_{12}^{p}(1,2) & \mathcal{R}_{12}^{p}(2,2) & \mathcal{R}_{12}^{p}(3,2) & \mathcal{R}_{12}^{p}(4,2) & \mathcal{R}_{12}^{p}(5,2) \\ \mathcal{R}_{12}^{p}(1,3) & \mathcal{R}_{12}^{p}(2,3) & \mathcal{R}_{12}^{p}(3,3) & \mathcal{R}_{12}^{p}(4,3) & \mathcal{R}_{12}^{p}(5,3) \\ \mathcal{R}_{12}^{p}(1,4) & \mathcal{R}_{12}^{p}(2,4) & \mathcal{R}_{12}^{p}(3,4) & \mathcal{R}_{12}^{p}(4,4) & \mathcal{R}_{12}^{p}(5,4) \\ \mathcal{R}_{12}^{p}(1,5) & \mathcal{R}_{12}^{p}(2,5) & \mathcal{R}_{12}^{p}(3,5) & \mathcal{R}_{12}^{p}(4,5) & \mathcal{R}_{12}^{p}(5,5) \\ \mathcal{R}_{12}^{p}(1,6) & \mathcal{R}_{12}^{p}(2,6) & \mathcal{R}_{12}^{p}(3,6) & \mathcal{R}_{12}^{p}(4,6) & \mathcal{R}_{12}^{p}(5,6) \\ \mathcal{R}_{12}^{p}(1,7) & \mathcal{R}_{12}^{p}(2,7) & \mathcal{R}_{12}^{p}(3,7) & \mathcal{R}_{12}^{p}(4,7) & \mathcal{R}_{12}^{p}(5,7) \\ \mathcal{R}_{12}^{p}(1,8) & \mathcal{R}_{12}^{p}(2,8) & \mathcal{R}_{12}^{p}(3,8) & \mathcal{R}_{12}^{p}(4,8) & \mathcal{R}_{12}^{p}(5,8) \end{bmatrix} \tag{3-26}$$

Also notate the basis vector $\{\boldsymbol{\Psi}_j(y)\}, 1 \le j \le 5$ as a matrix of coefficients of polynomials since $\boldsymbol{\Psi}_1(y)=1$, $\boldsymbol{\Psi}_2(y)=1$, $\boldsymbol{\Psi}_3(y)=2y^2-2$, $\boldsymbol{\Psi}_4(y)=4y^3-12y^2-4y+12$, ...;

$[\boldsymbol{\Psi}(j,l)]_{5\times 8}$ =

0	0	0	0	0	0	0	1
0	0	0	0	0	0	1	0
0	0	0	0	0	2	0	-2
0	0	0	0	4	-12	-4	12
0	0	0	8	-8	-24	8	16

Thus, in order to derive a subroutine like f_1 in (3-17), it is needed to write a procedure that provides matrix of coefficients of polynomials $\left[\mathcal{R}_{12}^{p}(j,l)\right]$ and evaluates the vector $\left\{\widehat{\boldsymbol{R_{12}}}(\boldsymbol{y})\right\}$ as well as:

$$[\boldsymbol{\Psi}(j,l)]_{\{(M-2)\times(M+1)\}} \xrightarrow{\substack{Operators\ in\ (2-10)and\ (2-11)\\ on\ (M,m,k,q,\mathrm{Re},R,s)}} \left[\mathcal{R}_{12}^{p}(j,l)\right]_{\{(M-2)\times(M+1)\}} \xrightarrow{(3-26)@y_s} \left\{\widehat{\boldsymbol{R_{12}}}(\boldsymbol{y_s})\right\}_{[1:(M-2)]}$$

Thereby, a subroutine as f_1 as (3-17) is established. Then, matrices [L] and [R] in (3-13) and (3-15) are set up by means of vectors $\widehat{\boldsymbol{L_{11}}}(y_s)$, $\widehat{\boldsymbol{L_{21}}}(y_s)$, $\widehat{\boldsymbol{L_{12}}}(y_s)$, $\widehat{\boldsymbol{L_{22}}}(y_s)$ and $\widehat{\boldsymbol{R_{11}}}(y_s)$, $\widehat{\boldsymbol{R_{21}}}(y_s)$, $\widehat{\boldsymbol{R_{12}}}(y_s)$, $\widehat{\boldsymbol{R_{22}}}(y_s)$ for s=3,4, …, M-2. In this case:

$[\mathrm{L}]_{[6\times6]}$ =

-28631	-55511	-116614	- 2560**i**	15360**i**	23040**i**
-56020	10240	-71080	- 2560**i**	20480**i**	10240**i**
-18391	60631	-116614	- 2560**i**	25600**i**	- 17920**i**
- 2**i**	0	- 2**i**	-1.9	9.7	17.5
2.7**i**	5.4**i**	5.4**i**	-3.3	20.1	26.8
14.1**i**	- 8.1**i**	30.3**i**	-5.5	38.8	27.7

$[\mathrm{R}]_{[6\times6]}$ =

306.5-3086.5**i**	868.1–14562**i**	1507-24643.9**i**	3285.1+21.8**i**	-17266.4-126.8 **i**	-29566.2- 231.2**i**
588.1-584.7**i**	-189.3-5427.4**i**	52.1+11095.9**i**	5005.8+50.5**i**	-31568.2-345.4**i**	-36980.4-345.4**i**
803.8+850.3**i**	-1862.3–12506**i**	4254.9+22164.5**i**	1533.9+258.2**i**	-9504.8–1948 **i**	-12600 -728.5**i**
0.75+0.02**i**	0.09-0.01**i**	0.92-0.03**i**	0.01-0.64**i**	-0.06+3.2**i**	-0.13+5.76**i**
0.29-0.05**i**	-1.6-0.08**i**	0.57-0.07**i**	0.03-**i**	-0.16+6**i**	-0.22+8**i**
4.25-0.3**i**	-3.3+0.27**i**	10.8-0.65**i**	0.09+0.9**i**	-0.6-6.2**i**	-0.4-4.4**i**

4. Code Implementation and Confirmation

4.1 Setting off the program

The pseudo-spectral method was described in previous chapter and accordingly a straightforward procedure was implemented in MATLAB. The computations were quite routine and easy to follow. The convergence of the algorithm was fairly acceptable as far as the input parameters are chosen not to be in the vicinity of the neutral stability curve. The Script of the program could be also found in appendix B.

An iterative algorithm was used to determine the convergent value of the growth rate. After fixing ω_i, other quantities such as phase speed, radial amplitude, radial frequency, azimuthal amplitude, and azimuthal frequency for travelling disturbance were computed.

The travelling disturbances in $(r-\theta)$ plane were investigated for an arbitrary swirl parameter and Reynolds number. Interacting with the axial velocity component, the disturbances also emanate in a helical form. In this study, the axial direction was not included in the stability analysis.

The base flow was set up to be:

$$U = 0 \quad ; \quad V = \frac{q.r}{\sqrt{1+r^4}} \quad ; \quad W = e^{-r^2} \tag{4-1}$$

This profile was chosen to be similar to Batchelor vortex model used by Fabre *et al* [25]. The only difference is that the azimuthal component was replaced by Vatistas vortex model.

Our objective was to implement stability analysis with the proper azimuthal component. As explained in section 1.4, the azimuthal component is acceptable only if its maximum value is coincidence with the core radius. In other words, the condition $V(r = r_c) = V_{max}$ should not be violated in any base flow model used in stability analysis.

Despite, the peak azimuthal component in Batchelor vortex model occurs at r=1.256 (the azimuthal velocity is similar to Burger's model, see Table 1-1). This model has been commonly used for viscous stability analysis, which I strongly believe that was not the correct base flow.

Nonetheless, it is required to compare and validate present method with a reliable study. Indeed, the dimensionless swirl parameter would be the best variable in quantifying the onset or cease of stability in a columnar vortex which in turn restrict the selection of base flow to so-called "q-vortex" models.

The overall drawback in the credibility of Batchelor vortex could be remedied by correcting the azimuthal component. The new velocity profile should be:

$$V_{modified} = \frac{q}{r}\left(1 - e^{1.256r^2}\right) \qquad (4\text{-}2)$$

Then, the highest value of azimuthal velocity relocates to r=1; the core radius. Both the original and the modified base flow were fed into the program and the results were compared in the next section.

4.2 Confirmation with previous studies

The accuracy of the numerical method was verified by comparing the results of present study for the growth rate with the previous stability studies. The comparisons of results are listed in Table 4-1.

Table 4-1

Re	m	k_{max}	q_{max}	Inviscid Study Lessen	Inviscid Study Duck	Viscous Study Khorroami	Present Method		
							Original Batchelor	Modified Batchelor	Vatistas Azimuthal
20000	-2	1.2	0.70	0.3138	0.3139	0.3127	0.3135	0.2849	0.2960
50000	-2	1.2	0.70	0.3138	0.3139	0.3133	0.3141	0.2852	0.2965
100000	-2	1.2	0.70	0.3138	0.3139	0.3135	0.3143	0.2854	0.2967
100000	-3	1.7	0.79	0.3544	0.3546	0.3540	0.3541	NaN	0.3201
100000	-4	2.15	0.82	0.3777	0.3775	0.3768	0.3769	NaN	0.3390

Calculations were performed for asymmetric disturbances (m<-1) and the results related to original Batchelor obviously agree with those of [9], [8], and [5]. This coincidence can assure us from the credibility of the generated MATLAB program (see appendix B). The trend of growth rate fairly complies with available results; however, a relatively large deviation is evident on the right-side columns of Table 4-1. Because the base flow of the "Modified Batchelor" is different than the "Vatistas Azimuthal".

4.3 Convergence test of the algorithm

The proposed method was proved to be computationally efficient. The convergence history is given in Table 4-2 for the particular asymmetric case of m=-3, k=1.65, q=0.75, Reynolds=1000.

Table 4-2

	Eigenvalue ($\boldsymbol{\omega} = \omega_r + \mathbf{i}\omega_i$)	
M	Primary mode	Secondary mode
20	0.2997493189 **i** - 0.8255926974	0.1785820337 **i** - 0.8231761633
25	0.2996236357 **i** - 0.8256629175	0.1764776611 **i** - 0.8232370169
30	0.2996168708 **i** - 0.8256644140	0.1764618726 **i** - 0.8232219030
35	0.2996169531 **i** - 0.8256633787	0.1764616424 **i** - 0.8232165578
Convergence value of 0.2996 for growth rate by considering 35 collocation points		

4.4 Verifying contours of growth rate

These contours known as topography of instability are very beneficial. It allows one to determine the destabilizing interval of swirl as well as the type of possibly amplified instabilities. In figures 4-1, 4-2, and 4-3 the unstable region is pictured as contours of growth rate for various Reynolds numbers. Plots of instability topography, were originally provided by Mao *et al.* [12]. In order to validate the present method, these contours were regenerated and compared for different Reynolds numbers. In the modified Batchelor Vortex model the disturbance is asymmetric (m=-2) and Reynolds number equals 100, 10^3, and 10^4 for figures 4-1, 4-2, and 4-3 respectively.

Inspecting all the figures, the regenerated contours are satisfactorily smooth all through the unstable region. The locations and values of maximum growth rate in both cases match fairly well. Furthermore, the unstable region in present study does not outspread wider than those by Mao's which ensures not having a contractive interpretation on any point (q,k). Nonetheless, the approach portrays major difficulties about convergence in the region close to the neutral stability. The corresponding curves are plotted by dashed curve in the contours of Mao in each of the figures. These were required to be detected using the inviscid stability theory, which was not the scope of present study.

It may be stated that the present study is in good agreement with previously established approaches of viscous stability analysis and it is capable of providing reliable results.

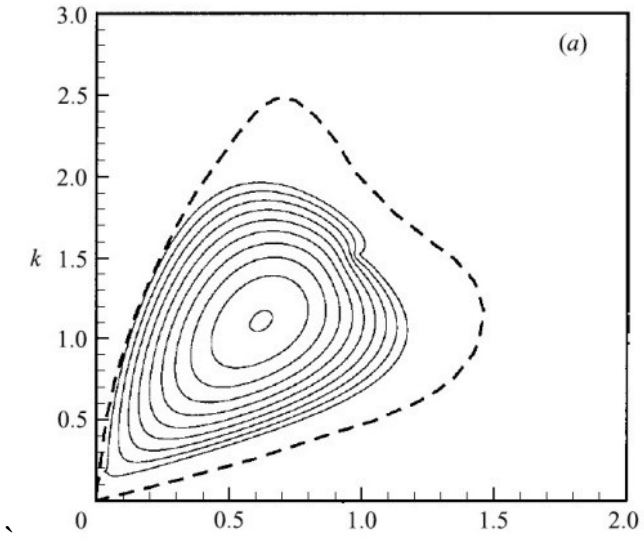

(a)

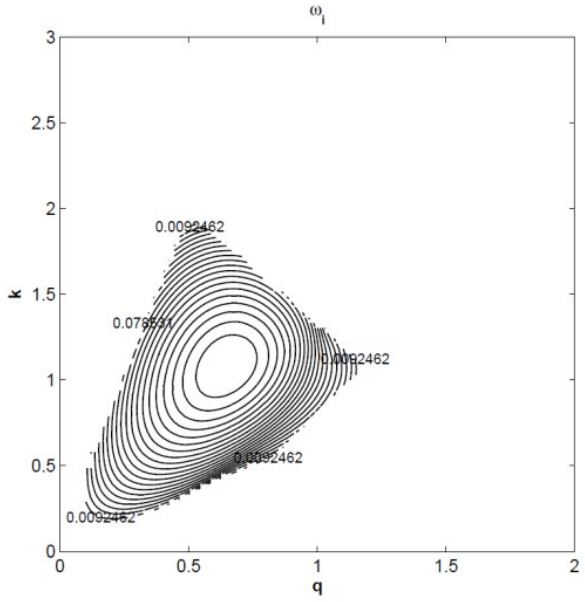

(b)

Figure 4-1 Contours of growth rate for Batchelor's vortex model

m=-2, Re=100, (a) Mao paper (b) Present study

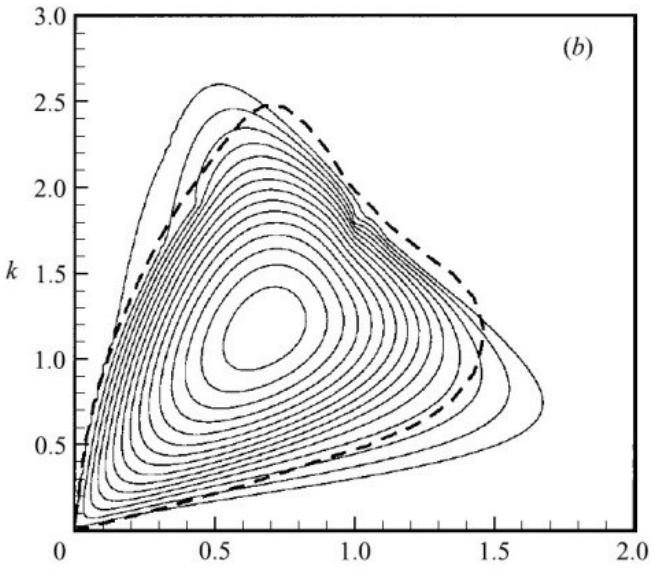

(a)

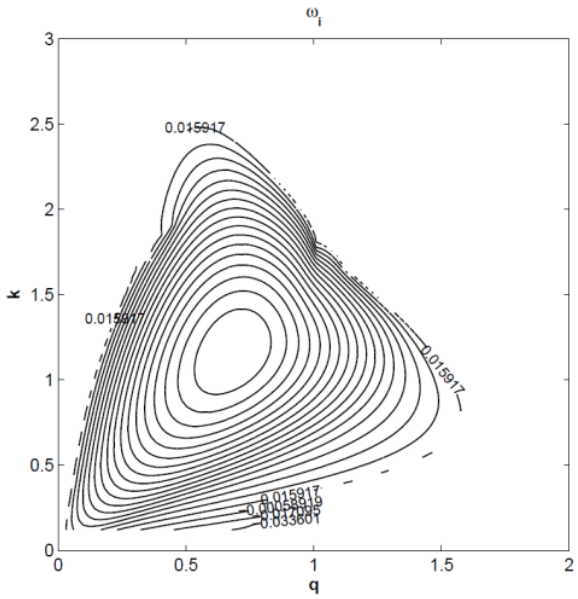

(b)

Figure 4-2 Contours of growth rate for Batchelor's vortex model

m=-2, Re=1000, (a) Mao paper (b) Present study

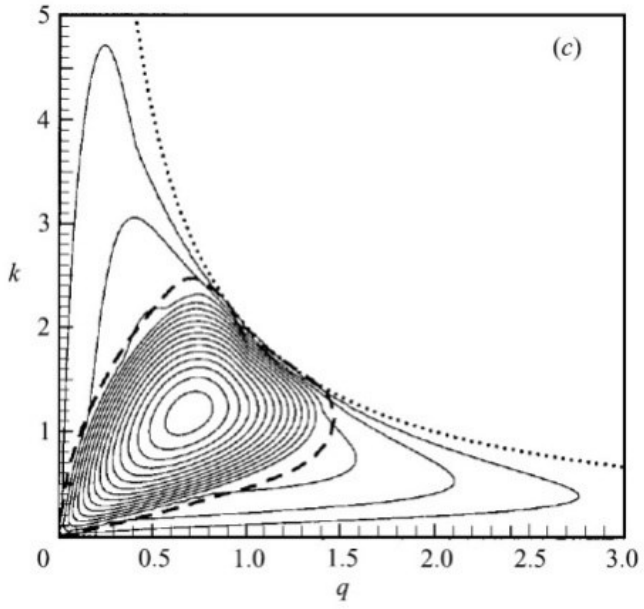

(a)

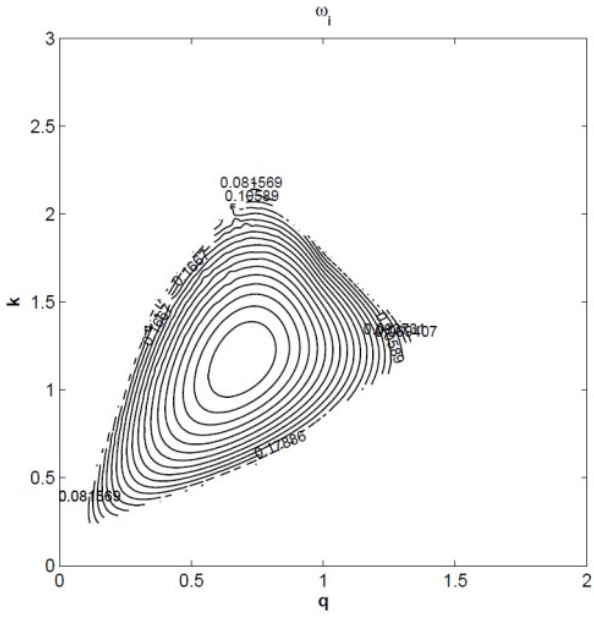

(b)

Figure 4-3 Contours of growth rate for Batchelor's vortex model m=-2, Re=10000, (a) Mao paper (b) Present study

5. Viscous Stability Analysis

5.1 Results for axisymmetric mode (m=0)

The number of mode captures depends on the number of collocation points, but since the primary and secondary modes are the most unstable ones we presented only the results related to these modes. The primary mode corresponds to the solution with the largest real part among all the eigensolutions.

Variation of growth rate and phase speed versus axial wavenumber for an axisymmetric disturbance (m=0) is plotted in figure 5-1. The swirl quantity equals to 0.26 and Reynolds number is 5×10^4. Some portion of the curve was not displayed due to numerical problem in the convergence. The solid curve represents the growth rate of the primary mode and dashed line corresponds to the secondary mode. The magnitude of growth rate is relatively small which means that the instability of the vortex build up slowly. The primary mode growth rate increases monotonically until reaches its maximum of 0.0710 at k=2.8176.

The profile of growth rate for primary and secondary modes overlap at $k \approx 1.85$. That occurs on the peak of secondary mode and is known to be the main cause of divergence in computing the eigensolutions.

The slope of phase speed curve represents the wave group velocity which is equal to -0.72 in figure 5-1 for both primary and secondary modes. However, the temporal branches of phase speed for the primary and secondary mode cross over each other.

Figures 5-2 and 5-3 show the associated eigenfunctions associated with this instability. Recall from section 2.3 that complex quantities F_1 and F_2 correspond

respectively to radial and azimuthal disturbances. The magnitudes of $\|F_1\|$ and $\|F_2\|$ were normalized everywhere by the largest one. Moreover, the zero frequency was set off to be at the location of the peak amplitude.

The observable points in the profile of disturbances are as following. They resemble impulse waves while their maximum occurs inside the vortex core (r<1). The position of peak amplitude for radial disturbance is on r_{max}=0.7479 which is farther than the one for the azimuthal disturbance; r_{max}=0.5953. This indicates that the unstable mode is a center mode. Looking at the frequencies in figures 5-2 and 5-3, little variations can be seen except an abrupt phase shift on the distance almost equal to 0.6. Based on the mode frequencies one can notices that the primary instability is almost stationary.

In figure 5-4, the real and imaginary parts of eigenvalues, ω_r and ω_i were presented for the first fifteen temporal viscous modes.

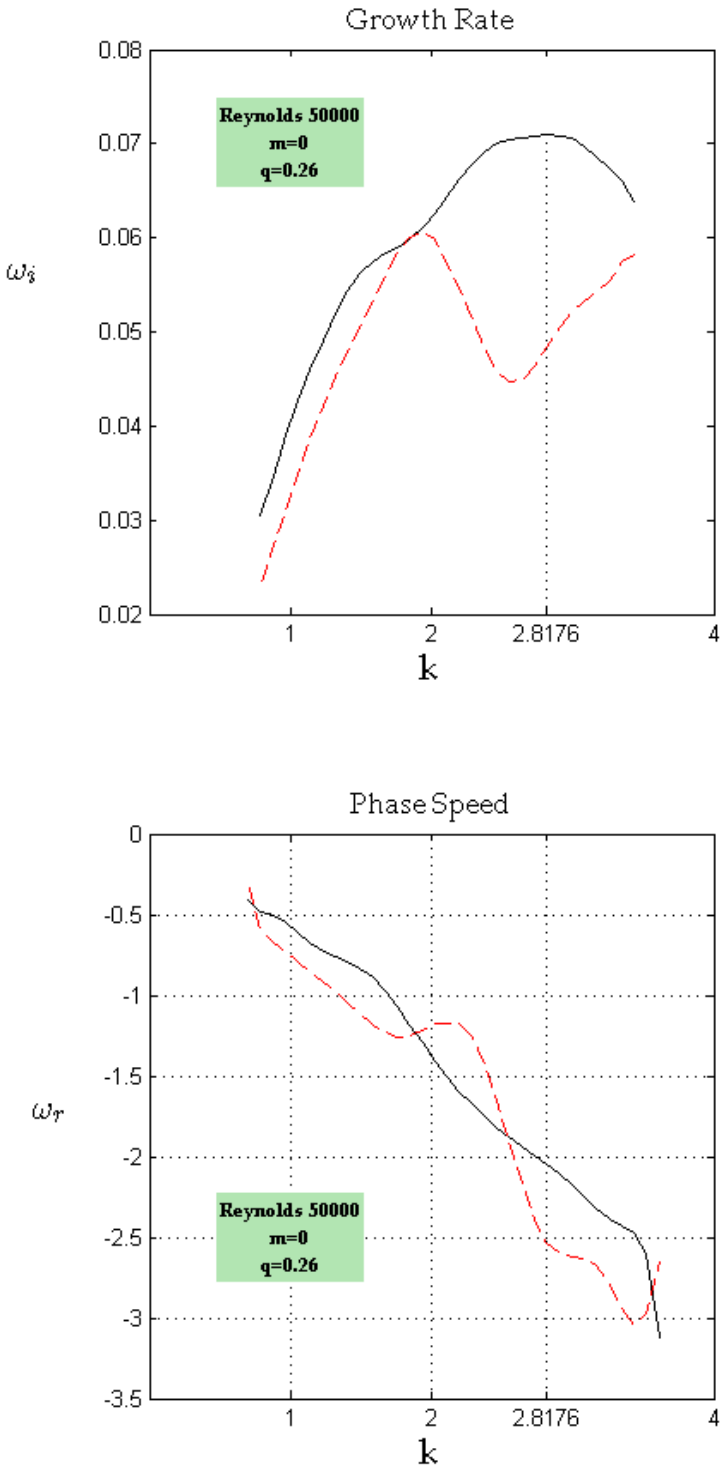

Figure 5-1 Primary and secondary mode for axisymmetric disturbance

(The solid and dashed lines represent primary and secondary modes respectively.)

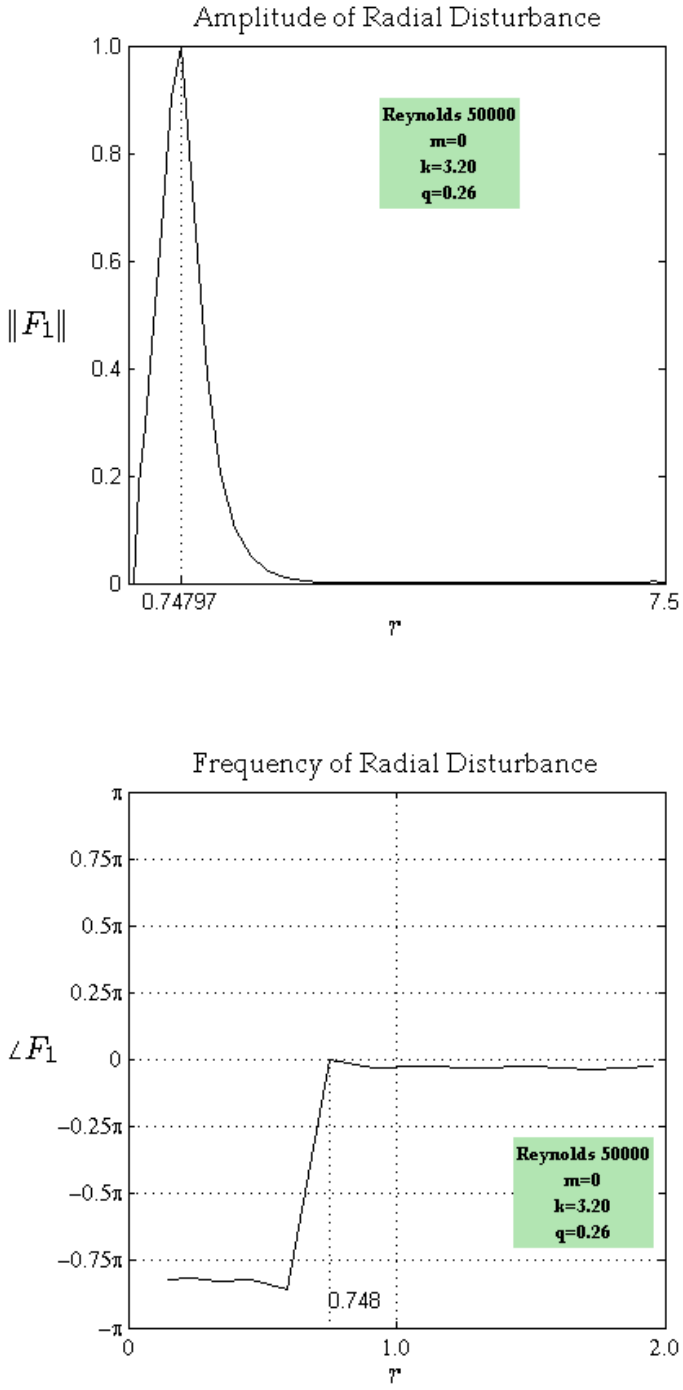

Figure 5-2 Propagation of radial axisymmetric disturbance

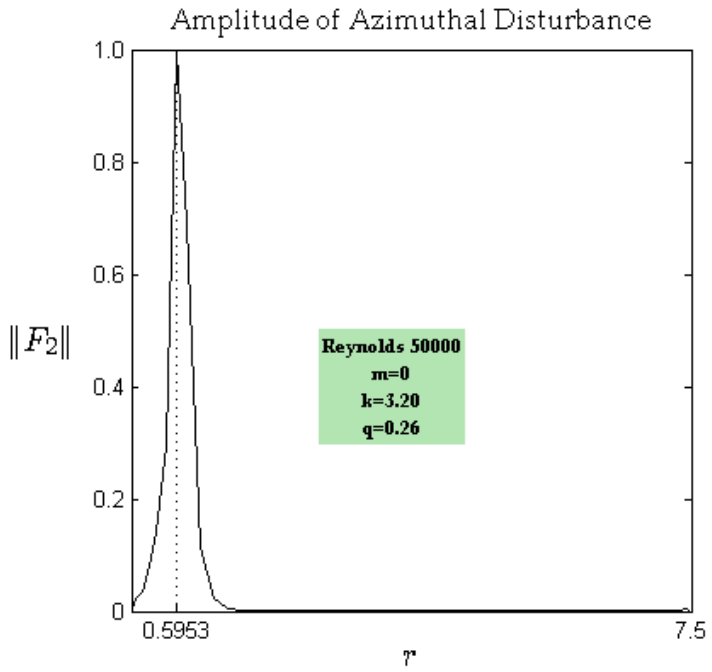

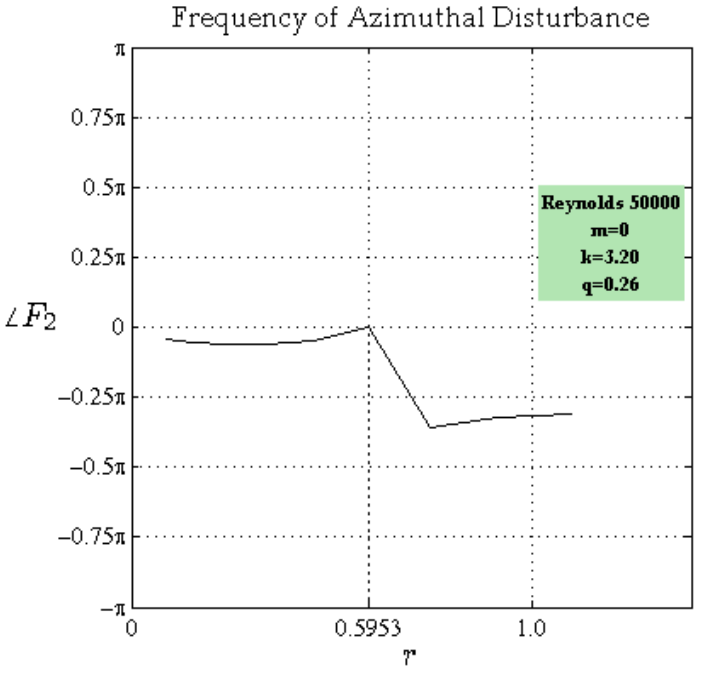

Figure 5-3 Propagation of azimuthal axisymmetric disturbance

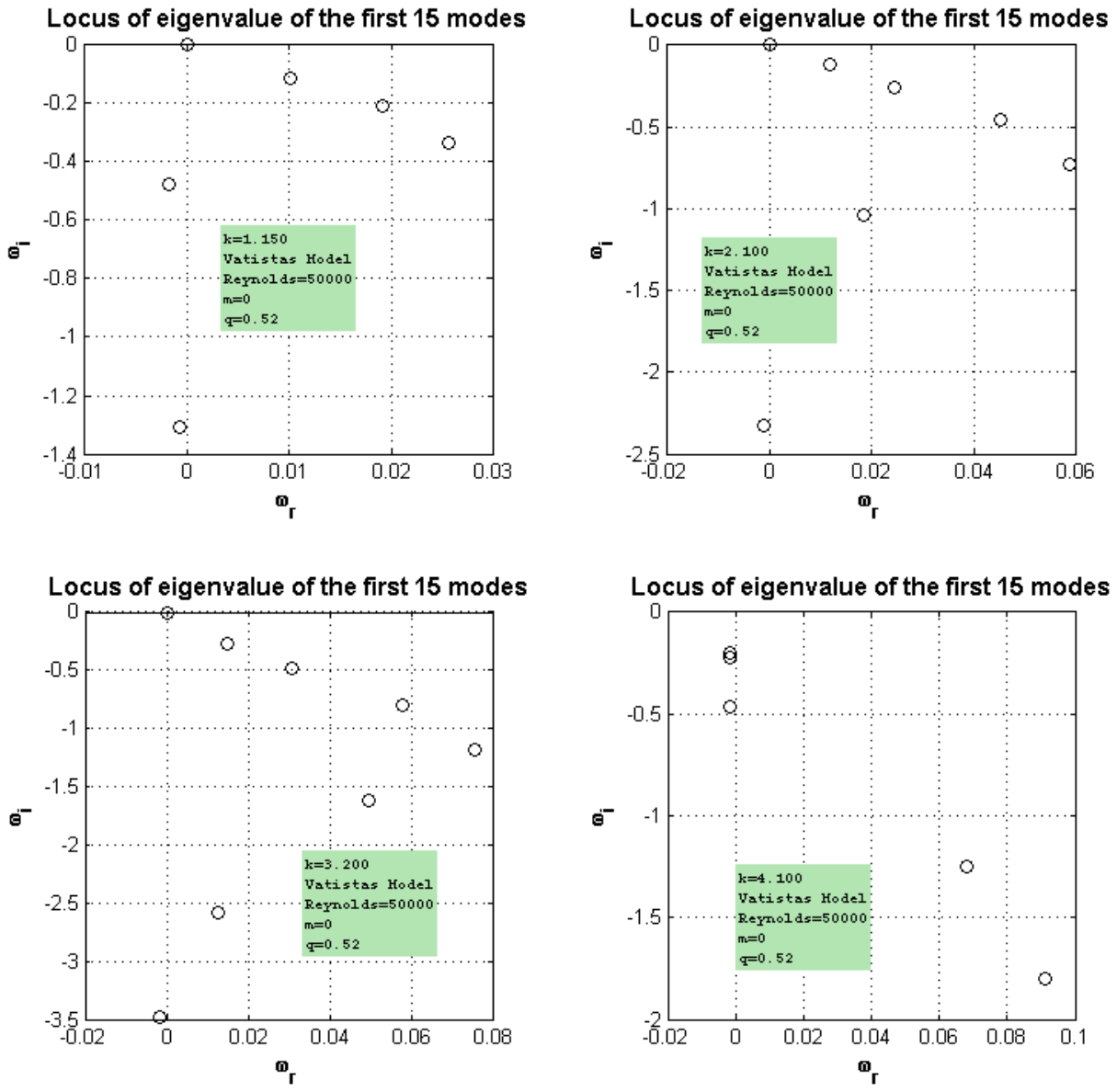

Figure 5-4 Locus of eigenvalues in axisymmetric disturbance

5.2 Results for the asymmetric mode (m=-2)

The dependence of the growth rate, ω_i, on the axial wave number, k, for an asymmetric disturbance (m=2) is shown in figure 5-5. Again, the solid line and dashed line represent primary and secondary modes respectively. Their profiles are fairly distinctive and look obviously smoother than those for axisymmetric disturbance. In addition, the growth rates in figure 5-5 have significantly greater order of magnitude compared to the results presented in figure 5-1.

The figure shows that the asymmetric instability occurs at lower axial wavenumber. This statement could be probed through jeopardizing the order of magnitude of variable k between figures 5-1 and 5-2 for which the instability as the value of growth rate is significant. Then, it may be concluded that the asymmetric disturbance travels in long-wave packets and comparatively the axisymmetric does in short-wave ones.

The first two strongest modes were satisfactorily plotted distinctively as quasi-parabolic profiles. In the same manner, other modes are expected to share the same shape. Unfortunately, the computational capability of present study did not allow for more refinement of eigensolutions.

Looking at figure 5-5, it is clear that the maximum of primary mode profile occurs in larger values of k than the peak of secondary mode; k=0.989 versus k=0.695. Furthermore, the primary mode instability lasts over a wider interval of axial wavenumber.

The order of magnitudes of growth rates shown in figures 5-1 and 5-5 are evidently different. For example, the axisymmetric disturbance in Figure 5-1 Primary and secondary mode for axisymmetric disturbancehas maximum growth rate equal to

0.0710. In contrast, the maximum value of the asymmetric growth rate equals 0.2634 for primary mode and 0.1389 for secondary mode (see figure 5-5). This means that asymmetrical modes are the most unstable ones.

The phase speed, ω_r decreases monotonically with the axial wavenumber by rate of -0.51. The curves of primary and secondary modes are very close to each other and have a quite constant rate of change. However, in the reality since a primary mode is the most unstable mode one should expect to observe the primary mode rather the second one.

Figure 5-6 shows the amplitude and frequency of the radial eigenfunctions F_1 for the particular case m=-2, k=0.5, q=0.4 and Reynolds=4000. Figure 5-7 is the plot of $\|F_2\|$ and $\angle F_2$; the azimuthal amplitude and frequency of asymmetric temporal instability for the similar asymmetric inputs. Again, the eigenfunctions are normalized with the maximum values.

If the normalized amplitude and azimuthal disturbances in figure 5-6 and 5-7 are compared with those in figures 5-2 and 5-3, it can be seen that the radial profiles in the former spread over larger domain than the latter.

The maximum value of radial amplitude in figure 5-6 is found to be at r=0.4136 which is again less than unity. Therefore, the asymmetric instability persists inside the vortex core and occurs even closer to the vortex centerline compared to the axisymmetric. The slope of $\angle F_1$ inside the vortex core is approximately -1.5 which simply indicates non-stationary characteristic of asymmetric disturbance. Despite, the horizontal phase speed for r>1 has the meaning of stationary asymmetric instabilities on the free stream region (outside of the vortex core).

As presented so far, the amplitude of disturbance has only one maximum. Nonetheless, there are two peaks in the profile shown in figure 5-7 which make the azimuthal asymmetric disturbance look different from a single impulsive profile. The largest azimuthal amplitude occurs at r=0.239, is apparently closer to the centerline compared to the radial amplitude in figure 5-6.

Neglecting all the phase shifts in figure 5-7, the slope of $\angle F_2$ on the distances close to unity is notably equal to -2.5. Thus one lead up to anticipating non-stationary instabilities of asymmetric type in the region with highest azimuthal velocity.

The locus of eigenvalues for asymmetric disturbance, m=-2, and q=1.0 is presented in figure 5-8 for different values of axial wavenumber. The distribution of eigenvalues are quite spurious. However, the arrangement bifurcates into possibly meaningful pattern, which is in turn an open question to address.

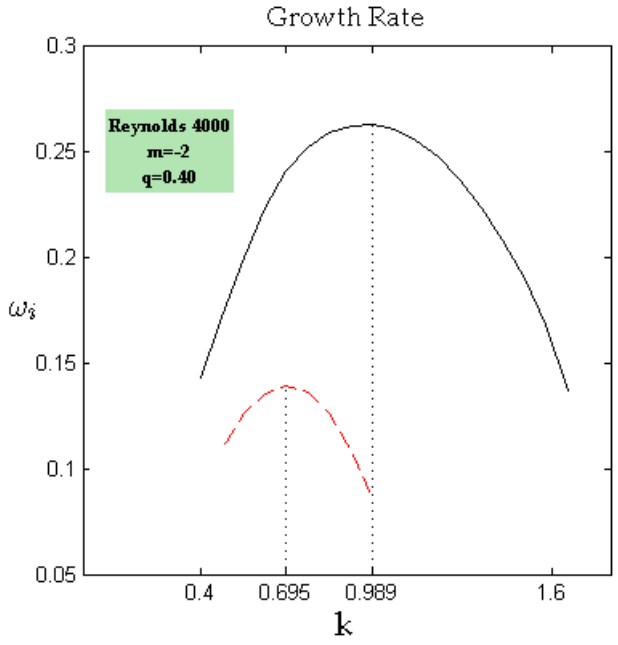

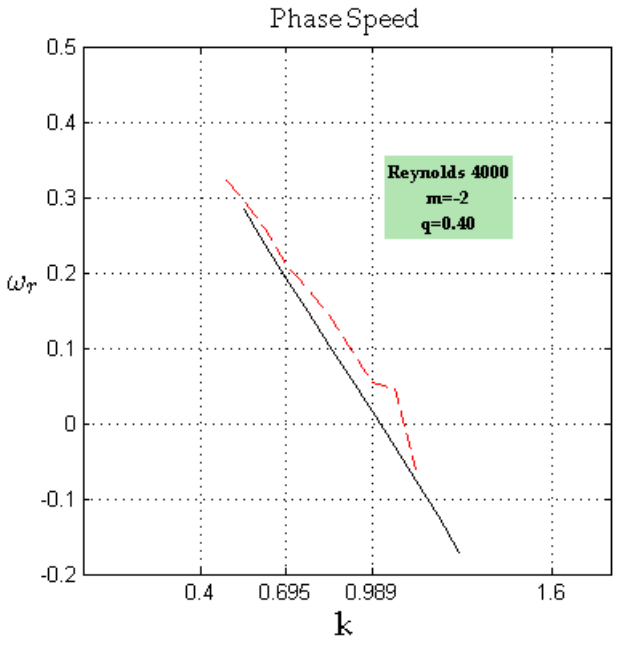

Figure 5-5 Primary and secondary modes for asymmetric disturbance

(The solid and dashed lines represent primary and secondary modes respectively.)

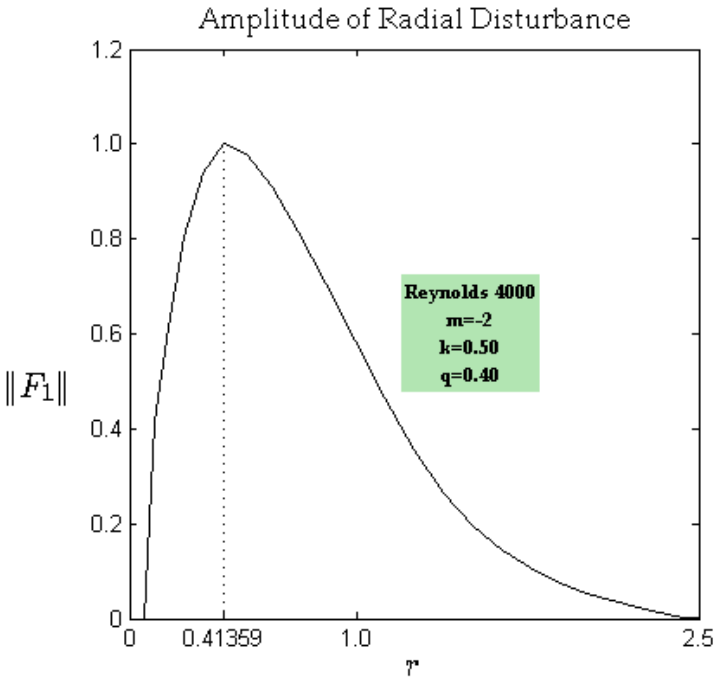

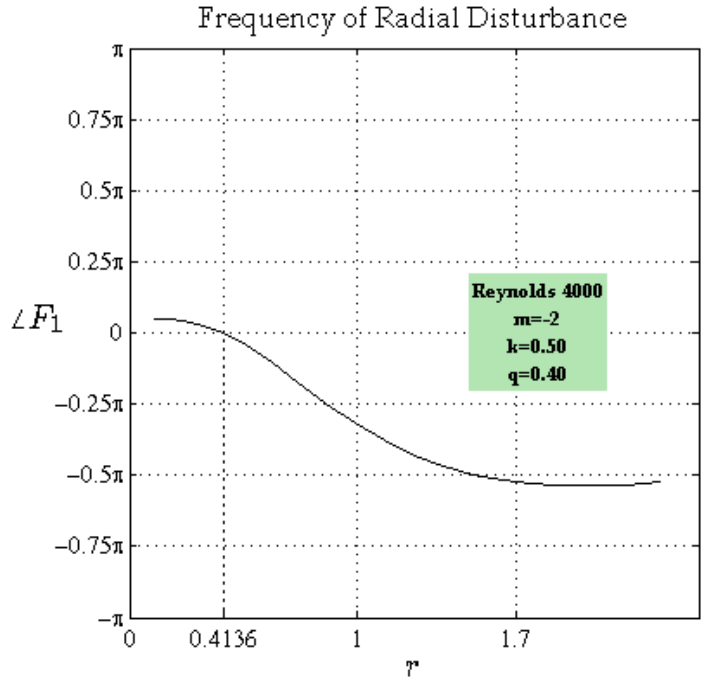

Figure 5-6 Propagation of radial asymmetric disturbance

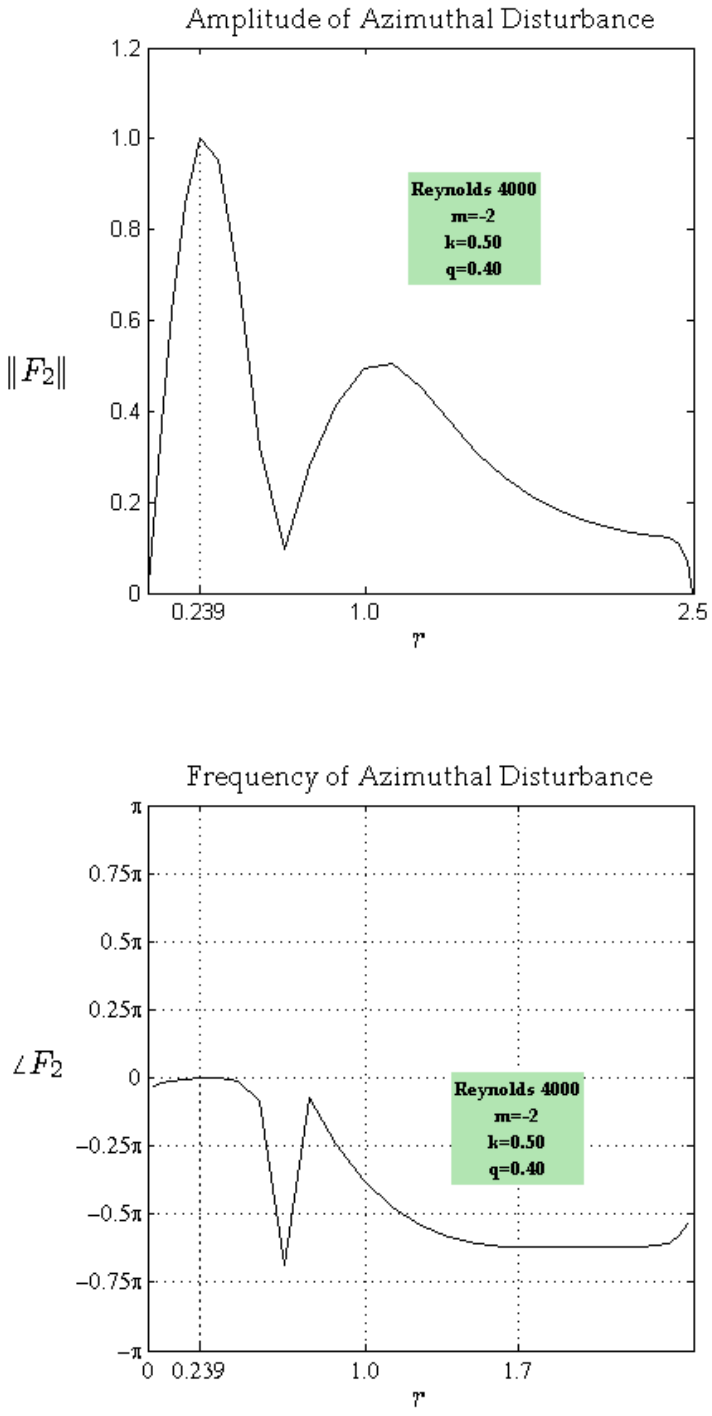

Figure 5-7 Propagation of azimuthal asymmetric disturbance

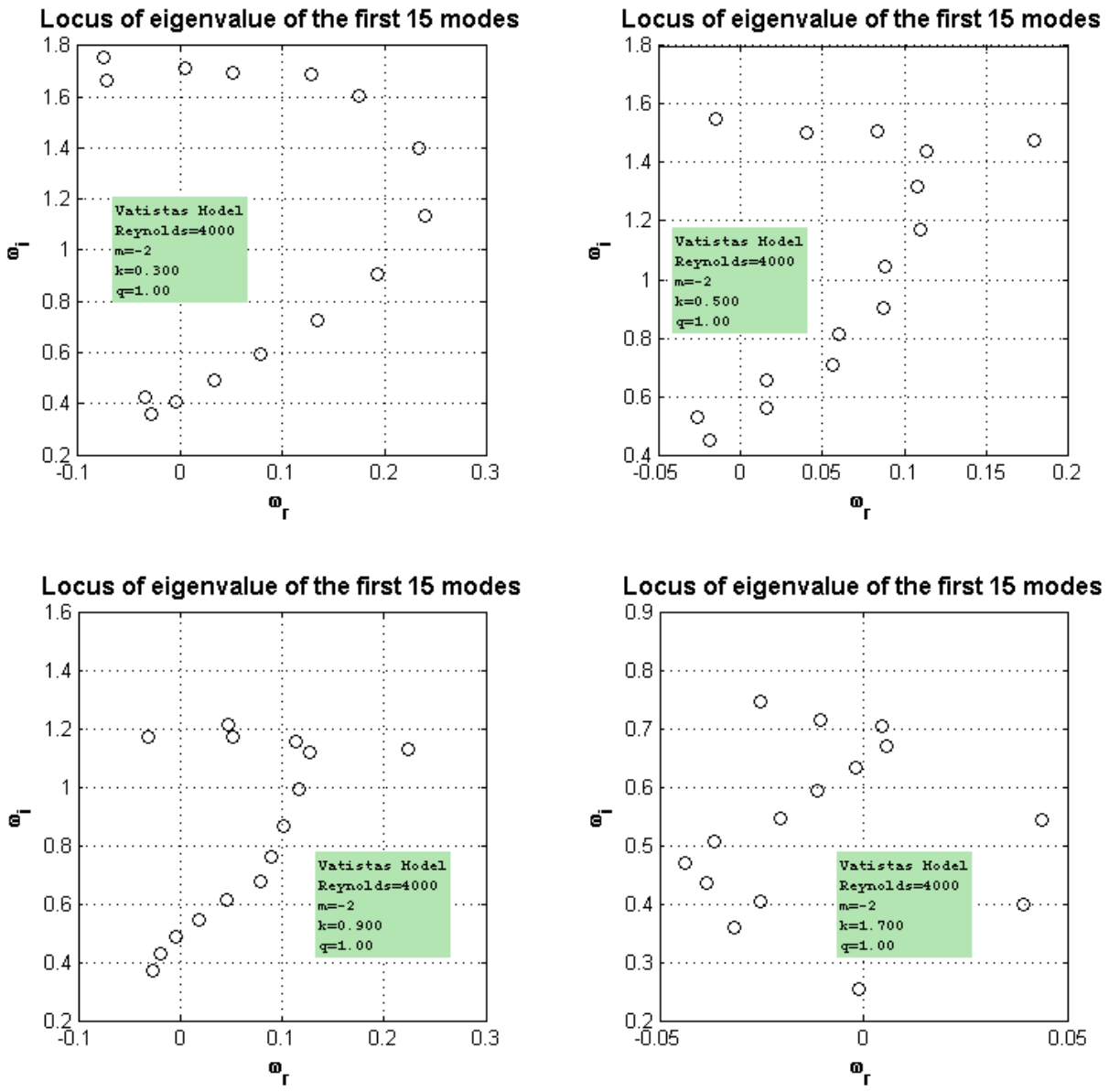

Figure 5-8 Locus of eigenvalues for asymmetric disturbance

5.3 Effect of swirl parameter on instability

In this subsection, the influence of swirl parameter on the instability was attempted. The unstable modes were recomputed with approximately doubling the values of swirl quantity. These “intense vortex” plots were compared illustratively with their conjugate figures in order to study the effect of intensifying swirl parameter on the main traits of unstable waves.

The behaviour of the growth rate and phase speed at a higher value of swirl parameter is depicted in figure 5-9 for axisymmetric disturbance, with Reynolds number equal 5×10^4, m=0, and q=0.52 (almost twice of the swirl quantity taken in section 5-1). As it can be seen, the axisymmetric instability shifts to higher values of axial wavenumber (short-wave) as the swirl parameter increases. Again, the profiles of growth rate for primary and secondary modes lie close to each other, which serve as a cause of computational divergence in the present algorithm.

Comparing figures 5-1 and 5-9, the peak of primary growth rate in the latter occurs at larger values of k. Consequently, the stronger vortex may cause the axisymmetric instabilities to shift from the long-wave to short-wave. In addition, increasing the swirl quantity apparently widens the range of axial wavenumber for which the growth rates of unstable axisymmetric waves are noticeable.

Looking at figure 5-9, the branches of phase speed cross over each other and decrease with an approximately equivalent rate. Besides, the slope is less than figure 5-1, which means the stronger the vortex, slower the group velocity is.

Finally, the increase in maximum value of growth rate from 0.0710 to around 0.10 is intriguing. It may be then concluded that increasing the value of q makes

axisymmetric instabilities slow down, have more amplification rate and shift up to a much short-wave zone.

Figures 5-10 and 5-11 assess the new amplitudes and frequencies of radial and azimuthal axisymmetric disturbances for larger swirl parameter. Comparing radial disturbances in figures 5-2 and 5-10, the position of the peak changes from 0.748 to 1.098, which means the maximum value was relocated away vortex core. Nonetheless, the stationary characteristics of the travelling waves did not change due to the horizontal frequency. Therefore, increasing the swirl parameter may shift the position of maximum growth rate to radial distances farther from the vortex centerline but does not necessarily interrupt other features of axisymmetric disturbance. In other words, instability shifts from center mode into an annular mode that occurs outside the vortex core.

Figure 5-11 should be compared back with figure 5-3, m=0, k=3.2, and the value of q increases from 0.26 to 0.52. Thereby, the new azimuthal amplitude increases to its maximum at r=0.9159 opposed to its previous peak location at r=0.5953. This means that the increasing the swirl also shifts the azimuthal instability farther. However, it can be seen that the impulsive profile of azimuthal wave is not modified and the amplitude falls offs quickly to zero after the peak. The unstable wave stays stationary. The implication is that every feature of the axisymmetric instability is immune to the swirl parameter except the position of maximum amplitude.

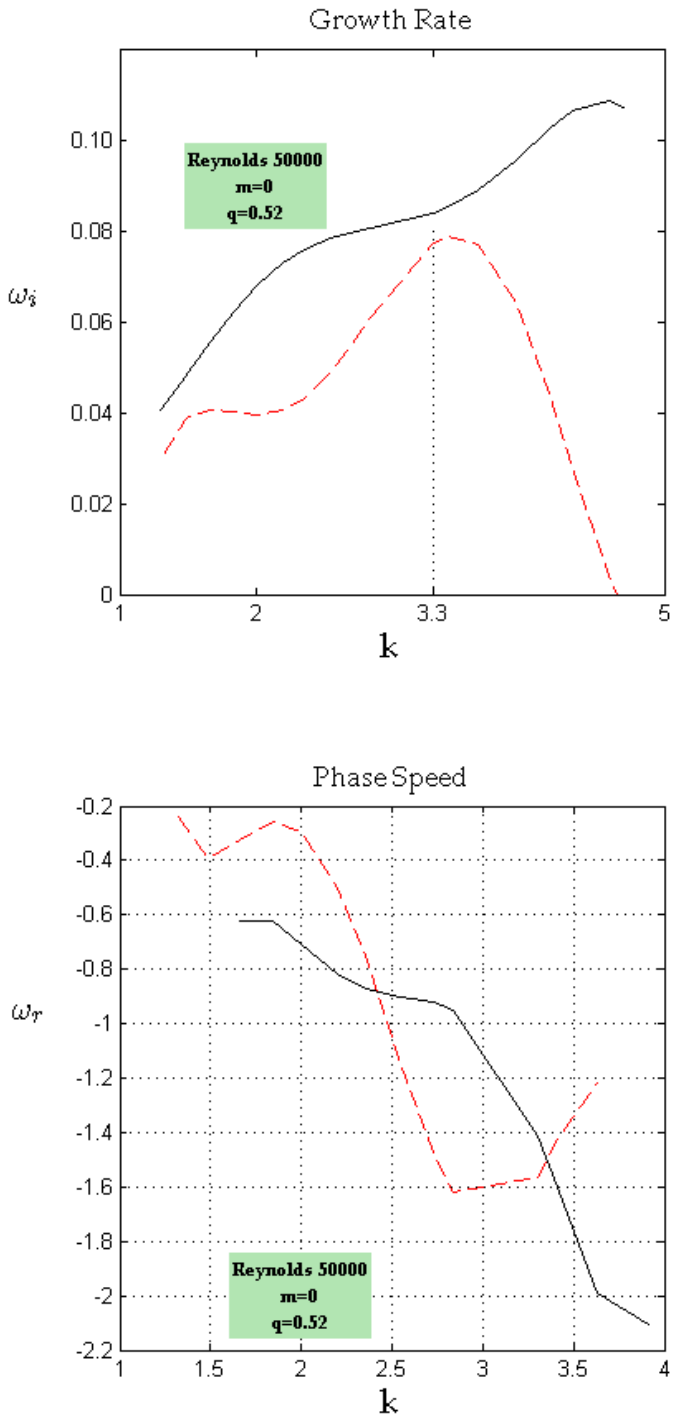

Figure 5-9 Primary and secondary modes for axisymmetric disturbance; intense vortex

(The solid and dashed lines represent primary and secondary modes respectively.)

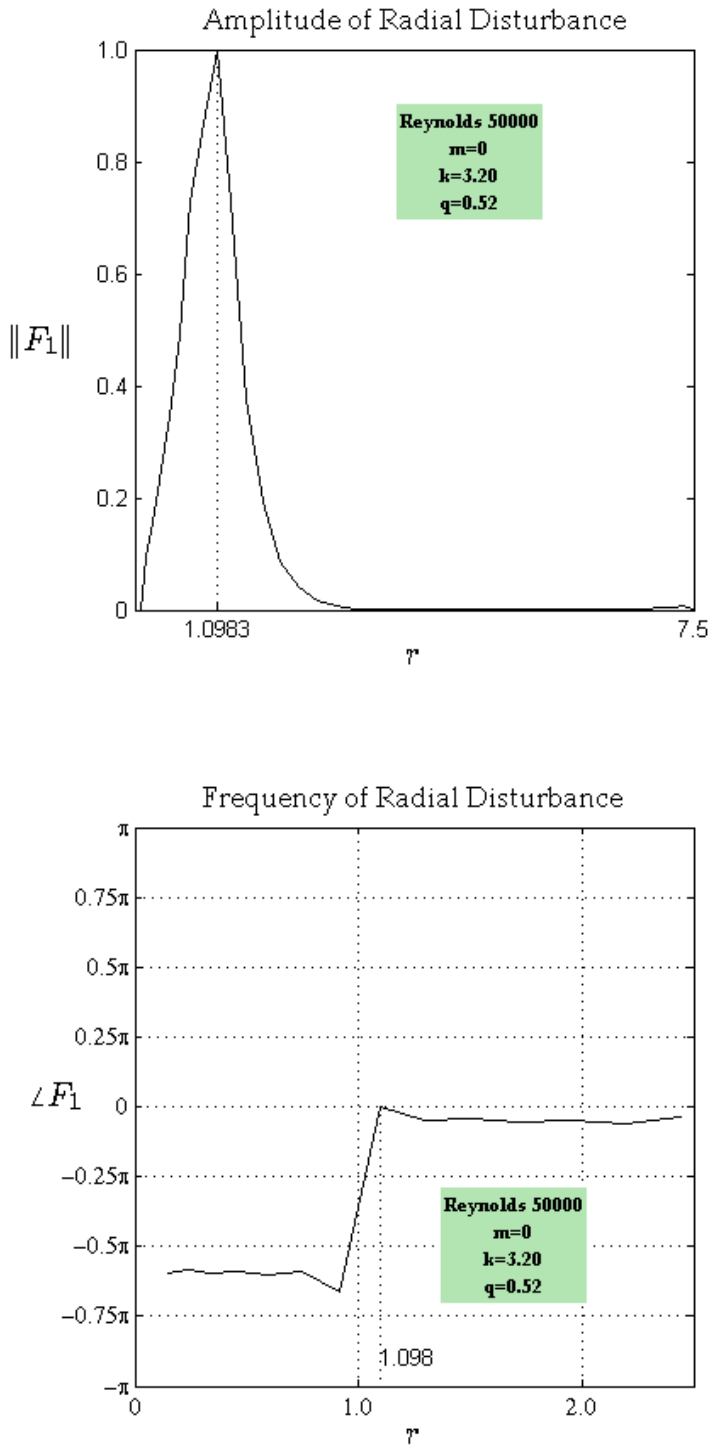

Figure 5-10 Propagation of radial axisymmetric disturbance; intense vortex

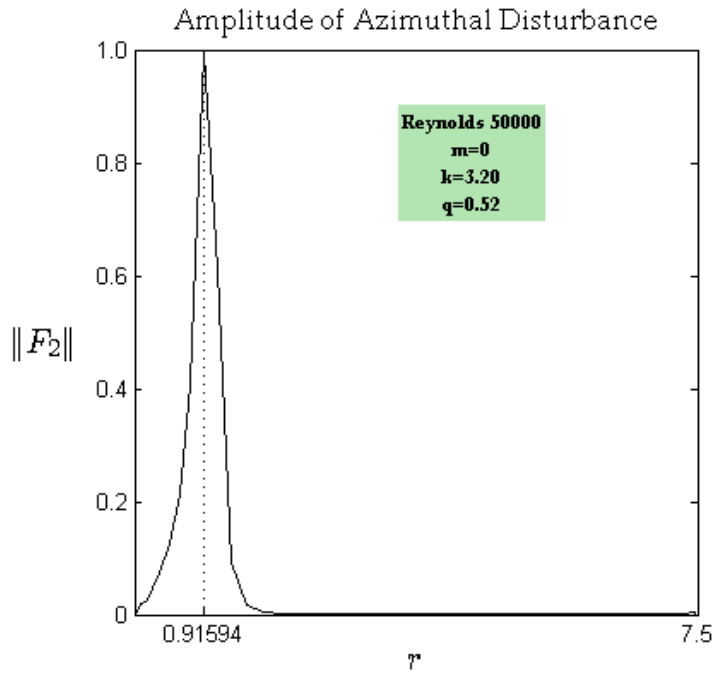

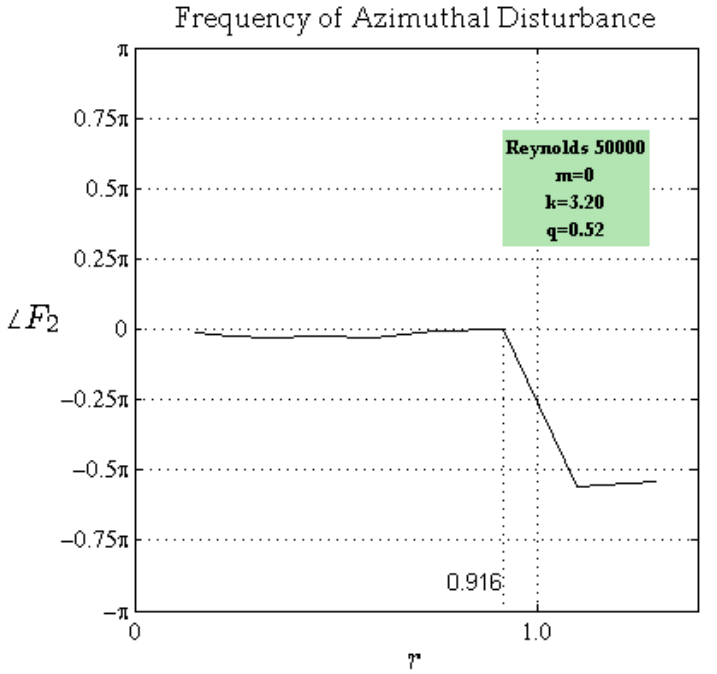

Figure 5-11 Propagation of azimuthal axisymmetric disturbance; intense vortex

Figure 5-12 illustrates the growth rate variations for a comparatively larger swirl quantity than section 5.2. The disturbance is asymmetric (m=-2), q=0.8, and Reynolds=4000. Again, only the first two predominant modes among the spectrum of eigensolutions were presented. The largest values of the growth rate are 0.2601 and 0.1814 for primary and secondary modes. These maximums were also taken place farther; their new position in figure 5-12 are r=1.3, 1.14 compared to the values r=0.989, 0.695 in figure 5-5. The phase speed for both primary and secondary mode were also shown in figure 5-12. As it is expected, the corresponding branches look to be undistinguishable. The magnitude of the declination rate of phase speed is -0.86, greater than slope -0.51 in figure 5-5. Therefore, the azimuthal instabilities propagate faster as the swirl quantity increases.

Figure 5-5 and 5-12 could be also compared in terms of order of magnitude of k for predominant instabilities. In this way, the range of axial wave number in intense vortex presented by figure 5-12 states larger orders than figure 5-5. From that, the majority of asymmetric instabilities in a stronger vortex possibly tend to occur in comparatively short-wave type.

Radial variations of magnitude $\|F_1\|$ and angle $\angle F_1$ for intense vortex are presented in figure 5-13. Compared to figure 5-6, the radial amplitude profile in figure 5-13 slightly shrinkages and offers its peak at a smaller radial distance r_{max}=0.3211. This is less than r_{max}=0.4136 in figure 5-6 and is obviously closer to the vortex centerline. Figure 5-13 also presents the frequency of radial asymmetric disturbance for strongest mode versus radial location. As it is observed, the asymmetric instabilities are not stationary in as much as the value of $\angle F_1$ decreases with declination rate approximately equal to -3.7 inside the vortex core. Although, the phase speed is almost horizontal outside of the core

implying that the instability should be interpreted as stationary waves far outside of the core.

The amplitude and frequency of azimuthal disturbance were also plotted in figure 5-14. Corresponding values for asymmetric disturbance are: Reynolds=4000, m=-2, k=0.50, and with a stronger swirl quantity; q=0.80. It is interesting to note that the location of the maximum azimuthal disturbance remained unchanged while the swirl quantity increases. The value of r_{max} equals 0.239 whether in figure 5-7 or figure 5-14. The slope of the frequency of azimuthal disturbance on the region near to the core radius has the approximate value of -4.0, which means there is a sharper declination rate compared to the rate of -2.5 in figure 5-7.

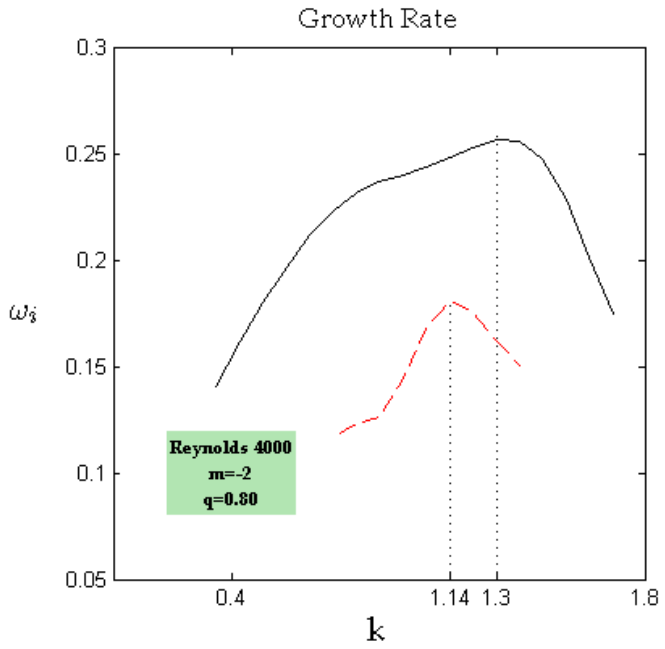

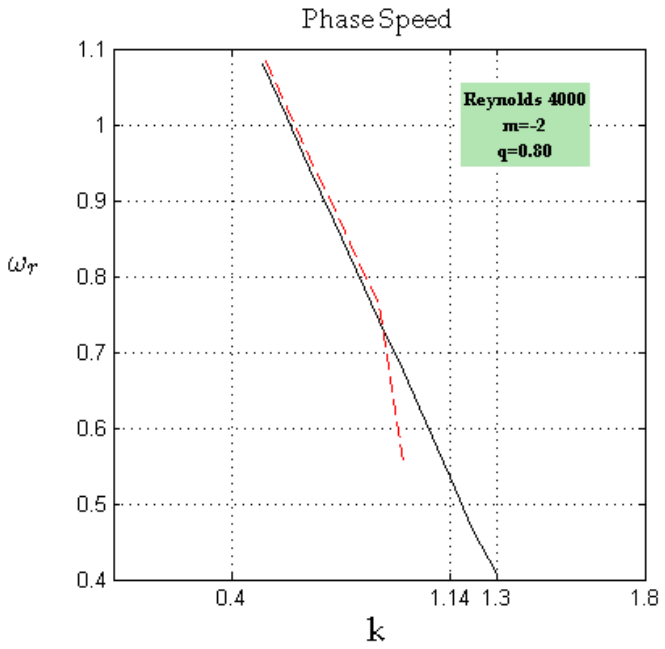

Figure 5-12 Primary and secondary mode for asymmetric disturbance, intense vortex

(The solid and dashed lines represent primary and secondary modes respectively.)

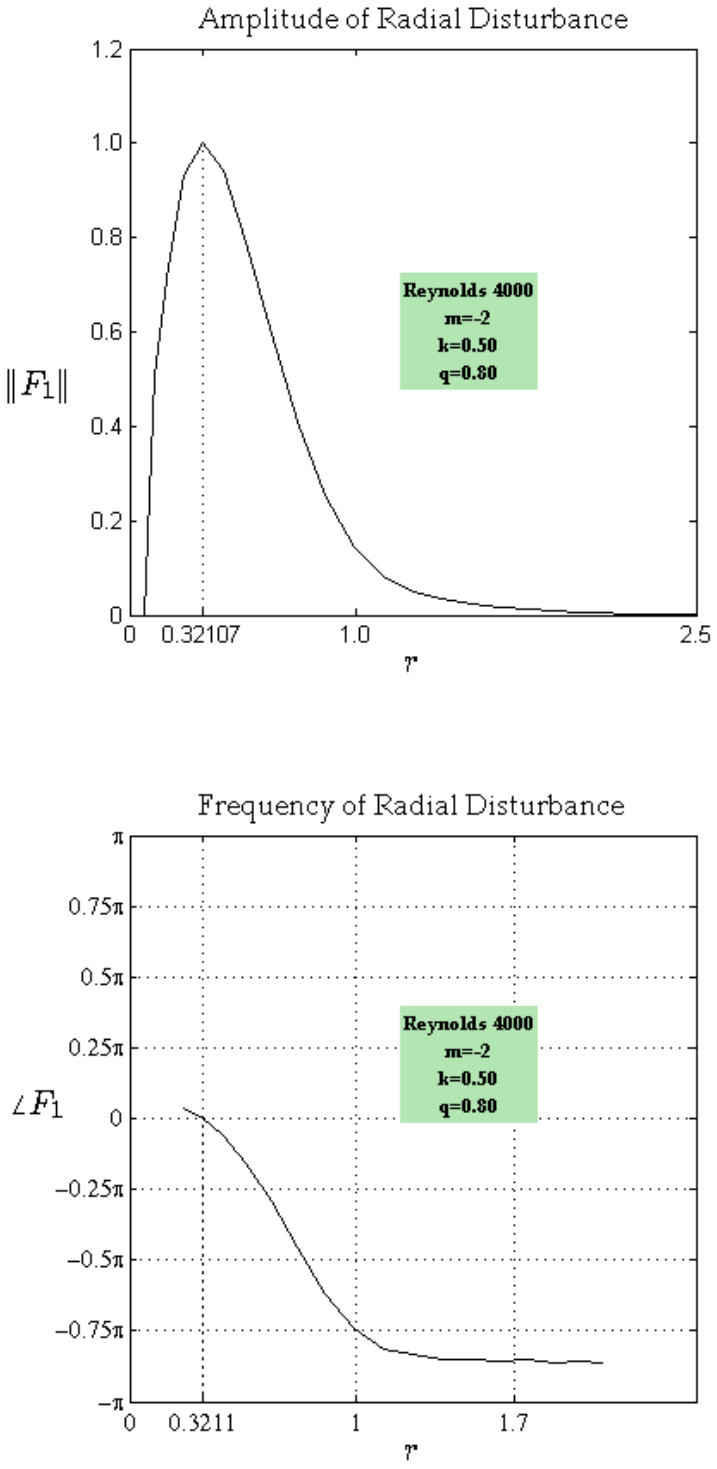

Figure 5-13 Propagation of radial asymmetric disturbance; intense vortex

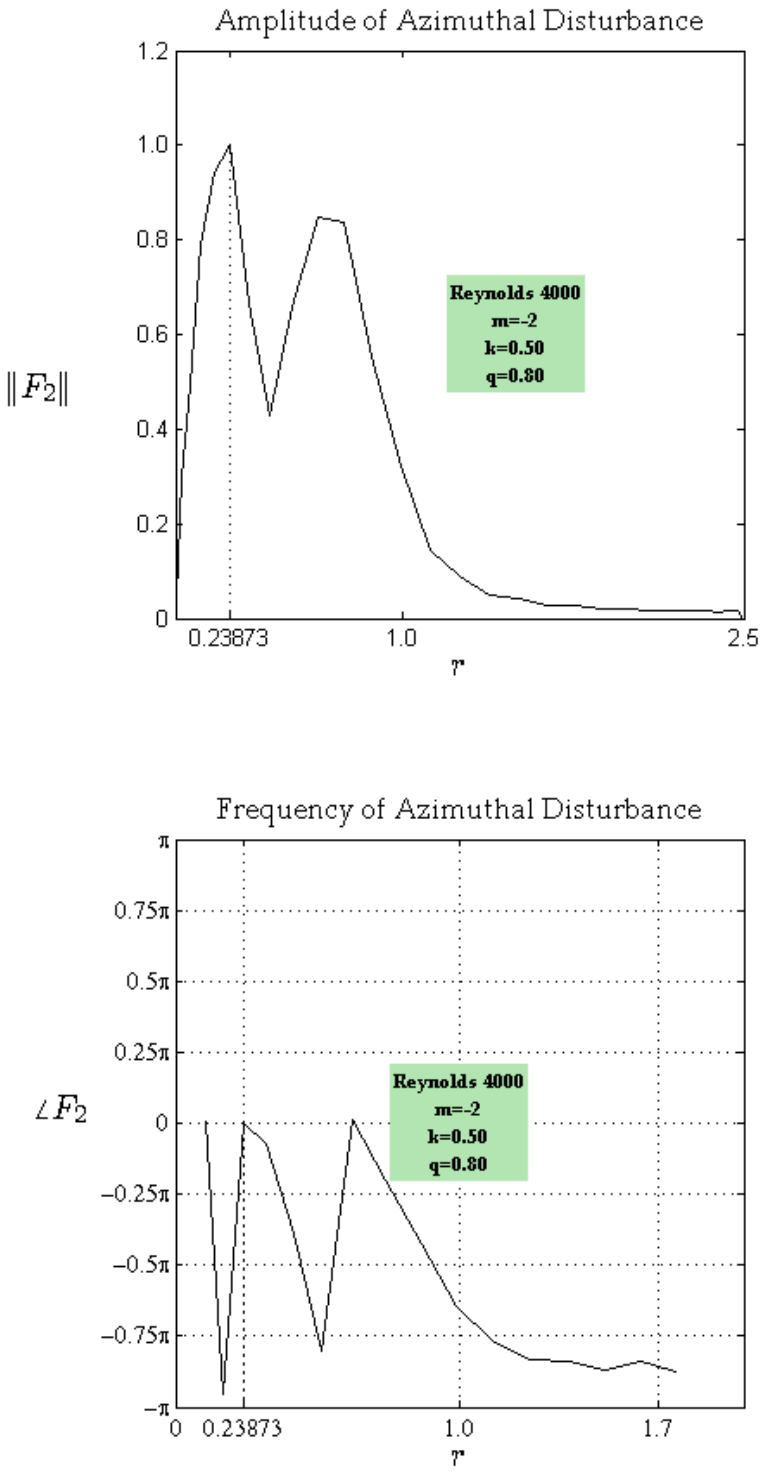

Figure 5-14 Propagation of azimuthal asymmetric disturbance; intense vortex

Table 5-1

q	k_{max}	$\omega_{i,max}$	$\frac{d\omega_r}{dk}$
0.19	0.626	0.1531	-0.64
0.4	0.942	0.2635	-0.64
1.1	0.879	0.2147	-0.89
m=-2, Reynolds=4000			

Figure 5-15 depicts the variations of growth rate ω_i with k for different swirl parameters. The disturbance is asymmetric (m=-2), Reynolds=4000, and q=0.19, 0.4, and 1.1. The main information was also summarized in Table 5-1.

As seen in a larger perspective, all profiles have similar quasi-parabolic pattern. However, the maximum growth rate and also the range of predominant instability depend strongly on the value of swirl quantity.

Inspecting figure 5-15 carefully, it can be observed that increasing the swirl quantity does not necessarily scale up/down the growth rate profile over k. Indeed, as the value of q increases from 0.19 to 0.4, both the peak of primary modes and the axial wave number range of predominant instabilities increase dramatically. Nevertheless, intensifying parameter from 0.4 to 1.1 decreases the scale of instability and shifts the growth rate curve to somewhere between the profile of q=0.19 and 0.4.

In conclusion, the swirl parameter strongly affects both the order of amplification of disturbances and the spectrum of travelling unstable waves. A maximum value shall exist for the value of swirl quantity for which the largest amplification rate occurs over the widest range of axial wave number. Furthermore, there should be also a critical swirl parameter, q_{cr} that represents the maximum destabilizing swirl parameter. For the

values of swirl quantity greater than q_{cr}, all instabilities decay in as much as the growth rate cross over the neutral stability curve.

Figure 5-16 displays the variations of ω_r of the primary mode with the axial wave number for different values values of swirl parameter. All the associated quantities are equivalent to those in figure 5-15. The sequence of values corresponds to quantities of "q". When q = 0.19, the slope is -0.64. At q = 0.40 the slope is slightly declined as compared to q = 0.19. At q = 1.10, the slope equals -0.89 which is at its most declined as compared to the other values of q. Consequently, as the graph shifts up, there is a sharper rate of declination that corresponds to higher group velocity. Therefore, stronger the vortex is, faster the asymmetric instability propagates, which is a generalized compliment of what was already discussed.

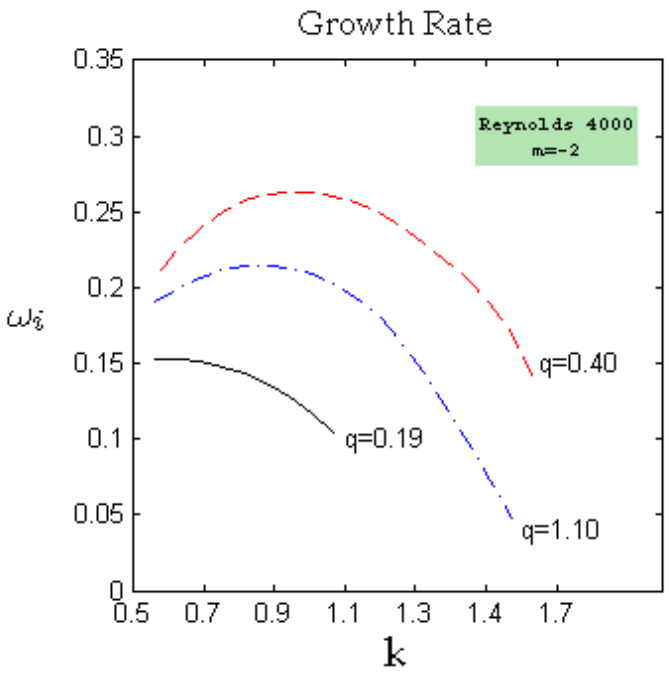

Figure 5-15 Effect of swirl parameter on the growth rate of, m=-2, q=0.19,0.4,1.1

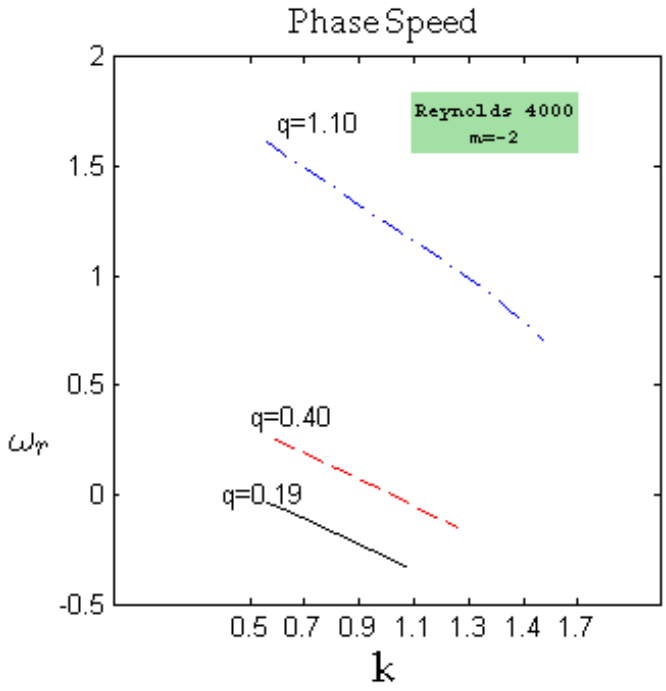

Figure 5-16 Effect of swirl parameter on the phase speed, m=-2, q=0.19,0.4,1.1

5.4 Effect of viscous forces on instabilities

The effect of Reynolds number on the asymmetric mode (m=-2) at q=0.8 is presented in figure 5-17 for two scenarios of axial wave number; k=0.70 and k=1.1. The primary and secondary modes were displayed with solid and dashed lines respectively.

The increase in growth rate over Reynolds number is noticeable. Thus, as the Reynolds number increases, the flow becomes more unstable. The secondary mode has the same variations but with a shift in the curve; since its growth rate is expectedly smaller than the primary mode.

It is evident that the growth rate varies more significantly in low Reynolds flow than high Reynolds flow. As the Reynolds number increases, it increases with lower rate and eventually reaches asymptotically to the value 0.251 for k=1.1 and 0.225 for k=0.7. Indeed, the stabilizing effect of viscous forces in low Reynolds number is the main decaying source. Accordingly, the instabilities become immune to viscous forces in high Reynolds number flows.

Figure 5-18 compares variations of ω_r for primary and secondary modes over Reynolds number for different values of k. The phase speeds of primary and secondary modes are not influenced significantly by Reynolds number. The asymptotical values are 0.916 and 0.574 for k=0.7 and k=1.1 respectively. An illustrative graph for the group speed is a matter of interest in investigating the effects of viscous forces. Unfortunately, the computational algorithm was not adequately rigorous to obtain those results.

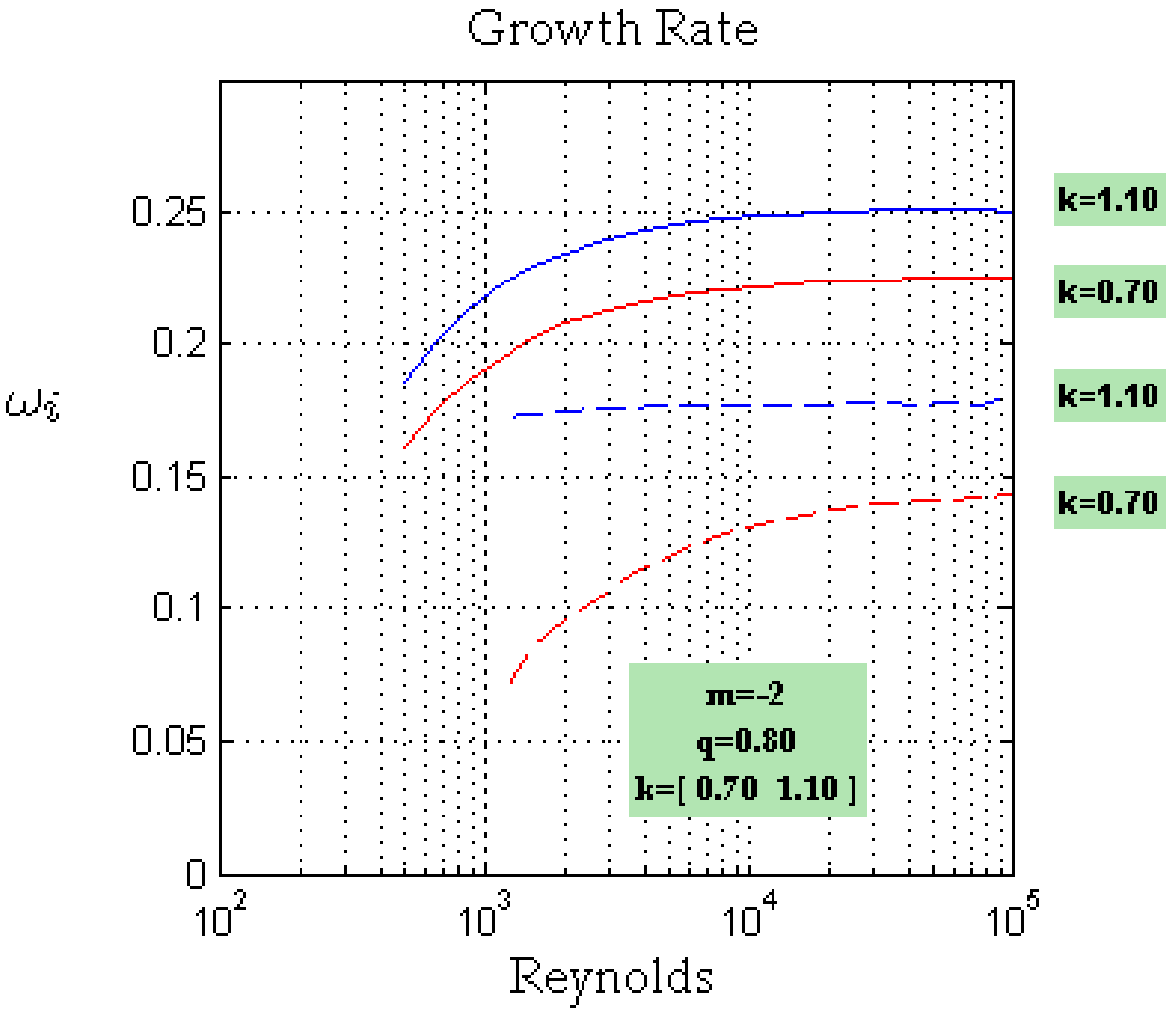

Figure 5-17 Growth Rate as a function of Reynolds number, m=-2, k=0.7,1.1

(The solid and dashed lines represent primary and secondary modes respectively.)

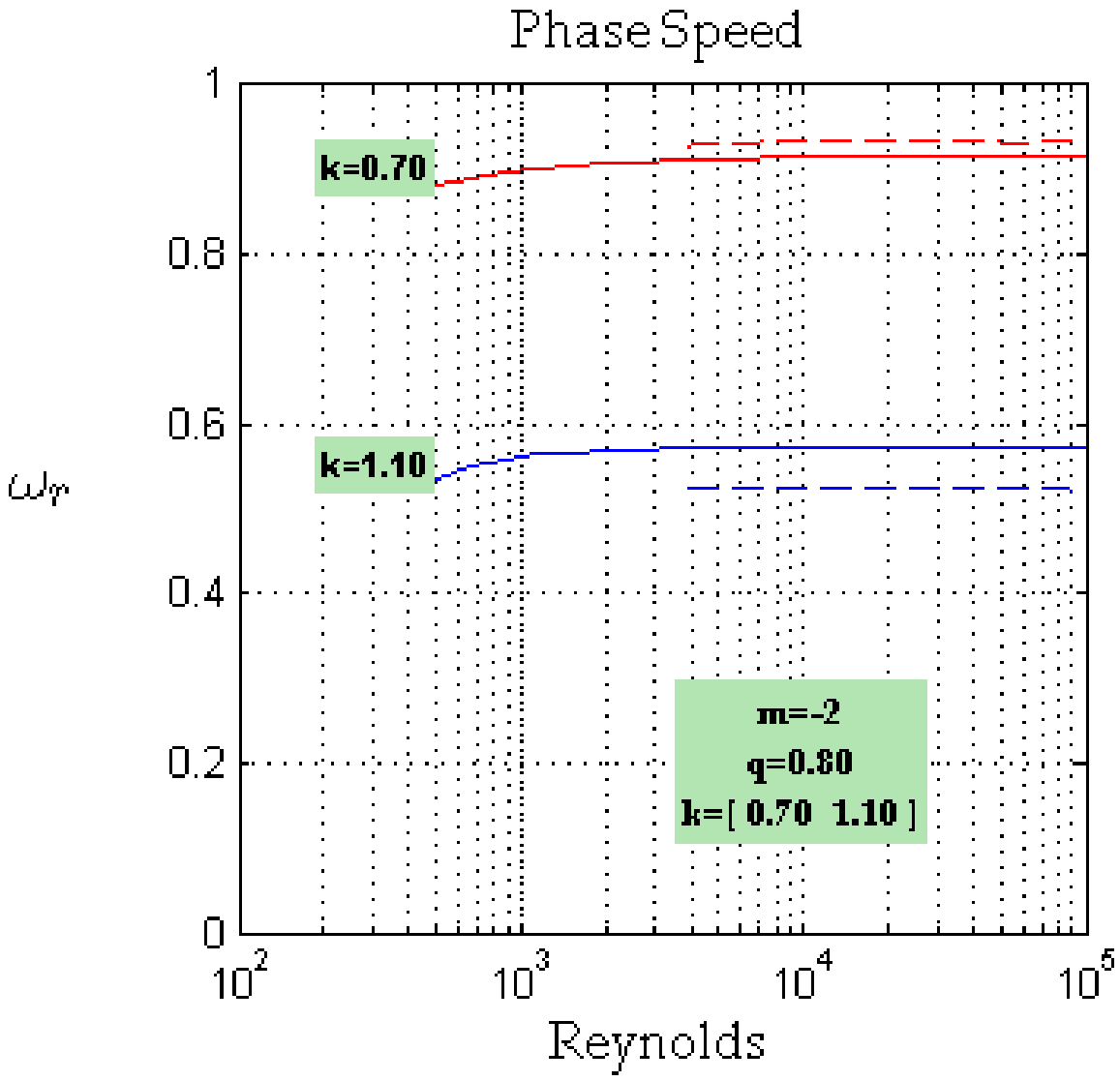

Figure 5-18 Phase Speed as a function of Reynolds number, m=-2, k=0.7,1.1

(The solid and dashed lines represent primary and secondary modes respectively.)

5.5 Topography of instabilities

The q-k plane was discretized and the growth rates were found at each point. An iterative method was employed to achieve convergent values for the growth rate. The entire unstable region was then mapped out with another subroutine. However, the algorithm did not adequately converge in the region close to the neutral stability. We attribute this to the singularity of eigensolutions for small growth rates. The curves of neutral stability are certainly of considerable interest and would be possibly a genuine topic for future studies.

The type of instability could be divided into two categories: long-wave type corresponding to smaller values of k, and short-wave type according to larger values of k. The outmost curve in the contour of growth rate is the neutral stability curve ($\omega_i = 0$).

Contours of growth rate for axisymmetric disturbance, m=-2 and Reynolds=100 are plotted in figure 5-19. An increment of 0.01 was considered for generating the contours. The flow is found to be entirely stable for swirl parameters larger than q_{cr}=1.52. This value as mentioned before is so-called critical swirl parameter and was evaluated to be around 1.5 for inviscid studies. The maximum growth rate equals 0.1837 occurring at q=0.586 and k=1.12. The unstable region is smooth everywhere. The range of unstable swirl is found out to be 0.1<q<1.5. Accordingly, the axial wave number of instabilities lies between 0.2 and 1.8.

Regarding the apex of the unstable region, the shortest unstable wavelength occurs at q=0.41. Accordingly, the largest axial wave number equals 1.82 for this swirl quantity. The border of the unstable region is the neutral stability curve and visibly distinguishable. It extends to shorter wavelength as the swirl parameter increases. This argument is supported by the positive slope on the bottom line of the unstable region in

figure 5-19. The strongest amplification of instabilities corresponds to the values of k is close to unity. Therefore, the axial wave number of unstable modes has as order of magnitude as the core radius (r_c).The shortwave limit is meaningfully determined by the largest axial wavenumber in the unstable region, which is the apex in contours. Here, it was found to be 1.82 for Reynolds=100. In the same manner, the zero-axis is the long-wave limit of instabilities. The unstable region in figure 5-19 lies near to the k=0 axis.

Figure 5-20 presents the topography of instabilities for the particular case of m=-2, Reynolds=1000. As mentioned before, the inner area is the unstable region and its border corresponds to neutral stability. Comparing figures 5-19 and 5-20, the unstable region is perceptibly extended as Reynolds number increases. The maximum growth rate is equal to 0.2895 at q=0.606 and k=1.15 (greater than figure 5-19). The critical swirl q_{cr} also increases roughly to 2.5. It was not possible to compute the value of swirl parameter for which the most shortwave instability happens, however the estimated value of 0.5 could be interpolated. Again, the unstable region looks to be fairly smooth. The growth rate goes smoothly toward zero as the swirl intensifies. There was also divergence in pseudo-spectral method for long wave disturbances (close to k=0 axis). Both the precision and convergence of the algorithm degrade for small values of k.

Ultimately, the topography of instability is mapped out in figure 5-21 for Reynolds equal to 10^4 and asymmetric disturbance (m=-2). The largest growth rate is found to be 0.3034 at q=0.606. In comparison, the largest growth rate in figure 5-21 is a bit greater than figure 5-20. But the values of q_{max} and k_{max} did not change. Thus, as Reynolds number increases, the value of swirl parameter and axial wave number for the most significant instability asymptote to a location in q-k plane. As seen in the plots, the numerical quality declines significantly for small magnitudes of growth rate. Thus, the results in the area close to the neutral stability would not be reliable.

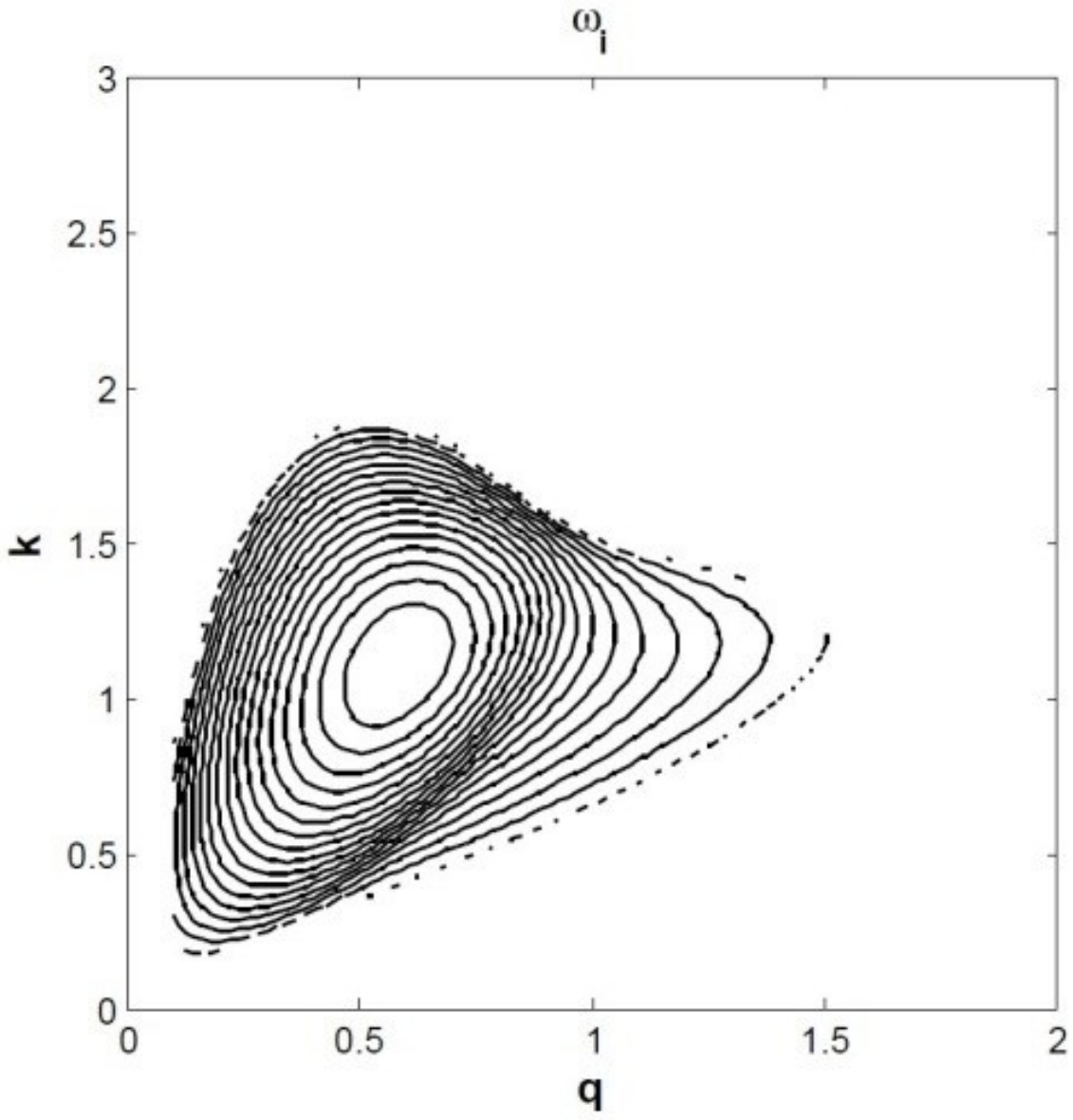

Figure 5-19 Contours of unstable region, m=-2, Reynolds=100

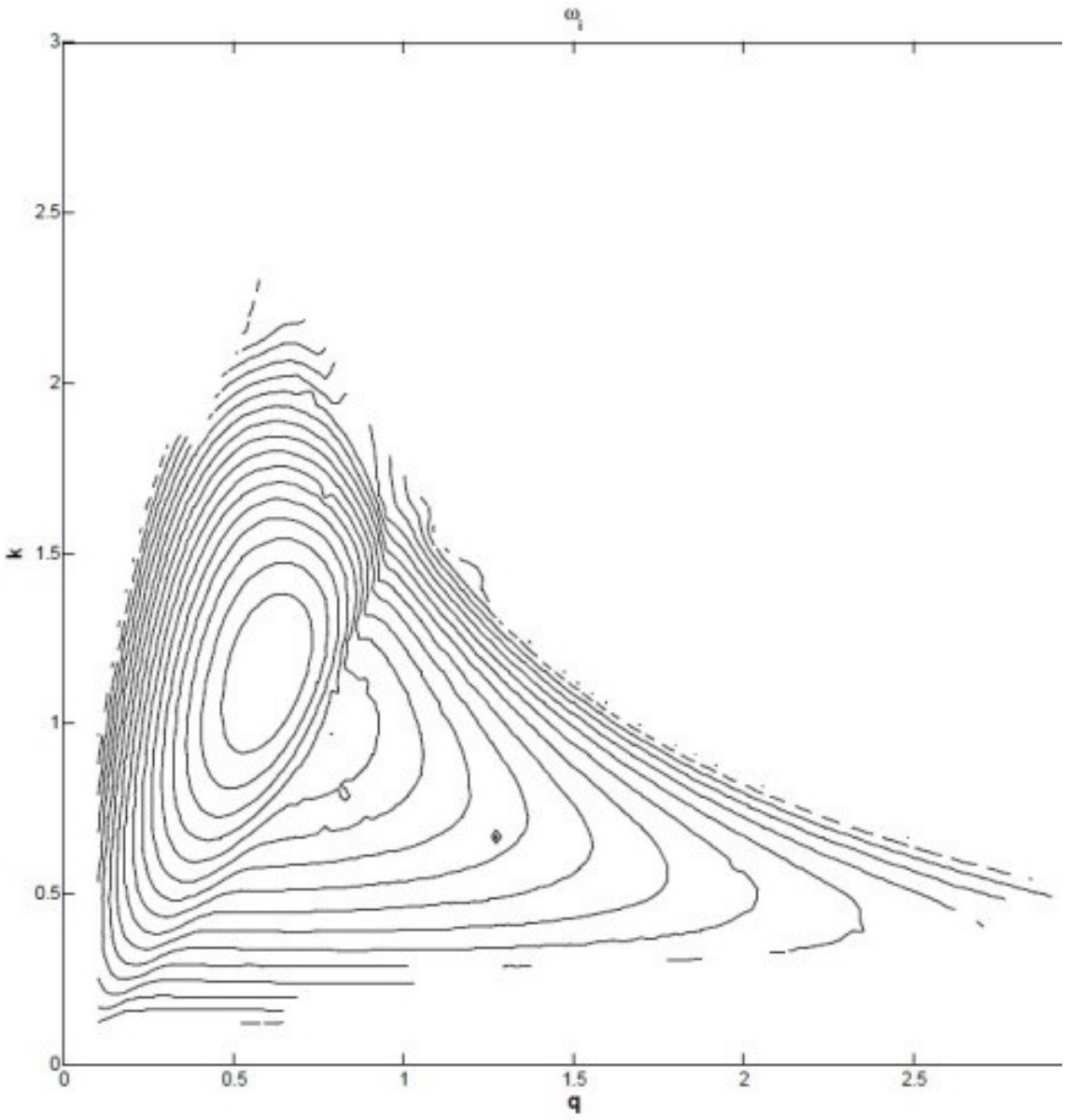

Figure 5-20 Contours of unstable region, m=-2, Reynolds=1000

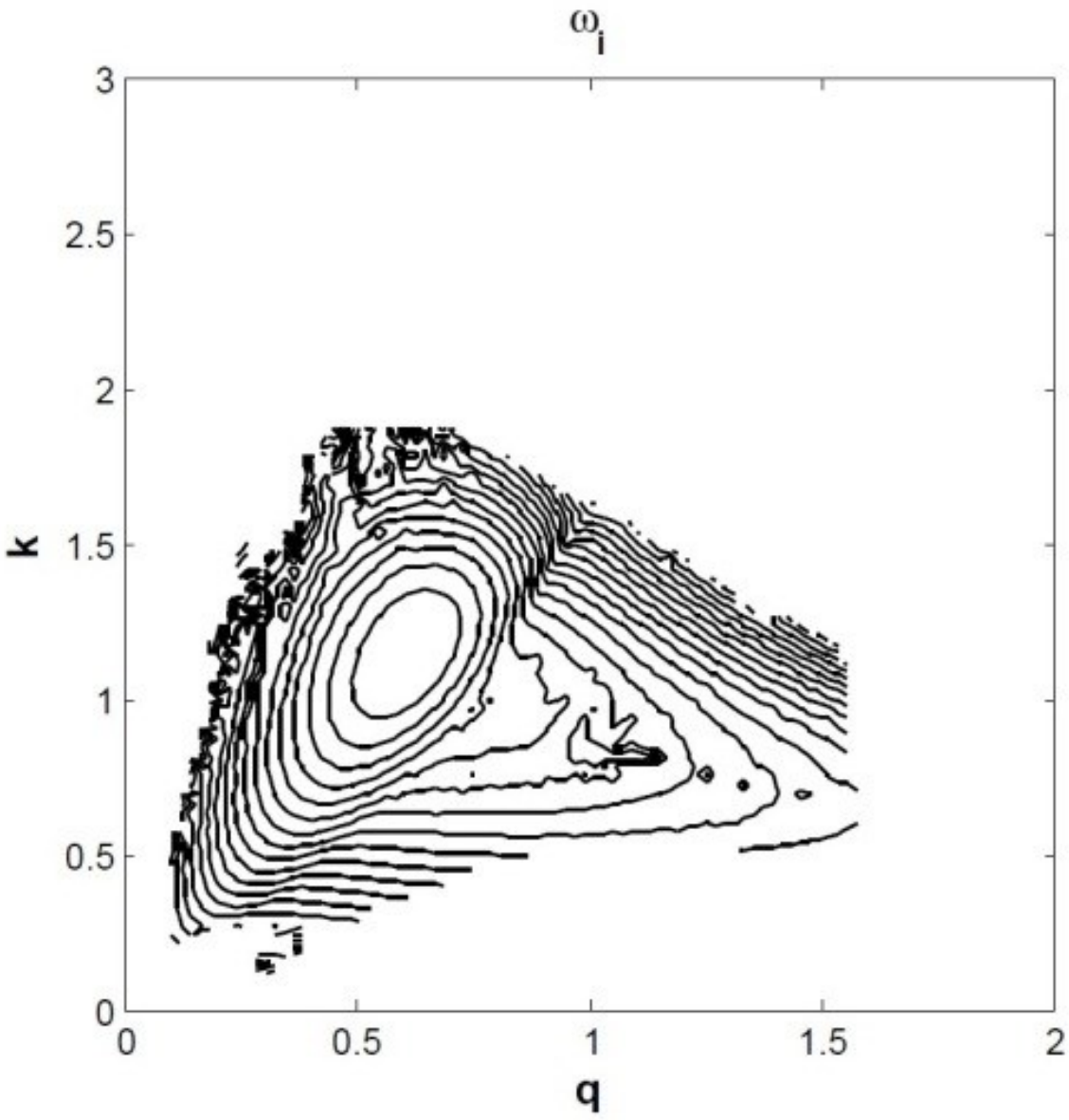

Figure 5-21 Contours of unstable region, m=-2, Reynolds=10000

6. Conclusion

In this study, the stability analysis of single cell unconfined columnar vortex was undertaken. The work parallels the investigation conducted with q-vortex model as the base flow. In the present study the azimuthal velocity in the q-vortex model is replaced by the azimuthal component of Vatistas vortex model. The base flow was subjected to three dimensional perturbation. The viscosity was included in the stability analysis. The perturbation equations were discretized using a pseudo-spectral method. The numerical code was validated by comparing the obtained results for the growth rate and topography of instability for the q-vortex model.

The evolutions of both axisymmetric and asymmetric disturbances were investigated. It was found that the asymmetrical instabilities occur comparatively at higher Reynolds number and in short-wave form and are resilient and stationary.

The results showed that intensifying the swirl has a drastic impact on the nature of the instability. In fact the instability switches from centre modes into annular modes. In an intense vortex, the instabilities propagates faster and their spectre is larger. Investigating the impact of Reynolds number, it was shown that the stronger the viscous forces are, the smaller the growth rate of instabilities is. The viscosity stabilises the vortex. Topographies of instabilities were mapped out for three different Reynolds number. As a result, the critical swirl quantity was found to be larger than inviscid threshold for stabilizing the flow; $q_{cr}>1.5$. Note that this critical value was recently re-evaluated and found equal to 2.3.

The maximum amplification rate was found to be when $q \approx 0.5$, which approximately coincided with the largest range of axial wavenumber and the shortwave limit which was about $k \approx 2.00$. The last results point out that major instabilities travel in the vortex having the same order of axial wave number as the core radius.

Similarly to the algorithm implemented by others, the present code did not produce reliable results in the region close to the neutral stability curve. This is because the singularities (critical layer) that needs a special treatments. One of the option to cure this drawback in is to embed a continuation method together with changing the integration path to ovoid the singularities at critical layer (critical radius). This can serve as guide for future work and we believe that this will overcome the difficulties that were faced at high Reynolds number, known in the studies of inviscid stability problems.

It was also discovered that changing R affects the convergence of the numerical solution. Thus, it is suggested that the maximum radius R be redefined in each iteration. In this way, better convergence would be obtained as the distribution of collocation points is manipulated. There is no doubt that more complication will be added as well.

A variety of new subtopics could be prospectively considered. Determining the neutral stability curve would be a beneficial analysis and could be considered as a case-study in future. Another open topic is the determination of the most amplified mode among all range of azimuthal wavenumber and the entire spectrum of eigensolutions. Another direction of future is to consider a stability full Vatistas model not just its tangential velocity.

The numerical procedure presented here lays the foundation of viscous stability analysis by pseudo-spectral method. The algorithm could be used as a valuable tool in

disseminating the knowledge of vortex stability. In addition, the program could be extended to be used in more complicated cases like compressible stability analysis.

"End"

Appendix A

Pseudo-spectral method with chebychev collocation

The Chebychev polynomial of degree n, $T_n(x)$, is defined by:

$$T_n(\cos\theta) = \cos(n\theta) \qquad \text{(A-1)}$$

Thus, by considering $x = \cos\theta$, the first five terms are:

$T_1(x) = 1$

$T_2(x) = x$

$T_3(x) = 2x^2 - 1$

$T_4(x) = 4x^3 - 3x$

$T_5(x) = 8x^4 - 8x^2 + 1$

...

Chebychev polynomials are the eigenfunctions of the singular Sturm-Liouville problem :

$$\frac{d}{dx}\left(p(x)\frac{d\phi_n}{dx}\right) + \big(\lambda_n w(x) - q(x)\big)\phi_n(x) = 0$$

with $p(x) = \sqrt{1-x^2}$, $w(x) = 1/\sqrt{1-x^2}$, $q(x) = 0$, $-1 \le x \le 1$, and the boundary conditions that $\phi_n(\pm 1)$ be finite[17]. The eigenvalues corresponding to $T_n(x)$ is $\lambda_n = n^2$. Hence, they satisfy the orthogonality relation

$$\langle T_n, T_m\rangle = \int_{-1}^{1} T_n(x)T_m(x)\,(1-x^2)^{-1/2}dx = \int_0^{\pi} \cos(n\theta)\cos(m\theta)d\theta \qquad \text{(A-2)}$$

$$= \begin{cases} 0 & (n \neq m) \\ \pi & (n = m = 1) \\ \dfrac{\pi}{2} & (n = m > 1) \end{cases}$$

Some properties of these bases are:

$$T_n(x) = 2xT_{n-1}(x) - T_{n-2}(x) \qquad n > 2$$

$$|T_n(x)| \le 1 \quad , |T_n{}'(x)| \le n^2$$

$$\frac{d^p}{dx^p} T_n(\pm 1) = (\pm 1)^{n+p} \prod_{k=0}^{p} \frac{n^2 - k^2}{2k+1} \tag{A-3}$$

Notice that is our study, the index of $T_n(x)$ was shifted by one unit and saved into the new functional vectors $\Gamma_n(y)$ as

$$\Gamma_n(y) = T_n(x)|_{x \to y;\, n \to n-1} = T_{n-1}(y)$$

As shown in §(3-1), we need to solve the eigenvalue problem in (3-2) for the entire domain at one time by deriving a compact correlation. The amplitude F_1 (y) was approximated in the subspace $\mathcal{R}_M = span\{\boldsymbol{\Phi}_1(y), \boldsymbol{\Phi}_2(y), \dots, \boldsymbol{\Phi}_M(y)\}$ and amplitude F_2 (y) in the subspace $\mathcal{R}_{M-2} = span\{\boldsymbol{\Psi}_n(y), \boldsymbol{\Psi}_n(y), \dots, \boldsymbol{\Psi}_n(y)\}$ and as equation (3-4) which we plug into the local LPE (3-6) and obtain:

$$\boldsymbol{\omega} \begin{bmatrix} L_{11}\rfloor_{@y_s} & L_{12}\rfloor_{@y_s} \\ L_{21}\rfloor_{@y_s} & L_{22}\rfloor_{@y_s} \end{bmatrix} \begin{bmatrix} \sum_{n=1}^{M} \phi_n \boldsymbol{\Phi}_n(y) \\ \sum_{n=1}^{M-2} \psi_n \boldsymbol{\Psi}_n(y) \end{bmatrix} = \begin{bmatrix} R_{11}\rfloor_{@y_s} & R_{12}\rfloor_{@y_s} \\ R_{21}\rfloor_{@y_s} & R_{22}\rfloor_{@y_s} \end{bmatrix} \begin{bmatrix} \sum_{n=1}^{M} \phi_n \boldsymbol{\Phi}_n(y) \\ \sum_{n=1}^{M-2} \psi_n \boldsymbol{\Psi}_n(y) \end{bmatrix}; \; s = 1,2,3,..,M \tag{A-4}$$

Notice that coefficients ϕ_n and ψ_n in (3-5) represent the weight of series expansion respectively on the modified chebychev basis $\{\boldsymbol{\Phi}_n\}_{n=1}^{M}$ and $\{\boldsymbol{\Psi}_n\}_{n=1}^{M-2}$. Hence, when derivational operators are applied they should come out of any expression. Thereon, equation (A-4) can be rewritten as

$$\begin{aligned} &\omega\left(\phi_1 L_{11}\{\boldsymbol{\Phi}_1(y)\}_{@y_s} + \phi_2 L_{11}\{\boldsymbol{\Phi}_2(y)\}_{@y_s} + \dots + \phi_M L_{11}\{\boldsymbol{\Phi}_M(y)\}_{@y_s}\right) \\ &+\omega\left(\psi_1 L_{12}\{\boldsymbol{\Psi}_1(y)\}_{@y_s} + \psi_2 L_{12}\{\boldsymbol{\Psi}_2(y)\}_{@y_s} + \dots + \psi_{M-2} L_{12}\{\boldsymbol{\Psi}_{M-2}(y)\}_{@y_s}\right) \\ &= \\ &\left(\phi_1 R_{11}\{\boldsymbol{\Phi}_1(y)\}_{@y_s} + \phi_2 R_{11}\{\boldsymbol{\Phi}_2(y)\}_{@y_s} + \dots + \phi_M R_{11}\{\boldsymbol{\Phi}_M(y)\}_{@y_s}\right) \\ &+\left(\psi_1 R_{12}\{\boldsymbol{\Psi}_1(y)\}_{@y_s} + \psi_2 R_{12}\{\boldsymbol{\Psi}_2(y)\}_{@y_s} + \dots + \psi_{M-2} R_{12}\{\boldsymbol{\Psi}_{M-2}(y)\}_{@y_s}\right) \end{aligned} \tag{A-5 a}$$

$$\omega\left(\phi_1 L_{21}\{\boldsymbol{\Phi}_1(y)\}_{@y_s} + \phi_2 L_{21}\{\boldsymbol{\Phi}_2(y)\}_{@y_s} + \ldots + \phi_M L_{21}\{\boldsymbol{\Phi}_M(y)\}_{@y_s}\right)$$

$$+\omega\left(\psi_1 L_{22}\{\boldsymbol{\Psi}_1(y)\}_{@y_s} + \psi_2 L_{22}\{\boldsymbol{\Psi}_2(y)\}_{@y_s} + \ldots + \psi_{M-2} L_{22}\{\boldsymbol{\Psi}_{M-2}(y)\}_{@y_s}\right) \quad \text{(A-5 b)}$$

$$=$$

$$\left(\phi_1 R_{21}\{\boldsymbol{\Phi}_1(y)\}_{@y_s} + \phi_2 R_{21}\{\boldsymbol{\Phi}_2(y)\}_{@y_s} + \ldots + \phi_M R_{21}\{\boldsymbol{\Phi}_M(y)\}_{@y_s}\right)$$

$$+\left(\psi_1 R_{22}\{\boldsymbol{\Psi}_1(y)\}_{@y_s} + \psi_2 R_{22}\{\boldsymbol{\Psi}_2(y)\}_{@y_s} + \ldots + \psi_{M-2} R_{22}\{\boldsymbol{\Psi}_{M-2}(y)\}_{@y_s}\right)$$

Expanding (A-5) for $3 \le s \le M-2$ and collect all coefficients for weight variables ϕ_i and ψ_i (i=1, 2, 3, ..., M) in matrix form as (A-6)

$$\boldsymbol{\omega}\begin{bmatrix} L_{11}\{\boldsymbol{\Phi}_1(y)\}_{@y_3} & \cdots & L_{11}\{\boldsymbol{\Phi}_5(y)\}_{@y_3} & \cdots & L_{11}\{\boldsymbol{\Phi}_M(y)\}_{@y_3} \\ L_{11}\{\boldsymbol{\Phi}_1(y)\}_{@y_4} & \cdots & L_{11}\{\boldsymbol{\Phi}_5(y)\}_{@y_4} & \cdots & L_{11}\{\boldsymbol{\Phi}_M(y)\}_{@y_4} \\ \vdots & & \vdots & \ddots & \vdots \\ L_{11}\{\boldsymbol{\Phi}_1(y)\}_{@y_{M-2}} & \cdots & L_{11}\{\boldsymbol{\Phi}_5(y)\}_{@y_{M-2}} & \cdots & L_{11}\{\boldsymbol{\Phi}_M(y)\}_{@y_{M-2}} \end{bmatrix}\begin{bmatrix} \phi_1 \\ \phi_2 \\ \vdots \\ \phi_{M-2} \\ \phi_{M-1} \\ \phi_M \end{bmatrix}$$

$$+\boldsymbol{\omega}\begin{bmatrix} L_{12}\{\boldsymbol{\Psi}_1(y)\}_{@y_3} & L_{12}\{\boldsymbol{\Psi}_2(y)\}_{@y_3} & L_{12}\{\boldsymbol{\Psi}_3(y)\}_{@y_3} & \cdots & L_{12}\{\boldsymbol{\Psi}_{M-2}(y)\}_{@y_3} & 0 & 0 \\ L_{12}\{\boldsymbol{\Psi}_1(y)\}_{@y_4} & L_{12}\{\boldsymbol{\Psi}_2(y)\}_{@y_4} & L_{12}\{\boldsymbol{\Psi}_3(y)\}_{@y_4} & \cdots & L_{12}\{\boldsymbol{\Psi}_{M-2}(y)\}_{@y_4} & 0 & 0 \\ \vdots & \vdots & \vdots & \ddots & \vdots & 0 & 0 \\ L_{12}\{\boldsymbol{\Psi}_1(y)\}_{@y_{M-2}} & L_{12}\{\boldsymbol{\Psi}_2(y)\}_{@y_{M-2}} & L_{12}\{\boldsymbol{\Psi}_3(y)\}_{@y_{M-2}} & \cdots & L_{12}\{\boldsymbol{\Psi}_{M-2}(y)\}_{@y_{M-2}} & 0 & 0 \end{bmatrix}\begin{bmatrix} \psi_1 \\ \psi_2 \\ \vdots \\ \psi_{M-2} \\ 0 \\ 0 \end{bmatrix}$$

$$=$$

$$\begin{bmatrix} R_{11}\{\boldsymbol{\Phi}_1(y)\}_{@y_3} & \cdots & R_{11}\{\boldsymbol{\Phi}_5(y)\}_{@y_3} & \cdots & R_{11}\{\boldsymbol{\Phi}_M(y)\}_{@y_3} \\ R_{11}\{\boldsymbol{\Phi}_1(y)\}_{@y_4} & \cdots & R_{11}\{\boldsymbol{\Phi}_5(y)\}_{@y_4} & \cdots & R_{11}\{\boldsymbol{\Phi}_M(y)\}_{@y_4} \\ \vdots & & \vdots & \ddots & \vdots \\ R_{11}\{\boldsymbol{\Phi}_1(y)\}_{@y_{M-2}} & \cdots & R_{11}\{\boldsymbol{\Phi}_5(y)\}_{@y_{M-2}} & \cdots & R_{11}\{\boldsymbol{\Phi}_M(y)\}_{@y_{M-2}} \end{bmatrix}\begin{bmatrix} \phi_1 \\ \phi_2 \\ \vdots \\ \phi_{M-2} \\ \phi_{M-1} \\ \phi_M \end{bmatrix}$$

$$+\begin{bmatrix} R_{12}\{\boldsymbol{\Psi}_1(y)\}_{@y_3} & R_{12}\{\boldsymbol{\Psi}_2(y)\}_{@y_3} & R_{12}\{\boldsymbol{\Psi}_3(y)\}_{@y_3} & \cdots & R_{12}\{\boldsymbol{\Psi}_{M-2}(y)\}_{@y_3} & 0 & 0 \\ R_{12}\{\boldsymbol{\Psi}_1(y)\}_{@y_4} & R_{12}\{\boldsymbol{\Psi}_2(y)\}_{@y_4} & R_{12}\{\boldsymbol{\Psi}_3(y)\}_{@y_4} & \cdots & R_{12}\{\boldsymbol{\Psi}_{M-2}(y)\}_{@y_4} & 0 & 0 \\ \vdots & \vdots & \vdots & \ddots & \vdots & 0 & 0 \\ R_{12}\{\boldsymbol{\Psi}_1(y)\}_{@y_{M-2}} & R_{12}\{\boldsymbol{\Psi}_2(y)\}_{@y_{M-2}} & R_{12}\{\boldsymbol{\Psi}_3(y)\}_{@y_{M-2}} & \cdots & R_{12}\{\boldsymbol{\Psi}_{M-2}(y)\}_{@y_{M-2}} & 0 & 0 \end{bmatrix}\begin{bmatrix} \psi_1 \\ \psi_2 \\ \vdots \\ \psi_{M-2} \\ 0 \\ 0 \end{bmatrix} \quad \text{(A-6-a)}$$

And

$$
\omega\begin{bmatrix} L_{21}\{\boldsymbol{\Phi}_1(y)\}_{@y_3} & \cdots & L_{21}\{\boldsymbol{\Phi}_5(y)\}_{@y_3} & \cdots & L_{21}\{\boldsymbol{\Phi}_M(y)\}_{@y_3} \\ L_{21}\{\boldsymbol{\Phi}_1(y)\}_{@y_4} & \cdots & L_{21}\{\boldsymbol{\Phi}_5(y)\}_{@y_4} & \cdots & L_{21}\{\boldsymbol{\Phi}_M(y)\}_{@y_4} \\ \vdots & & \vdots & \ddots & \vdots \\ L_{21}\{\boldsymbol{\Phi}_1(y)\}_{@y_{M-2}} & \cdots & L_{21}\{\boldsymbol{\Phi}_5(y)\}_{@y_{M-2}} & \cdots & L_{21}\{\boldsymbol{\Phi}_M(y)\}_{@y_{M-2}} \end{bmatrix}\begin{bmatrix} \phi_1 \\ \phi_2 \\ \vdots \\ \phi_{M-2} \\ \phi_{M-1} \\ \phi_M \end{bmatrix}
$$

$$
+\omega\begin{bmatrix} L_{22}\{\boldsymbol{\Psi}_1(y)\}_{@y_3} & L_{22}\{\boldsymbol{\Psi}_2(y)\}_{@y_3} & L_{22}\{\boldsymbol{\Psi}_3(y)\}_{@y_3} & \cdots & L_{22}\{\boldsymbol{\Psi}_{M-2}(y)\}_{@y_3} & 0 & 0 \\ L_{22}\{\boldsymbol{\Psi}_1(y)\}_{@y_4} & L_{22}\{\boldsymbol{\Psi}_2(y)\}_{@y_4} & L_{22}\{\boldsymbol{\Psi}_3(y)\}_{@y_4} & \cdots & L_{22}\{\boldsymbol{\Psi}_{M-2}(y)\}_{@y_4} & 0 & 0 \\ \vdots & \vdots & \vdots & \ddots & \vdots & 0 & 0 \\ L_{22}\{\boldsymbol{\Psi}_1(y)\}_{@y_{M-2}} & L_{22}\{\boldsymbol{\Psi}_2(y)\}_{@y_{M-2}} & L_{22}\{\boldsymbol{\Psi}_3(y)\}_{@y_{M-2}} & \cdots & L_{22}\{\boldsymbol{\Psi}_{M-2}(y)\}_{@y_{M-2}} & 0 & 0 \end{bmatrix}\begin{bmatrix} \psi_1 \\ \psi_2 \\ \vdots \\ \psi_{M-2} \\ 0 \\ 0 \end{bmatrix}
$$

$$
=
$$

$$
\begin{bmatrix} R_{21}\{\boldsymbol{\Phi}_1(y)\}_{@y_3} & \cdots & R_{21}\{\boldsymbol{\Phi}_5(y)\}_{@y_3} & \cdots & R_{21}\{\boldsymbol{\Phi}_M(y)\}_{@y_3} \\ R_{21}\{\boldsymbol{\Phi}_1(y)\}_{@y_4} & \cdots & R_{21}\{\boldsymbol{\Phi}_5(y)\}_{@y_4} & \cdots & R_{21}\{\boldsymbol{\Phi}_M(y)\}_{@y_4} \\ \vdots & & \vdots & \ddots & \vdots \\ R_{21}\{\boldsymbol{\Phi}_1(y)\}_{@y_{M-2}} & \cdots & R_{21}\{\boldsymbol{\Phi}_5(y)\}_{@y_{M-2}} & \cdots & R_{21}\{\boldsymbol{\Phi}_M(y)\}_{@y_{M-2}} \end{bmatrix}\begin{bmatrix} \phi_1 \\ \phi_2 \\ \vdots \\ \phi_{M-2} \\ \phi_{M-1} \\ \phi_M \end{bmatrix}
$$

$$
+\begin{bmatrix} R_{22}\{\boldsymbol{\Psi}_1(y)\}_{@y_3} & R_{22}\{\boldsymbol{\Psi}_2(y)\}_{@y_3} & R_{22}\{\boldsymbol{\Psi}_3(y)\}_{@y_3} & \cdots & R_{22}\{\boldsymbol{\Psi}_{M-2}(y)\}_{@y_3} & 0 & 0 \\ R_{22}\{\boldsymbol{\Psi}_1(y)\}_{@y_4} & R_{22}\{\boldsymbol{\Psi}_2(y)\}_{@y_4} & R_{22}\{\boldsymbol{\Psi}_3(y)\}_{@y_4} & \cdots & R_{22}\{\boldsymbol{\Psi}_{M-2}(y)\}_{@y_4} & 0 & 0 \\ \vdots & \vdots & \vdots & \ddots & \vdots & 0 & 0 \\ R_{22}\{\boldsymbol{\Psi}_1(y)\}_{@y_{M-2}} & R_{22}\{\boldsymbol{\Psi}_2(y)\}_{@y_{M-2}} & R_{22}\{\boldsymbol{\Psi}_3(y)\}_{@y_{M-2}} & \cdots & R_{22}\{\boldsymbol{\Psi}_{M-2}(y)\}_{@y_{M-2}} & 0 & 0 \end{bmatrix}\begin{bmatrix} \psi_1 \\ \psi_2 \\ \vdots \\ \psi_{M-2} \\ 0 \\ 0 \end{bmatrix}
$$

(A-6-b)

which enables us to extract a compact eigenvalue problem for discretized LPE.

Appendix B

Source program

```
function
[w_r,w_i,F1,F2,AMP1,FRQ1,AMP2,FRQ2]=Stability_Spectrum(model,number_mode,chebychev_number
,azimuthal_number,axial_number,vortex_intensity,reynolds,radius_max)

M=chebychev_number;
L=zeros(2*M-8,2*M-8);
R=zeros(2*M-8,2*M-8);
[Phi,Psi]=Collocation_Basis(chebychev_number,azimuthal_number);
for i=1:M-4

               [L11,L21,L12,L22,R11,R21,R12,R22]=Discretized_LPE(model,chebychev_number,a
               zimuthal_number,axial_number,vortex_intensity,reynolds,radius_max,Phi,Psi,
               i+2);

               L(i,1:M-4)=L11(5:M);
               L(i,M-3:2*M-8)=L12(3:M-2);
               L(i+M-4,1:M-4)=L21(5:M);
               L(i+(M-4),M-3:2*M-8)=L22(3:M-2);

               R(i,1:M-4)=R11(5:M);
               R(i,M-3:2*M-8)=R12(3:M-2);
               R(i+M-4,1:M-4)=R21(5:M);
               R(i+(M-4),M-3:2*M-8)=R22(3:M-2);

end

nmod=number_mode;                                          % numbers of mode

[Eigenvector,Eigenvalue]=eigs(L\R,nmod,'LR');     % eigensolutions for the multiple modes
w_r=real(Eigenvalue(logical(eye(size(Eigenvalue)))));
w_i=imag(Eigenvalue(logical(eye(size(Eigenvalue)))));

y=-cos(([1:M]-ones(1,M))*pi/(M-1));

FF1=zeros(M,nmod);     % Total amplitude of radial disturbance
FF2=zeros(M,nmod);     % Total amplitude of azimuthal disturbance

weight=zeros(1,M);
basis=zeros(1,M);
phi=weight;  % the weights of projection of the radial amplitude
Phi_s=basis; % Local amount of the modified chebychev basis in radial dimension
psi=weight;
Psi_s=basis;

for kk=1:nmod
   for s=5:M
      for j=5:M
         phi(1,j)=Eigenvector(j-4,kk);
         Phi_s(1,j)=polyval(Phi(j,:),y(s));
      end
      FF1(s,kk)=sum(phi.*Phi_s);
   end
```

```
   for s=3:M-2
      for j=3:M-2
         psi(1,j)=Eigenvector(j+M-6,kk);
         Psi_s(1,j)=polyval(Psi(j,:),y(s));
      end
      FF2(s,kk)=sum(psi.*Psi_s);
   end
end
F1=sign(real(FF1)).*FF1;
F2=sign(real(FF2)).*FF2;
AMP1=abs(F1);
FRQ1=angle(F1);
AMP2=abs(F2);
FRQ2=angle(F2);


function
[L11,L21,L12,L22,R11,R21,R12,R22]=Discretized_LPE(model,Cheb_No,Azimuthal_No,Axial_No,Vor
x_inten,Reynolds,Rad_Region,Phi,Psi,index)
%% Chebyshev Polynomials
M=Cheb_No;
m=Azimuthal_No;
k=Axial_No;
q=Vorx_inten;
Rey=Reynolds;
RR=Rad_Region;
Y_i=-cos(((index-1)*pi)/(M-1));    % Discretization
Rad=RR/2*(Y_i+1);                  % Mapping r to y
r=Rad;

%%  Defining Coefficients in Operators;

Z=2/RR;                            %chain rule    dy/dr
if strcmp(model,'Vatistas')        % Vatistas Model
   U=exp(-r^2);
   diff_U=-2*r*exp(-r^2);
   diff2_U=-2*exp(-r^2)-2*r*(-2*r*exp(-r^2));
   W=q*r/sqrt((1+r^4));
   diff_W=q*(1-r^4)/(1+r^4)^1.5;
   f=k^2+m^2/r^2+1i*k*U*Rey+1i*m*W*Rey/r;
   diff_f=-2*m^2/r^3+1i*k*Rey*diff_U+1i*m*Rey*(1/r*diff_W-1/r^2*W);
   E=W/r+diff_W;
end

if strcmp(model,'Batchelor')       % Batchelor Model
   U=exp(-r^2);
   diff_U=-2*r*exp(-r^2);
   diff2_U=-2*exp(-r^2)-2*r*(-2*r*exp(-r^2));
   W=q/r*(1-exp(-r^2));
   diff_W=-q/r^2*(1-exp(-r^2))+q/r*(2*r*exp(-r^2));
   f=k^2+m^2/r^2+1i*k*U*Rey+1i*m*W*Rey/r;
   diff_f=-2*m^2/r^3+1i*k*Rey*diff_U+1i*m*Rey*(1/r*diff_W-1/r^2*W);
   E=W/r+diff_W;
end

   if strcmp(model,'Modified Batchelor')    % Modified Batchelor Model
   U=exp(-r^2);
   diff_U=-2*r*exp(-r^2);
   diff2_U=-2*exp(-r^2)-2*r*(-2*r*exp(-r^2));
   W=q/r*(1-exp(-1.256*r^2));
   diff_W=-q/r^2*(1-exp(-1.256*r^2))+q/r*(2*1.256*r*exp(-1.256*r^2));
   f=k^2+m^2/r^2+1i*k*U*Rey+1i*m*W*Rey/r;
   diff_f=-2*m^2/r^3+1i*k*Rey*diff_U+1i*m*Rey*(1/r*diff_W-1/r^2*W);
   E=W/r+diff_W;
end

%%   Evaluating L11_p(Phi(y))
L11_p=zeros(M,M+1);
for i=1:M
   Phi_i=Phi(i,M-i+2:M+1);
   L11_1=Rey*Z*polyder(Z*polyder(Phi_i));
```

```
   L11_2=Rey*1/r*Z*polyder(Phi_i);
   L11_3=Rey*(-1/r^2-k^2)*Phi_i;

   [bb,i_max]=polyadds(L11_1,L11_2,L11_3);
   L11_p(i,M+2-i_max:M+1)=bb;
end

%%   Evaluating L21_p(Phi(y))
L21_p=zeros(M,M+1);
for i=1:M
   Phi_i=Phi(i,M-i+2:M+1);
   L21_1=(-1i*m/k^2)*(1/r)*Z*polyder(Phi_i);
   L21_2=(-1i*m/k^2)*(1/r^2)*Phi_i;
   [bb,i_max]=polyadds(L21_1,L21_2);
   L21_p(i,M+2-i_max:M+1)=bb;
end

%%   Evaluating L12_p(Psi(y))
L12_p=zeros(M,M+1);
for i=1:M-2
   Psi_i=Psi(i,M-i+2:M+1);
   L12_1=(1i*m*Rey)*(1/r)*Z*polyder(Psi_i);
   L12_2=(1i*m*Rey)*(-1/r^2)*Psi_i;
   [bb,i_max]=polyadds(L12_1,L12_2);
   L12_p(i,M+2-i_max:M+1)=bb;
end

%%   Evaluating L22_p(Psi(y))
L22_p=zeros(M,M+1);
for i=1:M-2
   Psi_i=Psi(i,M-i+2:M+1);
   L22_1=(1+m^2/(k^2*r^2))*Psi_i;
   i_max=i;
   L22_p(i,M+2-i_max:M+1)=L22_1;
end

%%   Substituting Y_i=y(index) into polynomials and finding [L11(y(index_y))]
     %    as a {1,1:M}vector that each array is respect to the i-th chebychev
     %    .... and also for L21,L12,L22
L11=zeros(1,M);
L21=zeros(1,M);
for i=1:M
   L11(i)=polyval(L11_p(i,M+2-i:M+1),Y_i);
   L21(i)=polyval(L21_p(i,M+2-i:M+1),Y_i);
end
L12=zeros(1,M-2);
L22=zeros(1,M-2);
for i=1:M-2
   L12(i)=polyval(L12_p(i,M+2-i:M+1),Y_i);
   L22(i)=polyval(L22_p(i,M+2-i:M+1),Y_i);
end


%%   Evaluating R11_p(Phi(y
R11_p=zeros(M,M+1);
for i=1:M
   Phi_i=Phi(i,M-i+2:M+1);
   R11_1=Z*polyder(Z*polyder(Z*polyder(Z*polyder(Phi_i))));
   R11_2=(2/r)*Z*polyder(Z*polyder(Z*polyder(Phi_i)));
   R11_3=-(3/r^2+f+k^2)*Z*polyder(Z*polyder(Phi_i));
   R11_4=(3/r^3-f/r-diff_f-k^2/r+1i*k*diff_U*Rey)*Z*polyder(Phi_i);
   R11_5=(-3/r^4+f/r^2-(1/r)*diff_f+k^2*f+k^2/r^2+1i*k*diff2_U*Rey)*Phi_i;
   [bb,i_max]=polyadds(R11_1,R11_2,R11_3,R11_4,R11_5);
   R11_p(i,M+2-i_max:M+1)=bb;
end

%%   Evaluating R21_p(Phi(y))
R21_p=zeros(M,M+1);
for i=1:M
   Phi_i=Phi(i,M-i+2:M+1);
   R21_1=(-1i/Rey/k^2)*(m/r)*Z*polyder(Z*polyder(Z*polyder(Phi_i)));
```

```
   R21_2=(-1i/Rey/k^2)*(2*m/r^2)*Z*polyder(Z*polyder(Phi_i));
   R21_3=(-1i/Rey/k^2)*(-f*m/r-m/r^3)*Z*polyder(Phi_i);
   R21_4=(-1i/Rey/k^2)*(m/r^4-f*m/r^2+1i*m*k*diff_U*Rey/r-2*k^2*m/r^2-i*k^2*E*Rey)*Phi_i;
   [bb,i_max]=polyadds(R21_1,R21_2,R21_3,R21_4);
   R21_p(i,M+2-i_max:M+1)=bb;
end

%%   Evaluating R12_p(Psi(y))
R12_p=zeros(M,M+1);
for i=1:M-2
   Psi_i=Psi(i,M-i+2:M+1);
   R12_1=(1i)*(m/r)*Z*polyder(Z*polyder(Z*polyder(Psi_i)));
   R12_2=(1i)*(-2*m/r^2)*Z*polyder(Z*polyder(Psi_i));
   R12_3=(1i)*(-f*m/r+3*m/r^3)*Z*polyder(Psi_i);
   R12_4=(1i)*(-3*m/r^4+f*m/r^2-m*diff_f/r +2*k^2*m/r^2+2*1i*W*k^2*Rey/r)*Psi_i;
   [bb,i_max]=polyadds(R12_1,R12_2,R12_3,R12_4);
   R12_p(i,M+2-i_max:M+1)=bb;
end

%%   Evaluating R22_p(Psi(y))
R22_p=zeros(M,M+1);
for i=1:M-2
   Psi_i=Psi(i,M-i+2:M+1
   R22_1=(1/Rey)*(1+m^2/(k^2*r^2))*Z*polyder(Z*polyder(Psi_i));
   R22_2=(1/Rey)*(1/r-m^2/(k^2*r^3))*Z*polyder(Psi_i);
   R22_3=(1/Rey)*(-1/r^2-f-f*m^2/(k^2*r^2)+m^2/(k^2*r^4))*Psi_i
   [bb,i_max]=polyadds(R22_1,R22_2,R22_3);
   R22_p(i,M+2-i_max:M+1)=bb;
end

%%   Substituting Y_i=y(index) into polynomials and finding [R11(y(index_y))]
     %    as a {1,1:M}vector that each array is respect to the i-th chebychev
     %    .... and also for R21,R12,R22
R11=zeros(1,M);
R21=zeros(1,M);
for i=1:M
   R11(i)=polyval(R11_p(i,M+2-i:M+1),Y_i);
   R21(i)=polyval(R21_p(i,M+2-i:M+1),Y_i);
end
R12=zeros(1,M-2);
R22=zeros(1,M-2);
for i=1:M-2
   R12(i)=polyval(R12_p(i,M+2-i:M+1),Y_i);
   R22(i)=polyval(R22_p(i,M+2-i:M+1),Y_i);
end

                    function [sum_poly,max_order]=polyadds(varargin)
                    n=nargin;
                    order=zeros(1,n);
                    for i=1:n
                    order(i)=size(varargin{i},2);
                    end
                    m=max(order);
                    coeffmat=zeros(n,m);
                    for i=1:n
                        coeffmat(i,(m-order(i)+1):m)=varargin{i};
                    end
                    sum_poly=ones(1,n)*coeffmat;
                    max_order=m;

function [Phi,Psi]=Collocation_Basis(Cheb_No,Azimuthal_No)
M=Cheb_No;
m=Azimuthal_No;

%% Gamma: Common Chebychev Polynomial
Gamma=zeros(M,M+1);
Phi=zeros(M,M+1);
Psi=zeros(M,M+1);
Gamma(1,M+1)=[1];
Gamma(2,M:M+1)=[1,0];
for i=3:M
```

```
   Gamma(i,:)=2*circshift(Gamma(i-1,:),[0 -1])-Gamma(i-2,:);
end

%%  Phi and Psi functions for the case m=0
if m==0
   Phi(1,:)=Gamma(1,:);
   Phi(2,:)=Gamma(2,:);
   Phi(3,:)=Gamma(3,:)-Gamma(1);
   Phi(4,:)=Gamma(4,:)-Gamma(2,:)-2*(Gamma(3,:)-Gamma(1,:));
   for i=5:M
      if mod(i,2)==1
         Phi(i,:)=Gamma(i,:)-Gamma(1,:)                                    ...
                  -(1/4)*(i-1)^2*(Gamma(3,:)-Gamma(1,:))                   ...
                  +(1/96)*((i-1)^4-4*(i-1)^2)*(Gamma(4,:)                  ...
                  -2*Gamma(3,:)-Gamma(2,:)+2*Gamma(1,:));
      else
         Phi(i,:)=Gamma(i,:)-Gamma(2,:)-(1/4)*(i^2-2*i)*(Gamma(3,:)-Gamma(1,:))    ...
                 +(1/96)*(-(i-1)^4-2*(i-1)^2+3)*(Gamma(4,:)-2*Gamma(3,:)          ...
                 -Gamma(2,:)+2*Gamma(1,:));
      end
   end
   Psi(1,:)=Gamma(1,:);
   Psi(2,:)=Gamma(2,:);
   for i=3:M-2
      if mod(i,2)==1
         Psi(i,:)=Gamma(i,:)-Gamma(1,:);
      else
         Psi(i,:)=Gamma(i,:)-Gamma(2,:);
      end
   end
end

%%  Phi and Psi function for the case m<-1
if m<-1
   Phi(1,:)=Gamma(1,:);
   Phi(2,:)=Gamma(2,:);
   Phi(3,:)=Gamma(3,:)-Gamma(1,:);
   Phi(4,:)=Gamma(4,:)-Gamma(2,:);
   for i=5:M
      if mod(i,2)==1
         Phi(i,:)=Gamma(i,:)-Gamma(1,:)-(1/4)*(i-1)^2*(Gamma(3,:)-Gamma(1,:));
      else
         Phi(i,:)=Gamma(i,:)-Gamma(2,:)-(1/8)*(i^2-2*i)*(Gamma(4,:)-Gamma(2,:));
      end
   end
   Psi(1,:)=Gamma(1,:);
   Psi(2,:)=Gamma(2,:);
   Psi(3,:)=Gamma(3,:)-Gamma(1,:);
   Psi(4,:)=Gamma(4,:)-6*Gamma(3,:)-Gamma(2,:)+6*Gamma(1,:);
   for i=5:M-2
      if mod(i,2)==1
         Psi(i,:)=Gamma(i,:)-Gamma(1,:)                                        ...
                  -(1/12)*((i-1)^4-(i-1)^2)*(Gamma(3,:)-Gamma(1,:))            ...
                  -(1/96)*((i-1)^4-4*(i-1)^2)*(Gamma(4,:)                      ...
                  -6*Gamma(3,:)-Gamma(2,:)+6*Gamma(1,:));
      else
         Psi(i,:)=Gamma(i,:)-Gamma(2,:)                                        ...
                  -(1/12)*((i-1)^4-(i-1)^2)*(Gamma(3,:)-Gamma(1,:))            ...
                  -(1/96)*((i-1)^4+2*(i-1)^2-3)*(Gamma(4,:)                    ...
                  -6*Gamma(3,:)-Gamma(2,:)+6*Gamma(1,:));
      end
   end
end
```

References

[1] Saffman P. G., Vortex Dynamics, New York, NY: Cambridge University Press, 1993.

[2] Batchelor G., An Introduction to Fluid Dynamics, Cambridge University Press, 2000.

[3] H. Schlichting, Aerodynamics of Airplanes, New York: McGraw-Hill, 1979.

[4] Batchelor G.K. , Gill A.E., "Analysis of the stability of axisymmetric jets," *J. Fluid Mech,* vol. 14, no. 4, pp. 529-551, 1962.

[5] Khorrami M. R., "A study of the temporal stability of multiple cell vortices," Progress Report, period ending 31 Oct. 1989 Old Dominion Univ., Norfolk, Virginia, 1989.

[6] Gottlieb D., Orszag S.A., Numerical Analysis of Spectral Methods: Theory and Applications, Society for Industrial and Applied Mathematics, 1987.

[7] Maxworthy T., " Wave motions on vortex cores," *Journal of Fluid Mechanics,* vol. 151, pp. 141-165, 1985.

[8] Duck P. W., Foster M. R., "The inviscid stability of a trailing line vortex," *Zeitschrift für Angewandte Mathematik und Physik (ZAMP),* vol. 31, no. 4, pp. 524-532, 1980.

[9] Lessen M., Paillet F., "The stability of a Trailing Line Vortex Part 2. Viscous Theory," *J. of Fluid Mechanics,* vol. 65, no. 4, pp. 769-779, 1974.

[10] Pedley T., "On the instability of viscous flow in a rapidly rotating pipe," *Journal of Fluid Mechanics,* vol. 35, no. 01, pp. 97--115, 1969.

[11] Maslowe S., "Instability of rigidly rotating flows to non-axisymmetric disturbances," *Journal of Fluid Mechanics,* vol. 64, no. 02, pp. 307--318, 1974.

[12] MAO X., Sherwin S., "Continuous spectra of the Batchelor vortex," *Journal of Fluid Mechanics,* vol. 681, pp. 1-23, 2011.

[13] Cottet G.H., Koumoutsakos P.D., Vortex Methods: Theory and Practice, Cambridge University Press, 2000.

[14] Helmholtz H., "LXIII. On Integrals of the hydrodynamical equations, which express vortex-motion," *Philosophical Magazine Series 4,* vol. 33, no. 226, pp. 485-512, 1867.

[15] Donnelly R., "Quantized vortices and turbulence in helium II," *Annual review of fluid mechanics,* vol. 25, no. 1, pp. 325-371, 1993.

[16] Hasimoto H., "Elementary Aspects of Vortex motion," in *IUTAM Symposium on Fundamental Aspects of Vortex Motion*, Tokyo, Japan, 1988.

[17] Kozel V., *Experimental and Theoritical Studies on Concentrated Columnar Vortices,* Montreal,, Quebec: Mechanical Engineering, Concordia University, 1991.

[18] Vatistas G. H., "New model for intense self-similar vortices," *Journal of Propulsion and and Power,* vol. 14, no. 4, pp. 462-469, 1998.

[19] Thomson W., "XXIV. Vibrations of a columnar vortex," *Philosophical Magazine Series 5,* vol. 10, no. 61, pp. 155-168, 01 September 1880.

[20] Mogens V. Melander, Hussain F., "Core dynamics on a vortex column," *Fluid Dynamics Research,* vol. 13, no. 1, pp. 1-37, 1994.

[21] Maxworthy T., "Waves on vortex cores," in *IUTAM Symposium on Fundamental Aspects of Vortex Motion*, Tokyo, Japan, 1988.

[22] Duraisamy K., *Studies in Tip Vortex, Formation, Evolution and Control,* Maryland: University of Maryland, 2005.

[23] Leibovich S., "Vortex stability and breakdown; survey and extension," *AIAA,* vol. 22, pp. 1192-1206, 1984.

[24] Leibovich S., K. Stewartson, "A sufficient condition for the instability of columnar vortices," *Journal of Fluid Mechanics,* vol. 126, pp. 335-356, 1983.

[25] Fabre D., Jacquin L., "Viscous instabilities in trailing vortices," *Journal of Fluid Mechanics,* vol. 500, p. 239–262, 2004.

[26] Vatistas G. H., Kozel V., "A simpler model for concentrated vortices," *Experiments in Fluids,* vol. 11, no. 1, pp. 73-76, 1991.

[27] Bagai A., Leishman J. G., "Flow visualization of compressible vortex structures using density gradient techniques," *Experiments in Fluids,* vol. 15, pp. 431-442, 1993.

[28] Brix S., Neuwerth G., Jacob D., "The inlet-vortex system of jet engines operating near the ground," in *18th applied aerodynamics conference*, Denver, 2000.

[29] Nguyen T., *An Investigation of Vortex Breakdown from the Point of View of Hydrodynamic Stability,* University of California, Berkeley, 1980.

[30] Rossow V. J., "Lift-generated vortex wakes of subsonic transport aircraft," *Progress in Aerospace Sciences,* vol. 35, no. 6, p. 507–660, August 1999.